Electrochemical Studies of Transition Metal Hexahalometallates.

Steven Hawkins

Submitted for the Degree of Ph.D.

Faculty of Science, University of Glasgow

November 6, 1989

ProQuest LLC.
789 East Eisenhower Parkway
P.O. Box 1346
Ann Arbor, MI 48106 – 1346

Abstract

This thesis determines the redox potentials of second and third row transition metal hexabromometallates using cyclic voltammetry methods in methylene chloride solution. The results are collated with the redox potentials of second and third row transition metal hexafluoro- and hexachlorometallates and the systematic trends exhibited by all the redox potentials are discussed. The contents of this thesis are divided as follows :-

In chapter one the nature of transition metal hexahalometallate bonding is discussed by drawing on ideas from ligand field theory and molecular orbital theory, both of which are described briefly. The contributions to the metal-halogen bond are described separately under a) purely electrostatic effects– which are treated using electronegativity differences, and b) covalency effects which are subdivided into σ - covalency and π - bonding. Lastly, chapter one includes a brief description of the vibrational and electronic spectra of transition metal hexahalometallates as these two methods were the principle means of identifying complexes.

Chapter two begins with a conceptual description of charge transfer reactions at electrode surfaces and then approaches the same subject mathematically to derive the Butler-Volmer equation, the fundamental equation of electrode kinetics. The D.C. and A.C. cyclic voltammetry techniques are described and for a D.C. cyclic voltammogram, the current-potential profile is discussed and illustrated for reversible, quasi-reversible and irreversible electron transfer processes. The effects of coupled chemical reactions and adsorption of reactant and/or product on the electrode surface are also reviewed.

Chapters three and four respectively describe the cyclic voltammetric investigations of the hexabromometallate complexes prepared in this work and the halogen/halide systems of chloride, bromide and iodide. The electrode potentials determined are compared with literature values wherever possible. Complex electrochemical activity at high oxidation potentials thwarted the detection of any of the possible $[MBr_6]^{0/1-}$ redox couples. Adsorption of hexabromometallate species onto the electrode at high oxidation potentials is put forward as a likely reason. Other

problems which were encountered include the reaction of tungsten hexabromide with the supporting electrolyte and the propensity of trivalent hexabromometallate anions to dimerize when countered by the sterically large tetra-n-butylammonium cation.

In chapter five, the electrode potentials of the transition metal hexabromometallate complexes determined in chapter three are collated with the electrode potentials of hexafluoro- and hexachlorometallate complexes already determined by previous workers. The systematic trends which emerged include :-

1. The electrode potentials of isovalent $[MX_6]^{z/z-1}$ redox couples increase regularly across a period except for a discontinuity at the $d^{3/4}$ couple.
2. The discontinuity is more pronounced for second row than third row transition metal hexahalometallates.
3. $[MX_6]^z$ complexes become more oxidizing with increasing oxidation state of the metal.
4. Third row transition metal hexahalometallate complexes are more reducing than their isoelectronic second row counterparts.

By using simple thermodynamic arguments it is derived that the standard electrode potential of a redox couple is proportional to the free energy difference between the reduced and the oxidized species, which is in turn composed of two separate contributions :-

- The entropy– which was associated with alterations to the solvation sphere which, it was concluded, have no influence on the systematic trends observed.
- The enthalpy– of which the principal contributions arise from
    1. the ionization enthalpy of the metal.
    2. the d^n configuration of the metal.
    3. the nature of the halide ligand.
    4. the nature of the solvent.

Chapter five concludes with a brief survey of some of the uses and applications of hexahalometallate redox potentials.

Finally, chapter six details the synthesis and characterisation of the compounds studied in this thesis. Included is a description of the electrochemical cell and its manipulation, and the preparation of the solvent and supporting electrolyte.

Acknowledgements

My sincere thanks go to my supervisor Prof.D.W.A.Sharp of Glasgow University for his invaluable help and encouragement throughout the duration of my studies. Special thanks also to Dr.J.M.Winfield of Glasgow University and Dr.L.J.Yellowlees of Edinburgh University for their numerous contributions and encouragement. I am indebted and grateful to all the technical staff, fellow students and the Friday night club at Glasgow University without whose help and generous friendship this thesis could not have been completed. To my brother John, who toiled at the word-processing over countless hours, and David Newton for technical support on the LaTeX type-setter, I offer my sincerest gratitude. I would also like to thank Hewlett-Packard Ltd. for the use of their computing facilities. Finally, my greatest thanks to all my family and Jane for their continual encouragement.

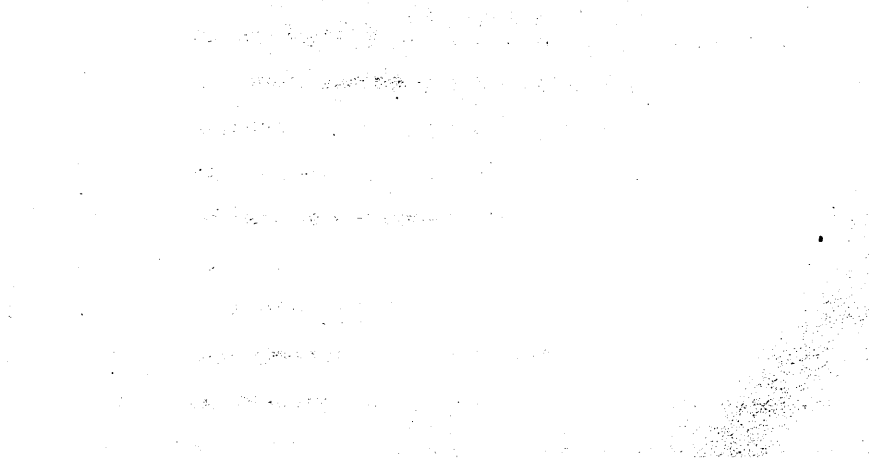

Contents

List of Figures

List of Tables

Chapter 1

1.1 Introduction

The hexahalometallate complexes of the second and third row transition elements comprise one of the most important categories of inorganic compounds; they are important compounds in their own right, such as the recent interest in hexahalotechnetate(IV) compounds as radiotracers in medical science for example [25]; the majority of transition metal hexahalometallate compounds are relatively easy to synthesize and are used as important precursors for more complex compounds; and the relative simplicity of their structures has enabled scientists to develop theories around them which were subsequently applied to more complex molecules.

As an important category of compounds, hexahalometallates have been the subject of a wide ranging number of studies for over a century although the bulk of research up till now has been mainly concerned with the properties of hexafluoro- and hexachlorometallates. The hexabromo- and hexaiodometallates of the second and third row transition elements have received less attention and one finds that the documented information becomes less and less extensive as one progresses from hexafluoro- to hexaiodometallates. With regard to this thesis, a number of electrochemical investigations concerning transition metal hexahalometallate complexes have already been published. In particular, the redox potentials of hexafluorometallates were investigated by D.W.A Sharp and co-workers [55] and the redox potentials

of hexachlorometallates were investigated by K. Moock *et al* [31,41] . The electrochemistry of hexabromometallate and hexaiodometallate compounds has been largely overlooked.

Therefore to extend the present understanding of hexahalometallate redox behaviour, this thesis attempts to develop further the trends already observed among and between the redox potentials of the hexafluoro- and hexachlorometallates of the second and third row transition elements. To this end, the bulk of the experimental results, which are described in chapter 3 , are concerned with the determination of the redox potentials of the second and third row transition metal hexabromometallate complexes in methylene chloride.

The remainder of this chapter will be devoted to a description of the nature of metal-halogen bonds in transition metal hexahalometallate species.In addition, a brief description of the vibrational and electronic absorption behaviour of hexahalometallates is included because these spectroscopic methods provide valuable means by which individual complexes can be identified.

1.2 Bonding in Transition Metal Hexahalometallate Complexes

Modern treatments of bonding in transition metal complexes using ligand field theory (L.F.T.) and molecular orbital (M.O.) theories are well documented [1] and a number of excellent textbooks have been written [2-5].

When discussing the bonding in transition metal hexahalometallate complexes, the structure adopted by each complex is assumed to be a regular octahedron and geometric distortions, principally Jahn-Teller effects, are neglected. The validity of this assumption was tested by Weinstock and Goodman [181] who could find no evidence for static Jahn-Teller distortions in the infra-red and Raman spectra of second and third row transition metal hexafluorides.(Although dynamic Jahn-Teller effects were discovered for the hexafluorides of Re, Tc, Os, and Ru, the distortion forces were small). Neglecting any Jahn-Teller effects simplifies the rigorous symmetry

and group theoretical treatments necessary with both L.F.T. and M.O.theory without greatly affecting the conclusions to be drawn from either.

Both theories have been extensively applied to hexahalometallate species in order to interpret various phenomena, although which theory is the most suitable approach for a problem is dictated by the nature of the problem and the individual merits of each theory. For example, L.F.T. is based on the electrostatic interactions between the metal and the ligands and has proved very useful when interpreting electronic absorption spectra. However L.F.T. becomes more restricted the less ionic character the central ion-ligand bonds show. In L.F.T. the complex ion is treated as a system whose electrons belong either exclusively to the central ion or to the ligands. In other words, the electrons are localized. This postulation specifically excludes covalent bonds and covalency contributions. In this respect molecular orbital theory as the name suggests, can accommodate varying degrees of bond covalency, but unfortunately M.O. analyses involve lengthy and complex calculations even for the simplest of molecules. M.O. calculations therefore necessarily involve a number of (sometimes incorrect) assumptions.

1.3 Ligand Field Theory

The conception of the crystal field theory (C.F.T.) , the predecessor of L.F.T. is attributed to Bethe (1929) [6]. C.F.T. assumes that the transition metal atom is ionized according to its formal positive oxidation number, and that the effects of the surrounding ligands can be obtained by representing them as point negative charges. For a transition metal atom in a simple cubic lattice, C.F.T. predicts that the 5 nd-orbitals are divided into two types - the e_g and t_{2g} sets. In an octahedral crystal field the two degenerate orbitals of the e_g set are of higher energy than the other three degenerate orbitals of the t_{2g} set. The reason for this can be quite easily understood;-

By convention the negative ligands are assumed to occupy points on the Cartesian axes (fig.1.1). If the negative charges of all six ligand ions were evenly distributed over a sphere surrounding the central metal ion, then the negatively charged nd orbitals of

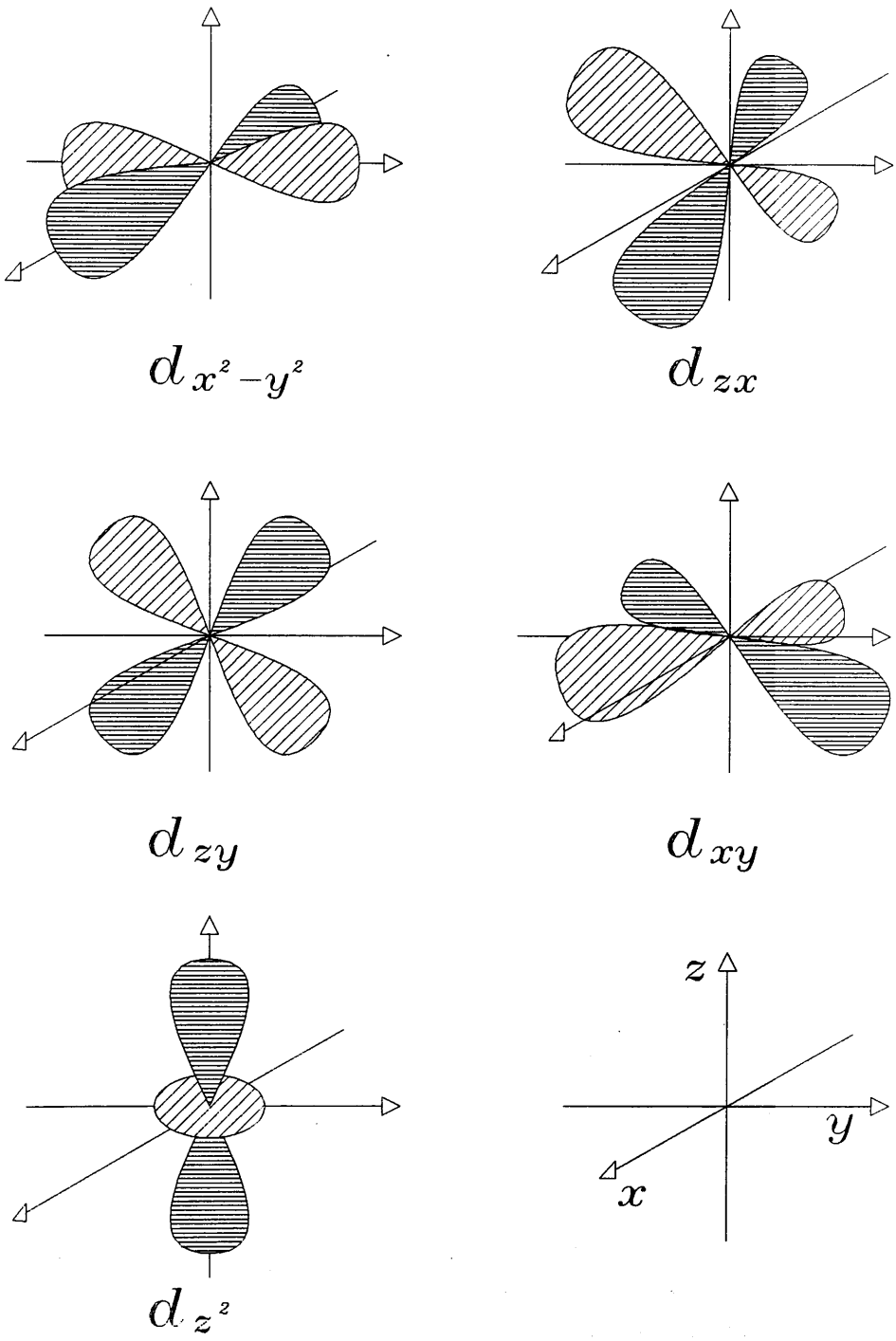

Figure 1.1: The *nd* orbital set

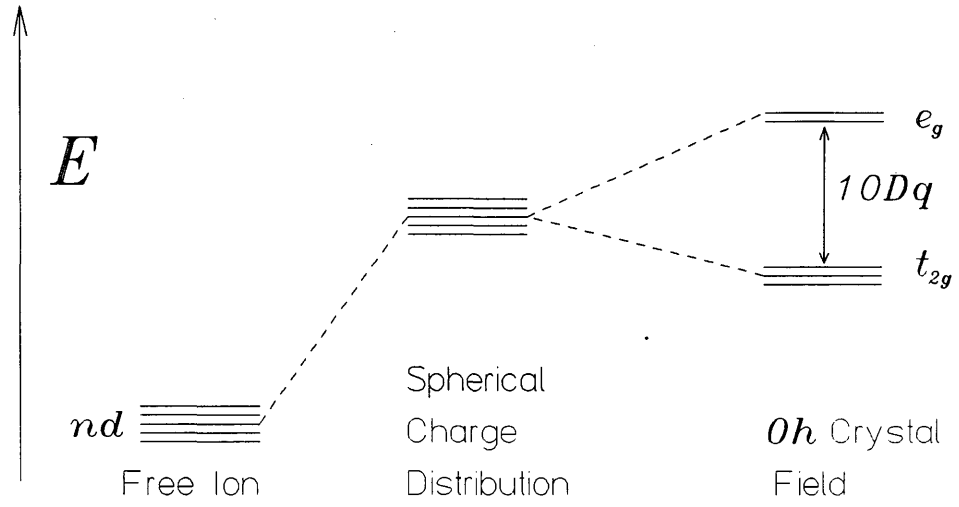

Figure 1.2: *d*-orbital splitting under an octahedral crystal field

the metal would each experience the same electrostatic repulsion, and their energies would be raised by the same amount above the energy of the nd orbitals in the free metal ion. But, when the negative ligand charges are located on the corners of an octahedron around the central metal ion, the nd orbitals which are directed towards the ligands ie. along the Cartesian axes, experience a greater repulsion than those which are directed between the Cartesian axes (fig.1.2). The energy separation between the e_g and t_{2g} orbitals is dependent on the identity of the central metal ion and the ligands and is known as 10 Dq. The 'centre of gravity' corresponding to the energy of a spherical charge distribution is always maintained.

The crystal field model was intended to explain the spectra of simple crystalline solids and for compounds such as bivalent transition metal oxides, it is probably not far from reality. However, to explain the spectra of the transition metal hexahalometallates it is necessary to admit that the nd orbitals can no longer remain 'pure' but must mix with ligand valence orbitals to form bonding and anti-bonding pairs. In effect, ligand field theory is a qualitative M.O. theory where changes produced by

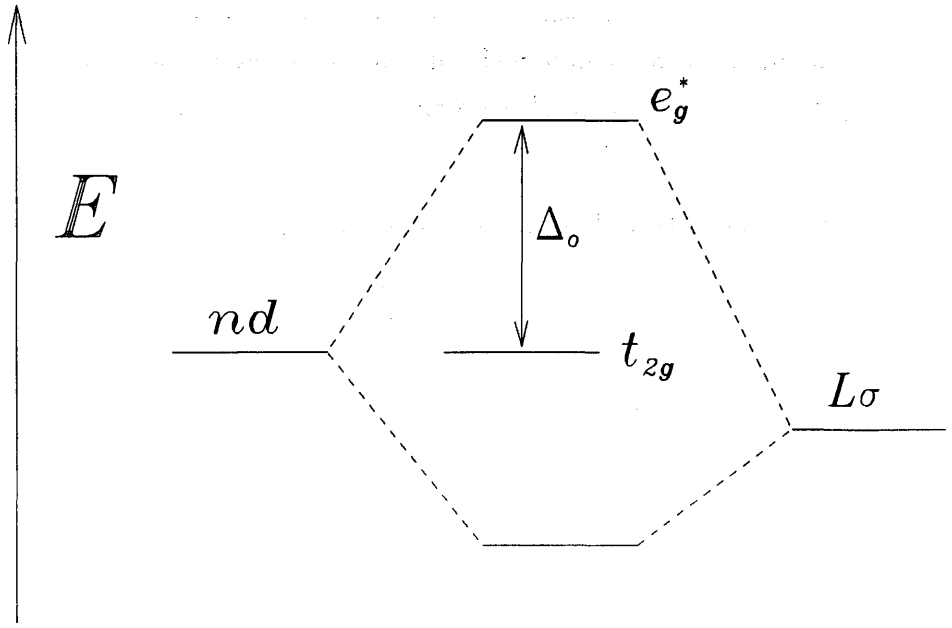

Figure 1.3: Octahedral ligand field formed by purely σ-bonding ligands.

the mixing of metal and ligand orbitals are accommodated by changing the appropriate details of the wave functions describing the effective d-orbital set [7]. As it is assumed that the degree of orbital mixing is small, the major features of C.F.T. behaviour remain.

In L.F.T., ligands with purely σ-bonding ability interact with the metal e_g set while the metal t_{2g} orbitals are essentially non-bonding (fig.1.3).

The 10 Dq value of C.F.T. is then associated in L.F.T. with Δ_o, the $e_g^* - t_{2g}$ energy difference. For all transition metals the size of Δ_o is found to increase according to the ligand identity following a sequence known as the spectrochemical series :-

$$I^- < Br^- < Cl^- < SCN^- < F^- < OH^- < \text{Oxalate} < H_2O \ll NO_2^- \ll CN^- \qquad (1.1)$$

The order of the halogen ligands in eqn.1.1 predicts an increasing Δ_o with decreasing ligand polarisability and atomic radii.This would also be predicted from C.F.T.

using a purely electrostatic model. However, the position of H_2O above OH^- and oxalate is not explainable with this argument because the C.F.T. neglects the possibility that the metal-ligand bond contains any degree of covalency. In L.F.T. the degree of orbital mixing is addressed by recourse to the nephelauxetic or 'cloud expanding' effect [8]:-

Jørgensen [8] defines the nephelauxetic ratio β as the ratio between the value of a representative parameter of interelectronic repulsion eg. the Racah repulsion parameter B, in the complex, to that of B in the free ion.

$$\text{nephelauxetic ratio } \beta = \frac{\text{B complex ion}}{\text{B free ion}} \tag{1.2}$$

Therefore the size of β decreases with decreasing interelectronic repulsion in a complex ion, corresponding to an increased delocalisation of the metal d electrons. The nephelauxetic series of ligands,defined by (1-β), for a given metal ion in a given oxidation state increases according to :-

$$F^- < H_2O < NH_3 < NCS^- < Cl^- \simeq CN^- < Br^- < I^- \tag{1.3}$$

The order of the ligands in eqn.1.3 corresponds with the reducing character of the ligands *viz.* their tendency to lose electrons. Hence an increase in the covalency of metal-ligand bonds arising from ligand to metal σ donation is expected between metal-fluorine and metal-iodine bonds.

Consequently , the nephelauxetic effect of ligands is used in L.F.T. to approximate the influence of bond covalency on the energy levels of a transition metal ion by multiplying the interelectronic repulsion parameters of the gaseous ion, observed experimentally, by the factor β.

1.4 Molecular Orbital Methods

Molecular orbitals are constructed from an appropriate combination of the valence atomic orbitals, governed by the linear combination of atomic orbitals approximation (L.C.A.O.). Metal and ligand valence orbitals are defined and then molecular orbital wave functions generated from them, provided the atomic orbital energies are similar and their symmetries are correct. To calculate the order of M.O. energies, reasonable approximations to the coulombic and exchange energies are adopted [12], and normally, semi-empirical calculations instead of *ab-initio* calculations are employed to reduce the computation and cost required.

When discussing the molecular orbitals of octahedral hexahalometallate complexes, the orbitals available for σ bonding on each halide ion are principally the valence ns orbital and that np orbital which is directed along the Cartesian axis, the pσ orbital. The relevant orbital interactions are similar to figure 1.3 However, those np orbitals which are perpendicular to the metal-ligand σ bond, the pπ orbitals, can overlap with the metal t_{2g} orbitals to form π-bonds. This property has a significant effect on the $e_g - t_{2g}$ energy separation, which in turn specifies the position of a ligand within the spectrochemical series.

The M.O. interpretation of the spectrochemical series is therefore based on the relevant energies of the metal based t_{2g} and e_g molecular orbitals. From L.F.T. (section 1.3) it was noted that the presence of a strong electrostatic interaction between the metal and ligand raised the e_g^* energy level thus increasing Δ_o. Ligand to metal π-bonding from occupied ligand pπ orbitals to metal t_{2g} orbitals is allowed by symmetry. This raises the energy of the previously non-bonding metal t_{2g} orbitals associated with L.F.T. and decreases the energy Δ_o .Therefore, the small ligand field splitting observed with halide ligands is attributed to the influence of occupied $p\pi$ orbitals of the appropriate symmetry available on the ligands.

On the contrary, a metal to ligand π^* interaction is only possible with those ligands possessing low lying unoccupied π^* orbitals of suitable symmetry (eg. CO, CN^-). Metal to ligand π^* bonding lowers the metal based t_{2g} M.O. energy and thus appreciably increases Δ_o .

(The possible existence of metal to ligand π donation in transition metal hexahalometallate species involving empty halide nd orbitals (not fluoride) has been speculated upon [13] and is discussed in section 1.7.)

To complicate matters,transition metal-halogen bonding occupies a region between the extremes of purely electrostatic and purely covalent bonding. However, to simplify the discussion the individual contributions to the metal-halogen bond in transition metal hexahalometallate species will be divided into the following three categories :-

1) Purely electrostatic effects
2) σ - covalency effects
3) π - bonding effects

The various group and periodic trends which emerge between transition metal hexahalometallate species are governed by the extent of each contribution 1),2) and 3) to the metal-halogen bond, which in turn is governed by the physical properties of both the metal and the halogen. In the following sections the different contributions will be discussed.

1.5 Electrostatic effects

The electrostatic contribution to the total energy of a bond M-X is most easily interpreted in terms of the electronegativity difference between the atoms or ions. According to Pauling [14], electronegativity is the power of an atom in a molecule to attract electrons to itself and therefore will be dependent on the valence state of the atom in the molecule. A large electronegativity difference Δ_{mx} is associated with a significantly ionic M-X bond.

$$\Delta_{mx} = \chi_x - \chi_m \tag{1.4}$$

Jørgensen [16] introduced the closely related concept of optical electronegativities

by which charge transfer absorption energies are related to electronegativity differences. The advantage of Jørgensens' method is that the electronegativities of metal ions in unusual oxidation states can be easily obtained. The optical electronegativities of the halogens and second and third row transition metal ions are shown in table 1.1. The data in table 1.1 indicates that the electrostatic nature of hexahalometallate bonds for a given metal ion decreases in the order :-

$$[MF_6]^z > [MCl_6]^z > [MBr_6]^z > [MI_6]^z \qquad (1.5)$$

(z=0, 1-, 2-, 3- etc.)

Another method of obtaining the same result is by comparison of stretching force constants. Verma *et al* [15] computed the force constants of second and third row transition metal hexahalometallate ions using general valence force field (G.V.F.F.), modified orbital valence force field (M.O.V.F.F.) and modified Urey-Bradley force field (M.U.B.F.F.) calculations. From the decrease of bond stretching force constant f_r(G.V.F.F.), K(M.O.V.F.F.) and K(M.U.B.F.F.) they deduced that the relative strengths of the chemical bonds in transition metal hexahalometallates was in the order of eqn.1.5, in accordance with the decrease in electronegativity; $F^- > Cl^- > Br^- > I^-$. Furthermore, it was observed by Verma *et al* that an increase in the stretching force constant occurred between isovalent second and third row hexahalometallates. This increase in bond strength down a group, for a given oxidation state, is predictable from the greater optical electronegativity values of second row transition metal ions compared with the corresponding third row metal ion.

In summary therefore, as a general rule the greater the electronegativity difference between the metal and the halogen, then the greater is the average bond strength of hexahalometallates. Hexafluorometallate bonds have the most electrostatic or ionic character and are consequently stronger than hexachlorometallate bonds which are stronger than hexabromometallate bonds which are stronger than hexaiodometallate bonds.

Table 1.1: Optical electronegativities of metal ions and ligands [16].

electron configuration	metal ion	electro-negativity
$4d^0$	Mo(VI)	2.1
$4d^3$	Mo(III)	1.7
$4d^3$	Tc(IV)	2.2
$4d^4$	Ru(IV)	2.4
$4d^5$	Ru(III)	2.1
$4d^5$	Rh(IV)	2.6
$4d^6$	Rh(III)	2.3
$4d^6$	Pd(IV)	2.7
$5d^0$	W(VI)	2.0
$5d^2$	Os(VI)	2.6
$5d^3$	Re(IV)	2.0
$5d^3$	Ir(VI)	2.9
$5d^4$	Os(IV)	2.2
$5d^4$	Pt(VI)	3.2
$5d^5$	Os(III)	1.9
$5d^5$	Ir(IV)	2.35
$5d^6$	Ir(III)	2.25
$5d^6$	Pt(IV)	2.6

	electronegativity			
ligand	F-	Cl-	Br-	I-
σ	4.4	3.5	3.3	3.0
π	3.9	3.0	2.8	2.5

1.6 The covalency of transition metal-halogen bonds

Using nuclear quadrupole resonance (N.Q.R.) analysis an estimation of the ionic, covalent and π character of a bond can be made. Unfortunately, the original procedure devised by Townes and Dailey [198] neglected any possibility of $p\pi$ to $d\pi$ ligand to metal π bonding. Therefore any π- character in the metal-ligand bond must be incorporated by estimating the π -bonding contribution using electron spin resonance measurements (E.S.R.). The data calculated by this method are listed in table 1.2.

The first notable feature of table 1.2 is that third row transition metal hexachlorometallates(IV) have approximately equal electrostatic and covalent contributions to the overall bonding. Secondly, the electrostatic contribution to the bonding remains roughly constant across the period which is largely to be expected because the metal(IV) ions have similar optical electronegativities (table 1.1). The same can be said for the decreasing electrostatic bonding contribution observed for a given metal ion (here Re) as the halide ligand is changed from (F^-) to Cl^- to Br^- to I^-. However the covalent contributions are more interesting. The, E.S.R. measurements show that π -bond character, namely $p\pi$(L) to $d\pi$(M), decreases across a period which is a result of the increasing metal t_{2g} orbital occupancy. At the same time the σ-covalency contribution to the metal-halogen bond increases such that the overall covalent contribution to the bond, $\sigma + \pi$, is roughly constant across a period.

Of course changing the halogen ligands will alter the numbers accordingly. By changing to the larger halogens the metal-halogen bond becomes increasingly more covalent. Townes and Dailey calculated the same π-bond character for hexachloro-, hexabromo- and hexaiodorhenate(IV) which is a curious result: because of the greater size or diffuseness of Br^- and I^- $p\pi$ orbitals, one would expect a greater π overlap with metal t_{2g} orbitals and a correspondingly greater π contribution.

A more rigorous approach was adopted by Cotton and Harris [22]. By employing extended Hückel molecular orbital calculations (E.H.M.O.), they were able to calculate charge distributions and metal-ligand covalencies for some hexachlorometallates(IV) in good agreement with the experimental data (table 1.3).

Table 1.2: The bond character of some metal-halogen bonds and the net charge on the central metal atom obtained by N.Q.R. measurements [19].

compound	ionic character	σ-bond character	π-bond character	net charge
$[PtCl_6]^{2-}$	0.44	0.56	0	0.64
$[IrCl_6]^{2-}$	0.47	0.48	0.054	0.82
$[OsCl_6]^{2-}$	0.47	0.43	0.108	0.82
$[ReCl_6]^{2-}$	0.45	0.39	0.16	0.70
$[WCl_6]^{2-}$	0.43	0.35	0.22	0.58
$[ReBr_6]^{2-}$	0.39	0.45	0.16	0.34
$[ReI_6]^{2-}$	0.32	0.52	0.16	-0.08

Table 1.3: $[MCl_6]^{2-}$ molecular properties obtained by E.H.M.O. calculations.

	$[ReCl_6]^{2-}$	$[OsCl_6]^{2-}$	$[IrCl_6]^{2-}$	$[PtCl_6]^{2-}$
metal charge	1.32	1.18	0.89	0.69
M-Cl bond order	0.438	0.454	0.475	0.475
σbond order	0.435	0.445	0.484	0.508
πbond order	0.003	0.009	-0.009	-0.003
% metal in t_{2g} M.O.	89	90	85	81

Cl orbital occupation				
	$[ReCl_6]^{2-}$	$[OsCl_6]^{2-}$	$[IrCl_6]^{2-}$	$[PtCl_6]^{2-}$
3s	1.93	1.93	1.91	1.91
3pσ	1.68	1.63	1.60	1.54
3pπ	3.94	3.95	3.96	3.99

The calculated data in table 1.3 agree with the predictions of the nephelauxetic theory as a progressively increasing M-Cl bond order and decreasing effective metal charge are observed when progressing across a period, mirroring the decreasing metal-halide electronegativity difference. However, a smaller bond order increase was observed than that which might have been expected from the large decrease in metal charge. The reason given by Cotton and Harris was, the increase in σ bond order is tempered by the increasingly negative π bond order due to the chlorine pπ orbitals donating into an antibonding metal t_{2g} orbital . (However, this reason neglected the presence of a full t_{2g} manifold with hexachloroplatinate(IV).)

Nonetheless, table 1.3 and to a lesser extent table 1.2 indicate that hexahalometallate bonds become increasingly covalent in the order:-

1. For a given metal ion, hexahalometallate bonds become increasingly covalent in character in the order

$$[MF_6]^{n-} < [MCl_6]^{n-} < [MBr_6]^{n-} < [MI_6]^{n-} \tag{1.6}$$

2. For the same halide ligand, the covalency of hexahalometallate bonds increases slightly across a period as a result of greater σ -donation from the halide ligands.

3. For a given halide ligand and within the same group,there is an increase in the covalency of hexahalometallate bonds between isovalent second and third row elements.

Although the first two items are predictable from electronegativity differences the third item indicates that electronegativity differences alone do not dictate the degree of electrostatic character in hexahalometallate bonds and that the average bond strength is the result of the combined ionic and covalent ($\sigma + \pi$) contributions to a bond.

Table 1.3 indicated that the π electron donation from chlorine pπ orbitals to a central metal ion decreases across a period such that the 3pπ orbital occupancies of the chloride ligands of $[PtCl_6]^{2-}$ are very nearly the maximum of 4.0. This is the

expected result of increasing the t_{2g} orbital occupancy which decreases the degree of $p\pi$ to t_{2g} bonding possible. As a consequence of reduced π bonding and reduced ionic character, the metal-halogen bond of hexahalometallate complexes should become progressively weaker across a period.

The $\nu_1(a_{1g})$ vibrational mode of octahedral transition metal molecules may be taken as the frequency closest to a measure of the metal-ligand bond strength. (Because the vibration does not alter the molecules' symmetry and there is no movement of the heavy central metal ion.) In table 1.4 the ν_1 stretching frequencies of second and third row hexafluorides decrease markedly across a period, indicating a progressive weakening of the metal-fluorine bond. Bond weakening is reflected by the chemical reactivity of second and third row hexafluorides which increases across each period [17]. Similarly, for the compounds WF_6, ReF_6, OsF_6 and IrF_6 the calculated stretching force constants f_r(M.V.F.F.) are found to decrease progressively [20].

Table 1.4: Symmetric stretching frequencies (ν_1) of the transition metal hexafluorides (ν in cm^{-1}).

compound	ν_1	compound	ν_1
MoF_6	741	WF_6	772
TcF_6	705	ReF_6	755
RuF_6	675	OsF_6	733
RhF_6	634	IrF_6	696
		PtF_6	655

In stark contrast with the second and third row transition metal hexafluorides, for the chloro- and bromo- series $[HfX_6]^{2-}$, $[ReX_6]^{2-}$, $[IrX_6]^{2-}$ and $[PtX_6]^{2-}$ the values of the force constants K(M.U.B.F.F.) show a progressive increase [21] (table 1.5). It is also an experimental fact that all complex chlorides and oxide chlorides with a d^0 configuration are thermally unstable with respect to dissociation to the parent halide or oxide halide, whereas the corresponding fluoro complexes are much more stable [13].

Table 1.5: M.U.B.F.F. stretching force constants of hexachloro- and hexabromometallate(IV) anions (K in mdyn/Å).

anion	K	anion	K
$[HfCl_6]^{2-}$	1.273	$[HfBr_6]^{2-}$	0.969
$[ReCl_6]^{2-}$	1.516	$[ReBr_6]^{2-}$	1.208
$[IrCl_6]^{2-}$	1.709	$[IrBr_6]^{2-}$	1.220
$[PtCl_6]^{2-}$	1.841	$[PtBr_6]^{2-}$	1.562

So why is the bond weakening influence of increasing the metal t_{2g} orbital occupancy and decreasing electronegativity difference for transition metal hexafluorides not relevant to hexachloro- and hexabromo- metallate complexes? A useful explanation is the possibility that chloride, bromide (and iodide) can accept electron density from the metal into empty low lying d orbitals. By this mechanism, the degree of metal to halogen $d\pi$ to $d\pi$ back-bonding would increase with increasing atomic number and therefore the metal-halogen bond strength would progressively increase across a period. Hence, there is an increase in stability of the hexachloro-, hexabromo- and hexaiodometallate complexes across a period because of an increased propensity for back-donation as the metal t_{2g} orbital electron population increases. Because fluoride ligands do not have available d orbitals back-bonding cannot occur and the opposite trend in stability is observed with transition metal hexafluorometallates because of the reasons outlined previously.

The concept of metal to halogen π back-bonding was developed by Woodward and Creighton [182] to explain an intensity anomaly in the Raman spectra of hexachloroplatinate(IV) species. More convincing evidence for π back-bonding was obtained by Owen and co-workers [23] who examined the E.S.R. spectrum of a hexachloroiridate(IV) sample. Instead of the expected 4 lines for iridium (I=3/2) they observed 16 lines arising from the unpaired t_{2g} electron, formally resident on the metal, interacting with the six chlorine nuclei. When the relevant data were analysed it was concluded [13] that a possible explanation of the π-bond orders calculated from the E.S.R. results was that the metal t_{2g} orbitals overlapped with both the chlorine $p\pi$

and dπ orbitals.

However, although evidence has developed which seems to validate the hypothesis of metal to ligand back donation in hexahalometallates there is so far no unequivocal proof. It should be remembered that although the idea of metal-halide back-bonding is generally accepted, the true extent may have been over-rated and conventional explanations in terms of donor-acceptor models relying on covalent character and polarisation may have been overlooked [184].

What does appear to be clear is that the bonding in hexafluorometallate complexes is predominantly electrostatic in nature and the average bond strengths of hexafluorometallates behave accordingly. As one progresses from hexachlorometallates to hexaiodometallates, the bonding becomes increasingly covalent in nature and the average bond strength results from a combination of electrostatic and σ and π covalency contributions including possibly π -back donation.

1.7 The vibrational spectra of hexahalometallates

Figure 1.4 illustrates the six normal modes of vibration and their symmetries for an octahedral AX_6 molecule. Vibrations ν_1, ν_2 and ν_5 are only Raman active whilst ν_3 and ν_4 are only infra- red active. Because ν_6 is inactive in both detection modes its frequency is normally estimated from an analysis of combination and overtone bands.

Table 1.6 lists the infra-red and Raman data of a number of hexabromometallate complexes (obtained from solid samples unless stated). For hexafluoro- and hexachlorometallates the order of the three stretching vibrations is normally $\nu_1 > \nu_3 > \nu_2$ (except $[PdCl_6]^{2-}$) while for hexabromometallates and presumably hexaiodometallates (the available data are limited) the order is normally $\nu_3 > \nu_1 > \nu_2$ (see for instance Nakamoto [185]). The identity of the countercation considerably affects the frequency of ν_1 and ν_3 which generally decrease with increasing cation size. This has been attributed to a decrease in cation-anion interactions as the cation size increases [186] but is more probably explainable by an increase in the metal-halogen bond length. Consequently, it is common procedure to obtain Raman measurements from

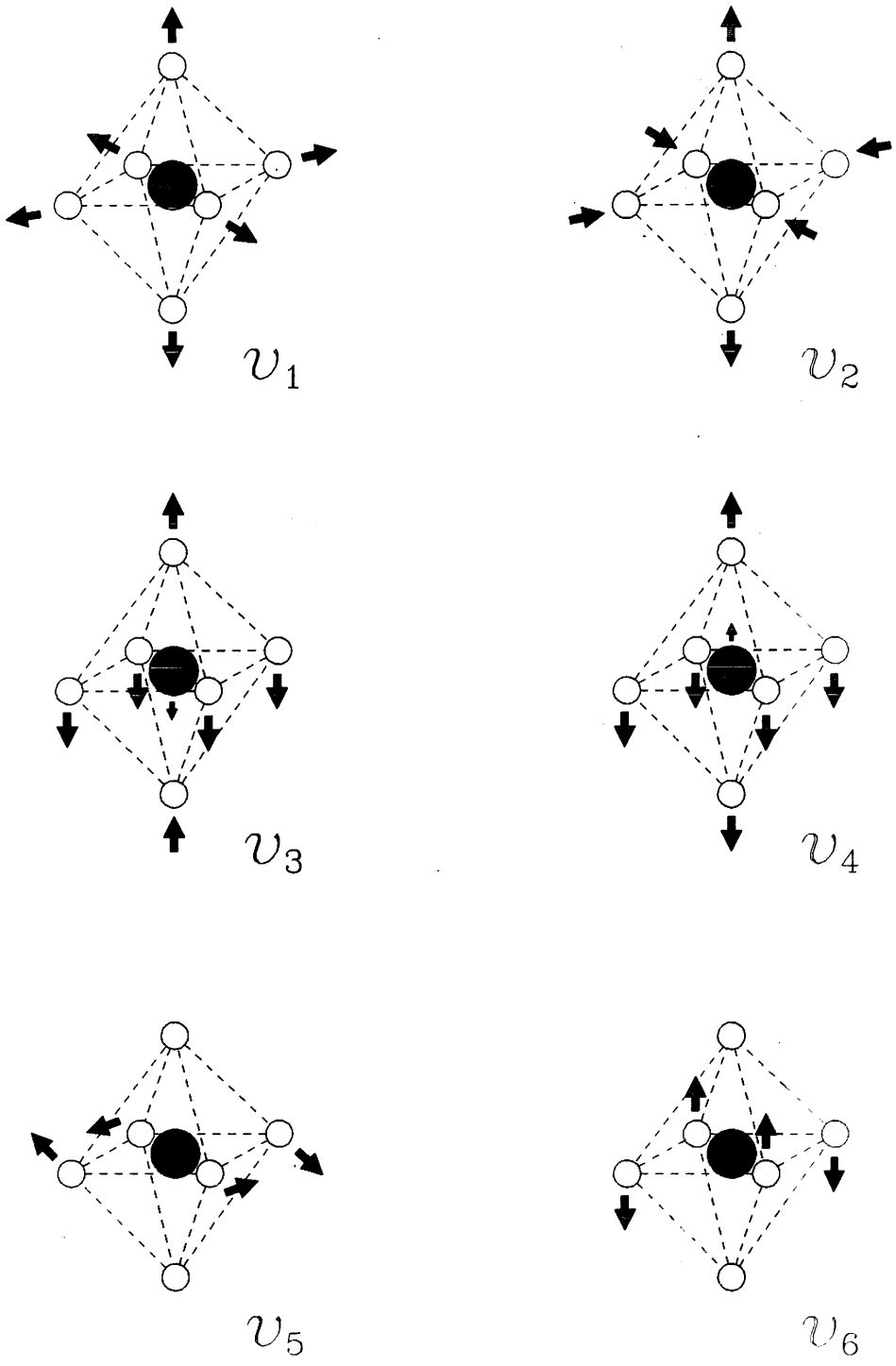

Figure 1.4: The normal modes of vibration of octahedral AX_6 molecules.

a solution of the compound in question if accurate values are required. In addition, solution spectra are often preferable because the intense colour of many hexabromo- and hexaiodometallate complexes makes Raman spectral data often unobtainable from crystalline samples.

The tetra-n-butylammonium salts of the hexabromometallate complexes prepared in this work were not amenable to powder Raman studies. All except a few tetra-n-butyl-ammonium complexes deteriorated in the Raman laser beam or the powdered samples were so intensely coloured that they did not effectively scatter the light from the laser. The latter problem, which was most widespread, could not be overcome by varying the wavelength within the range of available laser lines.

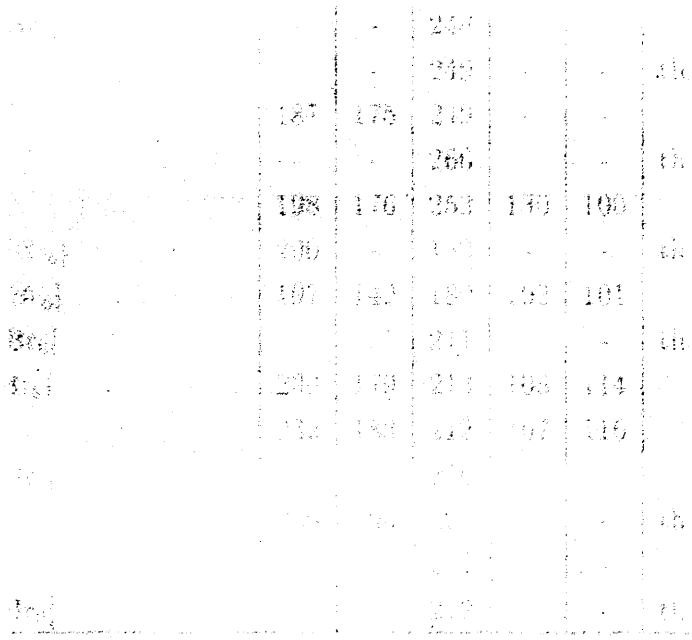

Table 1.6: Vibrational frequencies of hexabromometallates as crystalline solids (cm^{-1}).

compound	ν_1	ν_2	ν_3	ν_4^b	ν_5	ref.
$[Bu_4N]_2[ZrBr_6]$	-	-	219	-	-	this thesis
$[Et_4N]_2[ZrBr_6]$	194	144	223	106	99	144
$[Bu_4N][NbBr_6]$	-	-	237	-	-	this thesis
$Cs[NbBr_6]$	224	180	236	112	114	144
$[Et_4N][NbBr_6]$	219	179	239	112	-	147
$[PPh_4][NbBr_6]$	-	-	246	-	-	105
$[Bu_4]_2[MoBr_6]$	-	-	227	-	-	this thesis
$[PPh_3Me]_2[MoBr_6].2CH_2Br_2$	-	-	230	-	-	58[a]
$[Bu_4N]_2[RuBr_6]$	-	-	235	-	-	this thesis
$Cs_2[RuBr_6]$	-	-	240	-	-	163
$[Bu_4N]_2[RuBr_6]$	200	160	-	-	106	160
$[NH_4]_2[RuBr_6]$	-	-	248	-	-	158
$K_3[RhBr_6]$	-	-	249	-	-	this thesis
$K_3[RhBr_6]$	187	175	249	-	-	161
$K_2[PdBr_6]$	-	-	266	-	-	this thesis
$K_2[PdBr_6]$	198	176	253	130	100	154
$[Bu_4N]_2[HfBr_6]$	200	-	189	-	-	this thesis
$[Et_4N]_2[HfBr_6]$	197	142	189	102	101	144
$[Bu_4N][TaBr_6]$	-	-	211	-	-	this thesis
$[Et_4N][TaBr_6]$	230	179	213	106	114	147
$Cs[TaBr_6]$	232	183	212	107	116	144
$[PPh_4][TaBr_6]$	-	-	216	-	-	105
WBr_6	209	190	220	-	-	this thesis
WBr_6	-	-	217	-	-	159
$[Bu_4N][WBr_6]$	-	-	212	-	-	this thesis

(Table 1.6 continued)

compound	ν_1	ν_2	ν_3	ν_4^b	ν_5	ref.
$[PPh_4][WBr_6]$	-	-	210	-	-	159
$[Bu_4N]_2[WBr_6]$	-	-	200	-	-	this thesis
$Cs_2[WBr_6]$	-	-	214	-	-	157
$Cs_2[WBr_6]$	-	-	210	-	-	this thesis
$[Bu_4N]_2[ReBr_6]$	-	-	209	-	-	this thesis
$K_2[ReBr_6](aq)$	213	174	217	118	104	153
$[Hep_4N]_2[ReBr_6]$	-	-	208	-	-	155
$[Bu_4N]_2[OsBr_6]$	-	-	214	-	-	this thesis
$K_2[OsBr_6]$	-	-	224	-	-	164
$[Hep_4N]_2[OsBr_6]$	-	-	211	-	-	155
$[Bu_4N]_2[IrBr_6]$	-	-	221	-	-	this thesis
$[Bu_4N]_2[IrBr_6]$	215	182	221	-	112	162
$K_2[IrBr_6]$	-	-	235	82	-	152
$K_2[IrBr_6](aq)$	209	174	-	-	97	156
$[Bu_4N]_2[PtBr_6]$	-	-	231	-	-	this thesis
$K_2[PtBr_6]$	217	195	243	78	115	151
$K_2[PtBr_6]$	217	194	243	-	-	this thesis
$K_2[PtBr_6]$	207	190	240	90	97	153

[a] 262(m), 230(vs), 225(sh) (C_i symmetry)
[b] not observed in this work as spectra were only recorded between 4000 and 180cm^{-1}

1.8 The electronic spectra of hexahalometallates

The absorption spectra of hexahalometallates in the visible and ultra-violet regions are dominated by intense absorptions due to ligand to metal charge transfer (C.T.). Figure 1.5 indicates the source of these absorptions on a molecular orbital diagram where the γ_n nomenclature is used to indicate the orbital angular momentum of an electron [8]. The charge transfer classification arises because the lower $1t_{1g}$, $2t_{1u}$, $1t_{2u}$ and $1t_{2g}$ molecular orbitals are essentially ligand in character while the upper $2t_{2g}$ M.O. is essentially a metal d orbital. Then promotion of an electron from the $\Pi(x)$ orbitals to the nd orbitals in fig.1.5 is equivalent to electron transfer from the ligands to the metal. Therefore, ligand to metal C.T. is in essence a redox process decreasing the oxidation number of the central metal ion by one.

The wave numbers of these C.T. absorptions behave qualitatively as expected for an electron transfer from the halide to the central metal ion ie. they decrease with increasing oxidizing character of the central ion and with increasing reducing character of the halide ion. It is usually found that on passing from corresponding $4d^n$ to $5d^n$ hexahalometallates in the same oxidation state, there is a shift of the absorption bands ~6-9 kK (1kK=1000cm^{-1}) to higher wavenumber, as a result of the greater electronegativity (greater oxidizing ability) of the $4d^n$ metal ions (table 1.1). Similarly, there is a general decrease across a period for a series of hexahalometallates in a given oxidation state. For trivalent and tetravalent $4d^n$ and $5d^n$ hexahalometallates, Jørgensen [8] has deduced the linear interpolation formula :-

$$\begin{pmatrix} 4d^n & : & 51-7n \\ 5d^n & : & 58-7n \end{pmatrix} + \begin{pmatrix} F & +28 \\ Cl & +0 \\ Br & -6 \\ I & -15 \end{pmatrix} + \begin{pmatrix} \text{trivalent} & [\Pi(x) \rightarrow \gamma_5] & +15 \\ \text{tetravalent} & [\Pi(x) \rightarrow \gamma_5] & +0 \\ \text{trivalent} & [\Pi(x) \rightarrow \gamma_3] & +30 \\ \text{tetravalent} & [\Pi(x) \rightarrow \gamma_3] & +20 \end{pmatrix} \quad (1.7)$$

Formula 1.7 defines the wave number in kK of the first, strong absorptions identified as transitions to $2\gamma_{5g}$ and $2\gamma_{3g}$ and is accurate to ~2kK.

Complications arise in the interpretation of C.T.spectra due to parity forbidden

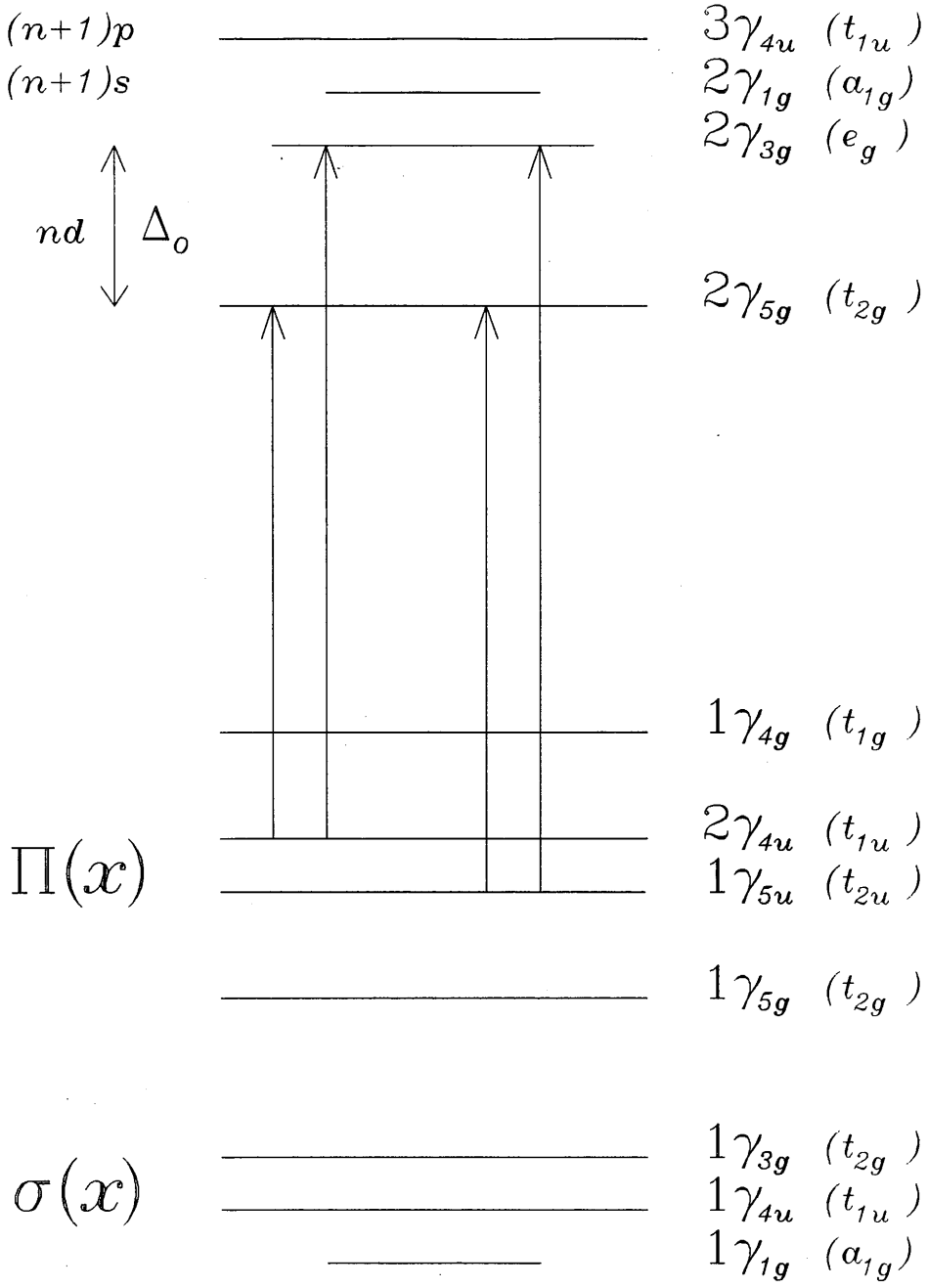

Figure 1.5: Schematic representation of parity allowed ligand to metal charge transfer transitions of hexahalometallate complexes.

C.T. transitions ($g \rightarrow g$, $u \rightarrow u$) which are normally weaker than parity allowed transitions ($g \rightarrow u$, $u \rightarrow g$). The Landé multiplet splitting factor ε_{nl} of the halides increases in the order $F^- > Cl^- > Br^- > I^-$ and is large enough for Br^- and I^- to make many more transitions resolvable. This splitting greatly increases the complexity of hexabromometallate and hexaiodometallate electronic absorption spectra. Nonetheless it can be observed experimentally, and in agreement with equation 1.7 that the energies of the first C.T. absorption $[\Pi(x) \rightarrow 2\gamma_{5g}]$ decrease in the order

$$[MF_6]^{n-} > [MCl_6]^{n-} > [MBr_6]^{n-} > [MI_6]^{n-} \tag{1.8}$$

for a given central metal ion and oxidation state. As expected, order 1.8 agrees with the change in the coulombic energies of the ligand atomic orbitals (sect. 1.5). In addition the width of the first C.T. $[\Pi(x) \rightarrow 2\gamma_{5g}]$ absorption also increases in the order of eqn.1.8 and this is thought to be due to an intrinsic change in the π-electron and metal t_{2g} orbital electron delocalisation.

Chapter 2

2.1 Electrode reactions

To understand reactions it is generally necessary to develop a conceptual scheme of the process occurring. An electron transfer at an electrode surface will generally proceed by several steps and can adopt various paths. But the path taken initially will be that one which requires the lowest overall activation energy. The model presented by Vlček [52] describing the nature of charge transfer reactions of coordination compounds is valid for most types of charge transfer reactions and occurs via seven stages [54] :-

1. The reactant is brought to the vicinity of the electrode by mass transfer.
2. A chemical reaction occurs which yields the species actually entering the inner part of the electrical double layer.
3. A structural rearrangement occurs yielding the species that takes part in the actual electron transfer reaction.
4. The electron transfer itself takes place.
5. A structural reorganization occurs leading to the immediate product of charge transfer.
6. A chemical reaction of the immediate product of charge transfer occurs which yields the species stable in solution.

7. The final product of charge transfer is removed to the bulk of the solution by mass transfer.

Direct knowledge of the charge transfer process at an electrode is limited but can be presumed to require some form of contact between reactant and electrode surface. Consequently, some form of structural rearrangement of reactant and product is necessary and can be visualized as the overlap of a molecular orbital of the redox species with an orbital of the electrode. During this transient régime, the electron transfer itself can occur and the process can be viewed as passing through a transition state in which both reactant and product are bonded by some means to the electrode surface.

The actual electron transfer step is assumed to be an extremely rapid adiabatic process by analogy to the Franck- Condon effect [53] and that the transfer occurs in a time interval significantly less than the formation of the transition state.

The following treatment of electron transfer kinetics discussed in this chapter can be found in greater detail in most electrochemistry texts and references [27], [28] and [53] were found to be particularly useful to the present author.

2.2 The electron transfer process

Consider the electrode reaction

$$O + ne \longrightarrow R \tag{2.1}$$

O = oxidant, R = reductant, n = number of electrons

Under equilibrium conditions and unit activities of O and R (a valid assumption normally given the concentrations of O and R are usually less than 10^{-2}M), then the Nernst equation gives :-

$$E_{eq} = E^o + \left(\frac{RT}{nF}\right) ln \left[\frac{C_o}{C_r}\right] \tag{2.2}$$

E_{eq} = equilibrium potential, E^o = standard electrode potential, R = gas constant, F = Faraday constant, C_o = concentration of oxidant, C_r = concentration of reductant.

The equilibrium potential E_{eq} refers to a situation of dynamic equilibrium between oxidized and reduced forms at the electrode surface which must be established rapidly in order to satisfy the conditions of thermodynamic reversibility. During an electrochemical experiment under reversible conditions, the applied cell potential E corresponds to E_{eq} and it can be easily deduced that when the concentrations C_o and C_r are equal then the applied cell potential E equals E^o. Because the cell is at equilibrium no net current flows, but if the applied cell potential E is altered then the surface concentrations of O and R, namely C_o^σ and C_r^σ, must change in order to satisfy the Nernst equilibrium conditions. This will cause a current to flow through the electrode-solution interface which is dependent on the equilibrium thermodynamics and the rate of electron transfer.

When a current passes through an electrode, the electrode adopts a different potential from the equilibrium value it would have in the absence of a current. This 'electrode polarization' phenomenon can be defined in terms of the overpotential η. This is equivalent to the electrode potential E minus the equilibrium potential E_{eq} ie :-

$$\eta = E - E_{eq} \tag{2.3}$$

At a dynamic equilibrium the rates of the forward and backward reactions are equal, therefore there is no overall chemical change and so no net current will flow.

$$\begin{aligned} k_f &= k_b \\ -I_f &= I_b = I_o \end{aligned} \tag{2.4}$$

k = rate constant, I = partial current density, I_o = exchange current density (the negative sign reflects the convention that a cathodic current i_c (ie: a reduction) is negative and an anodic current i_a (ie: an oxidation) is positive.)

At any given potential E, the current density is given by

$$I = I_f + I_b \tag{2.5}$$

Each partial current density will be dependent on the concentration of electroactive species at the electrode surface and the rate of electron transfer [27]

$$I_f = -nFk_fC_o^\sigma \quad \text{and} \quad I_b = nFk_bC_r^\sigma \tag{2.6}$$

However, the kinetic behaviour of an electroactive species is also strongly affected by the interfacial potential difference. By application of transition state or electrochemical potential arguments [28] the variation of the rate of heterogeneous charge transfer with potential is given by

$$k_f = k^o \exp\left[\frac{-\alpha nF(E-E^o)}{RT}\right] \quad \text{and } k_b = k^o \exp\left[\frac{(1-\alpha)nF(E-E^o)}{RT}\right] \tag{2.7}$$

where k^o = standard rate constant of heterogeneous electron transfer and α and $(1-\alpha)$ are the transfer coefficients for the cathodic and anodic reactions respectively.

Assuming $C_o^\sigma \simeq C_o$ under the conditions where a very small current flows then from equations 2.4, 2.6 and 2.7

$$\begin{aligned} I_o &= nFC_ok^o \exp\left[\frac{-\alpha nF(E-E^o)}{RT}\right] \\ &= nFC_rk^o \exp\left[\frac{(1-\alpha)nF(E-E^o)}{RT}\right] \end{aligned} \tag{2.8}$$

Substituting for $E - E^o$ from the Nernst equation 2.2

$$I_o = nFC_o k^o \exp\left[\frac{-\alpha nF}{RT} \cdot \frac{RT}{nF} \ln\left(\frac{C_o}{C_r}\right)\right]$$

$$= nFC_o k^o \left(\frac{C_o}{C_r}\right)^{-\alpha}$$

$$= nFk^o C_o^{(1-\alpha)} C_r^{\alpha} \tag{2.9}$$

From $I = I_f + I_b$

$$I_o = nFk^o \left[C_r \exp\left[\frac{(1-\alpha)nF(E-E^o)}{RT}\right] - C_o \exp\left[\frac{-\alpha nF(E-E^o)}{RT}\right]\right] \tag{2.10}$$

by substituting for k^o from equation 2.8 and $E - E^o$ from 2.2 and 2.3 then

$$E - E^o = \eta + \left(\frac{RT}{nF}\right) \ln\left(\frac{C_o}{C_r}\right) \quad \text{and}$$

$$I = I_o \left[\exp\left[\frac{(1-\alpha)nF}{RT}\eta\right] - \exp\left[\frac{-\alpha nF}{RT}\eta\right]\right] \tag{2.11}$$

Equations 2.10 and 2.11 are different forms of the Butler- Volmer equation,a fundamental equation of electrode kinetics which describes how the current density varies with the exchange current density, overpotential and transfer coefficients.

With a high positive overpotential, $|I_b| \gg |I_f|$, the anodic current density approximates to the form

$$\log I = \log I_o + \frac{(1-\alpha)nF}{2.3RT}\eta \tag{2.12}$$

and similarly with a high negative overpotential where $|I_f| \gg |I_b|$ the cathodic current density approximates to

$$\log I = \log I_o - \frac{\alpha n F}{2.3RT}\eta \tag{2.13}$$

If the overpotential is small ($\eta < RT/nF$) then by expanding the exponential functions and neglecting all the terms in the series except the first two, we obtain

$$I = I_o \frac{nF}{RT}\eta \tag{2.14}$$

The two limiting forms of the Butler-Volmer equation are called the Tafel equations and can be used to determine I_o and α at high over potentials.

2.3 Electron transfer kinetics

The kinetics of electrochemical reactions can be divided into three main categories depending on the magnitude of the rate constant of electron transfer k^o.

a) Reversible case : $k^o > 10^{-1}\text{cms}^{-1}$

The rate of heterogeneous charge transfer is so fast that a dynamic equilibrium is established at the electrode interface and the Butler-Volmer equation (2.10) can ultimately be reduced to the Nernst equation (2.2). The current does not have a kinetic dependence and is determined solely by the charge flux at the electrode ie: by mass transport. The current is effectively diffusion controlled because all reactant (in our case the oxidant O in equation 2.1) is immediately consumed upon reaching the electrode surface.

b) Irreversible case : $k^o < 10^{-5}\text{cms}^{-1}$

The rate of heterogeneous charge transfer is extremely slow and being the slowest step has the greatest influence on the current ie. charge transfer control where the concentrations of O and R will be far removed from thermodynamic equilibrium. Consequently the Nernst equation and any comparisons of electrochemical potentials with thermodynamic equilibrium potentials do not apply. Substantial overpotentials may be necessary to achieve a significant rate of charge transfer.

c) Quasi-reversible case : $10^{-1} > k^{o} > 10^{-5}\text{cms}^{-1}$

Both the rate of charge transfer and of mass transport contribute to the current and the Nernst equation is only approximately valid.

2.4 The mass-transport process

As well as the rate of charge transfer, the current-potential profile of an electron transfer reaction is also dependent on mass-transport which in an electrochemical system can be described by three processes, diffusion, convection and electrophoretic migration. The latter two can be neglected if the experimental solution is quiescent and the dependence of the current density on diffusional mass transport can be described by Ficks' second law

$$\frac{\partial c_i}{\partial t} = D_i \frac{\partial^2 c_i}{\partial x^2} \tag{2.15}$$

D_i = diffusion coefficient of species i

Solving for spherical diffusion to the electrode under the appropriate boundary conditions produces a current-time profile described by

$$|I| = nFDC_o \left[\frac{1}{(\pi Dt)^{\frac{1}{2}}} + \frac{1}{r} \right] \tag{2.16}$$

where r is the electrode radius.

It can be shown that at a microelectrode, consisting of a flat disc of a few hundred micrometers radius, a diffusion field of this type exists. The time dependent term in equation 2.16 predominates at shorter time scales but at longer time scales, the current reaches a limiting value defining the steady state contribution to the diffusional current :-

$$|I| = \frac{nFDC_o}{r} \tag{2.17}$$

This is the reason why the current at a spherical or microelectrode as in the present work remains finite whereas at larger electrodes the current approaches zero.

2.5 Cyclic voltammetry

From the previous two sections we observed that the current-potential ($I-E$) response is dependent on both the rate of heterogeneous charge transfer and mass transport. All $I-E$ responses are dependent on these two quantities and expressions describing the behaviour of systems can be derived by combining the two principal equations in an appropriate manner. However, in the present work we are not primarily concerned with a rigorous mathematical treatment. The qualitative effects of charge transfer, mass transport, sweep rate, temperature etc. can be readily observed on a cyclic voltammogram (the plotted $I-E$ response). Cyclic voltammetry (C.V) using both the A.C. and D.C. modes was used exclusively in this thesis to determine the redox potentials of transition metal hexahalometallates.

In order to determine the D.C. current-potential response, a linear voltage ramp is generated between potentials E_1 and E_2 and the current recorded. By applying a triangular waveform the potential can be cycled back and forth between E_1 and E_2 with the time duration for one cycle varying with the sweep rate ν ($Vsec^{-1}$).

Scan rates generally range from a few $mVsec^{-1}$ up to a few hundred $Vsec^{-1}$. Conventional chart recorders produce distorted responses above approximately 500 $mVsec^{-1}$ and oscilloscopes or computerised recording devices must then be utilized.

As an alternative, if a relatively high frequency alternating potential is superimposed on the slowly varying ramped potential, then a sinusoidal response in the current can be detected and this forms the basis of A.C. cyclic voltammetry.

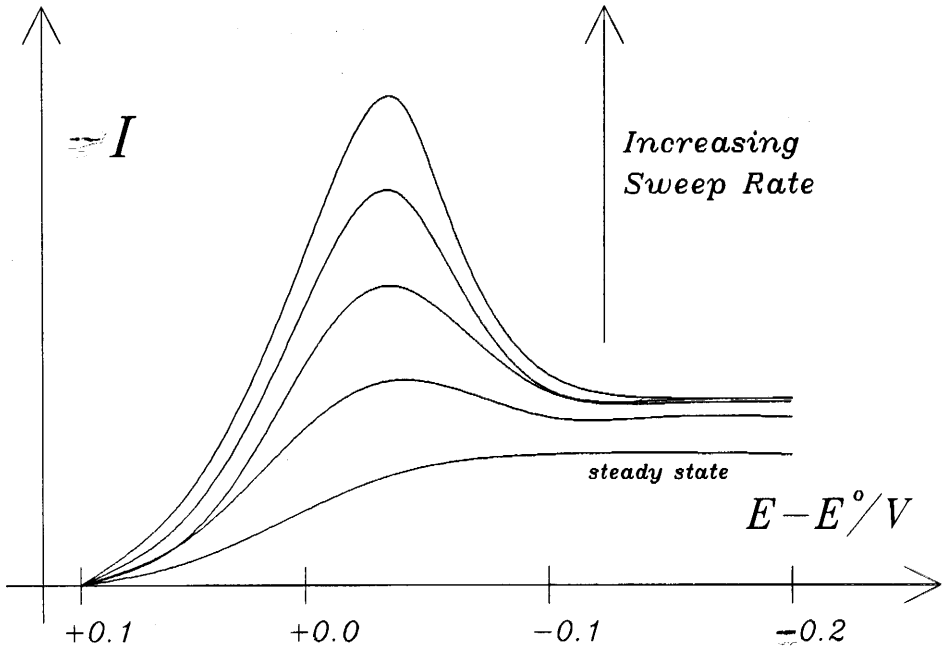

Figure 2.1: Current-potential response at several sweep rates for the reaction $O + e \longrightarrow R$.

2.6 The D.C. experiment

For the reduction process, equation 2.1, $O+ne \longrightarrow R$, if a very slow scan rate is used, steady state conditions (for a reversible reaction) are maintained. The concentration ratio C_o^σ/C_r^σ for a reversible reaction is given by the Nernst equation, and as the potential becomes more negative the ratio must alter to satisfy the Nernst conditions. In other words, the concentration of O at the surface must decrease. This will produce a concentration gradient in the region close to the electrode surface known as the Nernst diffusion layer and a small current will flow. As more and more O is reduced, the concentration gradient and the current increases until $C_o^\sigma \simeq 0$ and the current has reached the diffusion limiting or plateau current value (fig. 2.1).

With faster sweep rates, a steeper concentration gradient is developed and a larger current flows, which is proportional to the gradient. At the same time, relaxation processes of diffusion and convection attempt to reverse the slope of the gradient. However, as the potential is scanning more and more negatively the concentration of

O at the surface becomes increasingly depleted until it is effectively zero. At this point the concentration gradient begins to decrease due to relaxation and consequently the current decreases. The faster the sweep rate, the steeper the concentration gradient and the greater the current will flow in the external circuit since relaxation has less time to take effect.

When the potential sweep is reversed, the exactly analogous process of $R \longrightarrow O + ne$ occurs and a peaked current-potential response is obtained with the opposite sign. Therefore combining the forward and backward reactions, the overall C.V. trace of the typical one electron reversible reaction 2.1 (n=1) appears similar to figure 2.2.

However, for the cases of quasi-reversible and irreversible processes, the $I - E$ response is modified compared with figure 2.2. By assigning various experimental parameters in their calculations to reasonable values, Nicholson and Shain [30] were able to compute normalised current functions for different rates of charge transfer which resemble $I - E$ traces observed experimentally. The examples shown in figure 2.3 clearly indicate that there are marked differences between the $I - E$ responses of reversible, quasi-reversible and irreversible charge transfer processes. When passing from a reversible through to an irreversible process, a) to c) in fig. 2.3, the overpotential necessary to produce a significant current becomes increasingly large. For a totally irreversible process c), the rate of charge transfer for the return reaction is so small that no return wave can be observed.

Generally, to obtain thermodynamic information from voltammetric experiments, expressions for the current derived by solving Ficks' second law for the appropriate boundary conditions, are matched with the experimental observations. However, for some general results such as whether or not the electron transfer is reversible, the information can be obtained more quickly merely by studying the peak potentials and peak currents on a conventional cyclic voltammogram.

Thus for reversible and quasi-reversible charge transfer reactions without a coupled chemical reaction and irrespective of sweep rate

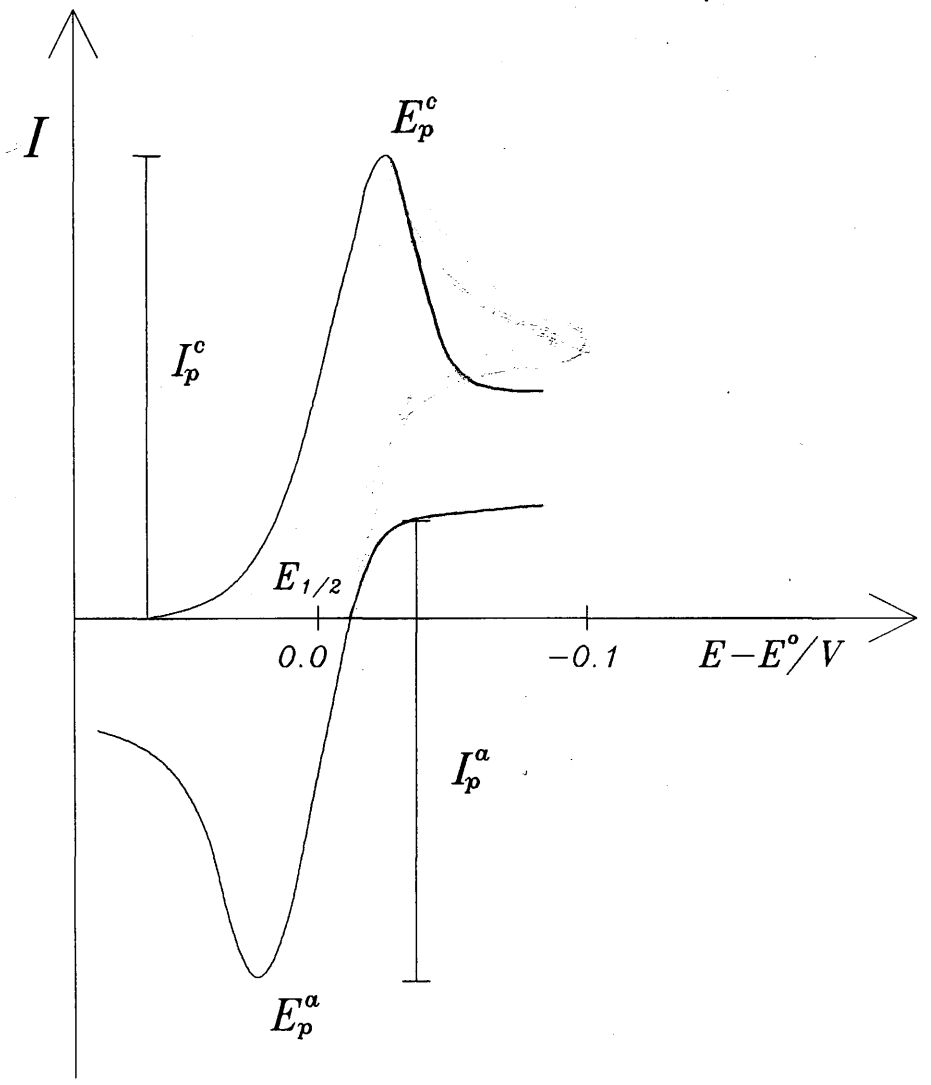

Figure 2.2: C.V. trace for the reversible reaction $O + e \longrightarrow R$.
Initially only O present, E_p^a = anodic peak potential, E_p^c = cathodic peak potential, I_p^a = anodic peak current, I_p^c = cathodic peak current, $E_{1/2}$ = half wave potential

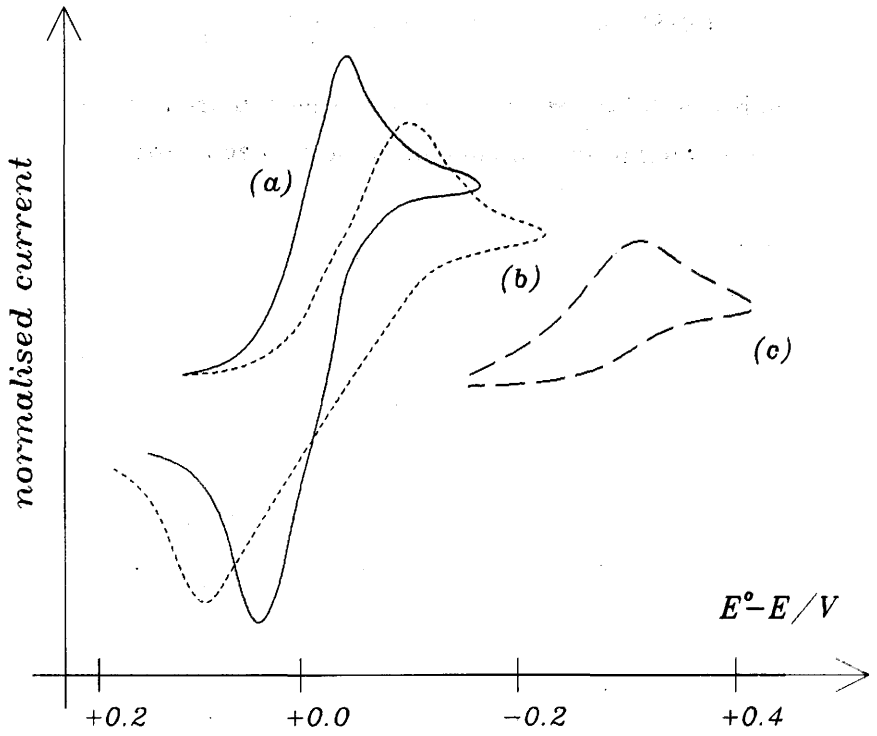

Figure 2.3: Cyclic voltammograms for a) reversible b) quasi-reversible and c) irreversible charge transfer.

$$\frac{I_p^a}{I_p^c} = 1.0 \tag{2.18}$$

The relationship 2.18 is invalid for an irreversible charge transfer. Under Nernstian conditions ie: a reversible (fast) electron transfer, the peak potential separation $|E_p^a - E_p^c|$ or ΔE_p is given by :-

$$\Delta E_p = 2.3\frac{RT}{nF} = \frac{59}{n} \quad mV \qquad \text{(at 298K)} \tag{2.19}$$

The peak potential separation is somewhat more useful as a diagnostic than the ratio of the peak currents as it is often difficult to determine the precise values of I_p^a and I_p^c. In the case of quasi-reversible electron transfer, the separation ΔE_p is greater than $59/n$ mV and for irreversible processes ΔE_p is very large if in fact the return wave can be observed at all.

2.7 The effect of varying the sweep rate

For a reversible process, the value of $|E_p^a - E_p^c|$ will remain constant at $59/n$ mV irrespective of the sweep rate since the rate of charge transfer is always great enough to maintain Nernstian equilibrium at the electrode surface. And similarly, for an irreversible process, $| E_p^a - E_p^c |$ will always be much greater than $59/n$ mV at normal experimental sweep rates of 100-200 $mVsec^{-1}$.

However, at low potential sweep rates of the order of 10 $mVsec^{-1}$ or less, the rate of electron transfer of an irreversible process can be greater than that of mass transport, and a seemingly reversible cyclic voltammogram is recorded. As the sweep rate is increased the rate of mass transport becomes comparable to that of electron transfer and a region seemingly of quasi-reversibility is reached. The most noticeable effect of this, apart from increased peak currents due to steeper concentration gradients, is an increased peak potential separation. At still higher sweep rates the separation ΔE_p becomes even larger indicating an irreversible electron transfer process. Therefore, the maintenance of $\Delta E_p = 59/n$ mV regardless of the sweep rate is another useful

criterion for determining whether an electrochemical reaction is reversible or not. However, one must not immediately interpret a large ΔE_p as evidence for quasi-reversibility or irreversibility, because the effect of an uncompensated IR drop on a reversible couple also results in a peak potential separation greater than $59/n$ mV.

2.8 The A.C. experiment

As already noted in section 2.5, the integral features of an A.C. voltammetric experiment are a slowly and linearly varying mean voltage $E_{D.C.}$ plus superimposed on this a rapidly varying sinusoidal component $E_{A.C.}$ with a peak to peak amplitude of perhaps 5 mV. The measured responses are the magnitude of the A.C. current at the frequency of $E_{A.C.}$ and its phase angle with respect to $E_{A.C.}$ which is equivalent to measuring the impedance. Then, the mean surface concentrations enforced by $E_{D.C.}$ are equivalent to the effective bulk values for the A.C. perturbation. In order that an A.C. current can be detected, both the oxidized and reduced forms must be present at the electrode in the timescale of the perturbation. Hence, for a totally irreversible electrochemical reaction, the rate of charge transfer will be too slow to observe any response. In the case of a simple reversible reaction 2.1, the A.C. response appears as a single symmetrical peak centred at E_p (see for example fig 3.2.1).

One of the obvious advantages of an A.C. response is that E_p and consequently $E_{1/2}$ ($E_p \equiv E_{1/2}$ in A.C. voltammetry) can be more easily determined than for a D.C. experiment.

For a fully reversible process, the A.C. return wave superimposes on the forward wave and, as with D.C. cyclic voltammetry

$$\frac{I_f}{I_r} = 1.0 \tag{2.20}$$

If a process is not reversible, then two separate peaks are usually distinguishable because the forward and return waves occur at slightly different $E_{1/2}$ potentials and the return wave has a smaller peak current. This provides a useful visual indication of

reversibility but it can be derived that another prerequisite for reversibility is that the peak width at half the peak current should be equivalent to $90/n$ mV in the absence of any ohmic drop.

2.9 The stirred voltammetry method

Conventional polarographic analysis involves the oxidation or reduction of compounds at an electrode consisting of mercury falling dropwise from a fine bore capillary glass tube. This resembles the stirred voltammetry method since in both methods the limiting current flow is not determined by the diffusional mass transport of the electroactive species as in cyclic voltammetry, but by the diffusion coefficient of the electroactive species in the stirred and therefore homogeneous solution. Low sweep rates are used as the currents are much larger and differentiation between oxidation and reduction processes is discernible from the sign of the current. In this thesis, stirred voltammetry was used principally for this reason but this method can also be used to determine the number of electrons transferred in one electrochemical step. For instance, if a solution of known concentration is oxidized or reduced with constant stirring, then by recording the constant current produced, and the time taken for complete reaction, the total number of electrons transferred can be calculated.

2.10 More complex electrochemical reactions

So far we have only considered the simple one electron process $O + e \rightleftharpoons R$. However, there are many other reaction types which can be investigated electrochemically although it is not within the scope of this thesis to discuss them all so we shall confine ourselves here to a discussion of those which were relevant to this work.

2.11 Coupled chemical reactions

In the language of electrochemists the simple electron transfer reaction 2.1 would be termed an E mechanism, with E standing for electron transfer. Such reactions involve either an oxidation or a reduction in which both O and R remain stable over the lifetime of the experiment eg.

$$[TaBr_6]^{1-} + e \rightleftharpoons [TaBr_6]^{2-} \tag{2.21}$$

$$[Fe(C_5H_5)_2]^0 \rightleftharpoons [Fe(C_5H_5)_2]^{1+} + e \tag{2.22}$$

However, an electron transfer process can also be coupled to one or more chemical steps and indeed to other electron transfer steps. The simplest of these is electron transfer followed by an irreversible chemical reaction as with :-

$$\begin{aligned} &(Estep) \qquad O \rightleftharpoons R \\ &(Cstep) \qquad R \xrightarrow{k} X \end{aligned} \tag{2.23}$$

the cyclic voltammogram of the EC reaction is very much dependent on the sweep rate and the chemical reaction rate constant k . The observation of an anodic return wave requires either a fast sweep rate, a slow reaction rate or both. An example of an EC mechanism is the oxidation of p-aminophenol [50] at a platinum electrode in aqueous acidic solutions. The quinoneimine formed undergoes a hydrolysis reaction to form benzoquinone :-

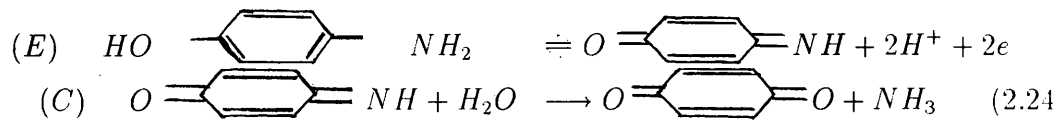

(2.24)

More complex mechanisms such as ECE and $ECCEE$ etc. are possible. The reduction of hexabromoplatinate(IV) at a platinum electrode in methylene chloride

(chapter 3) occurs via a complex mechanism (2.25), but exactly which mechanism is not known.

$$[PtBr_6]^{2-} \longrightarrow \text{`}[PtBr_6]^{3-}\text{'} \longrightarrow [PtBr_4]^{2-} + 2Br^- \qquad (2.25)$$

Often the effects of a following reaction can be diminished by cooling the experimental solution. Such was the case with bis(tetra-n-butylammonium)hexabromorhenate(IV) which underwent an irreversible reduction in methylene chloride at 298 K. When the solution was cooled to 223 K, the previously irreversible reduction exhibited quasi-reversible behaviour indicating that the effect of a following reaction had been greatly diminished. A number of the transition metal hexabromometallates discussed in this thesis exhibited a similar behaviour and are discussed more fully in chapter 3.

The effects of following reactions on a C.V. trace can also be explored by the use of very fast sweep rates. If the chemical reaction is fast, then R is rapidly removed from the region near the electrode and no return C.V. wave can be observed at low sweep rate. But by decreasing the timescale of the experiment using a fast sweep rate it is sometimes possible to observe a return wave, corresponding to oxidation of R, before the following chemical reaction can occur.

Finally, if the primary electron transfer, for example a reduction, is followed by a slow chemical reaction then sometimes a small secondary couple near to the original redox couple can be observed. If, by holding the potential stationary for a given length of time at a point subsequent to the reduction, the size of the secondary couple is increased then the secondary couple is shown to be dependent on the primary reduction and is identified as an electroactive 'daughter' product of the initial species.

2.12 Adsorption

Thus far, the systems discussed have been confined to electrode-solution interfaces where an excess of ions with opposite charges to that of the electrode are found

and where only long range electrostatic forces are operational. These ions are non-specifically adsorbed species (sometimes referred to here as dissolved) with the locus of their centres at a distance from the electrode know as the outer Helmholz plane . It is also possible for anions to become specifically adsorbed at the electrode surface where they are identified by short-range strong interactions. The locii of specifically adsorbed ions make up the inner Helmholz plane. Specific adsorption, unlike non-specific adsorption, is dependent on the chemical properties of both the ions and the electrode, and can have significant effects on the voltammetric response:

To describe simple electrochemical adsorption, the Langmuir isotherm borrowed from classical surface chemistry was found to be appropriate [32]. However, rather than calculating adsorption energies specifically, which except for the simplest systems is a difficult task, experimentalists are generally more concerned with identifying systems where adsorption occurs. In this respect D.C. cyclic voltammetry provides an excellent tool for this purpose because with a little previous knowledge, different types of adsorption systems can be quickly recognized. The following discussion concerns reaction 2.1, $O + e \rightleftharpoons R$.

2.12.1 O and R strongly adsorbed

For a case where adsorbed O and R are the only electroactive species (within the relevant potential range) then the cyclic voltammogram for a reversible reaction will look something like figure 2.4.

The symmetric appearance of the cyclic voltammogram arises because only the fixed amount of O adsorbed on the electrode is reduced, so there is no distortion by mass transport. When both O and R are specifically adsorbed, then O_{ads} is easier to reduce than dissolved O to R_{ads}, and R_{ads} is easier to oxidize than dissolved R to O_{ads}. The coincidence of the peak potentials for the oxidation and reduction processes depends on large and equivalent free energies of adsorption for O and R, reversibility of electron transfer, and adherence to a Langmuir isotherm. This is not an unlikely situation, but normally one encounters complications due to non-Nernstian behaviour distorting the symmetry of the waves and more commonly, the involvement of waves

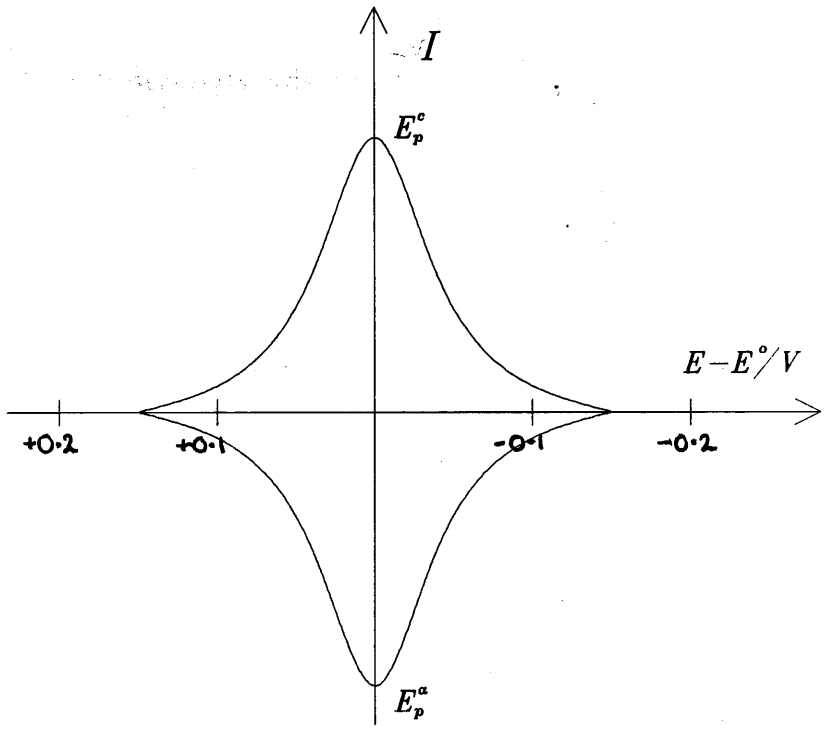

Figure 2.4: Cyclic voltammogram for the reversible reaction $O_{ads} + e \longrightarrow R_{ads}$.

due to non-specifically adsorbed species.

There are several different possibilities in this respect depending on whether both dissolved and adsorbed species are electroactive, whether O, R or both are specifically adsorbed, whether this adsorption is strong or weak and whether the electron transfer is reversible. However, for simplification we shall only describe the case for strong and weak product (R) adsorption where both adsorbed and dissolved species are reversibly electroactive and then draw some analogies about the others.

2.12.2 Product R strongly adsorbed

The C.V. of the reversible reaction

$$O + e \rightleftharpoons R_{ads} \tag{2.26}$$

resembles figure 2.5. The distinctive feature of the C.V. is an adsorption pre-wave with the same symmetric shape as figure 2.4. The reason this appears at a more positive potential than the dissolved wave is that the adsorption energy of R makes the reduction of O to adsorbed R easier than reduction to dissolved R. The difference between adsorbed and dissolved potentials is related to the magnitude of the free energy of adsorption and the bulk concentration of O.

The size of the pre-wave peak current is limited by the surface coverage possible and to a large extent the dissolved wave resembles that which would have existed if no adsorption had occurred. In the event of non-Nernstian behaviour, the peaks would all show deviations from this until, for an irreversible reaction no return waves would be exhibited.

In the event of only strong reactant (O) adsorption, a post-wave would be observed at a more negative potential. The reasoning is that it is then more difficult to reduce adsorbed O to R than reduce dissolved O to R.

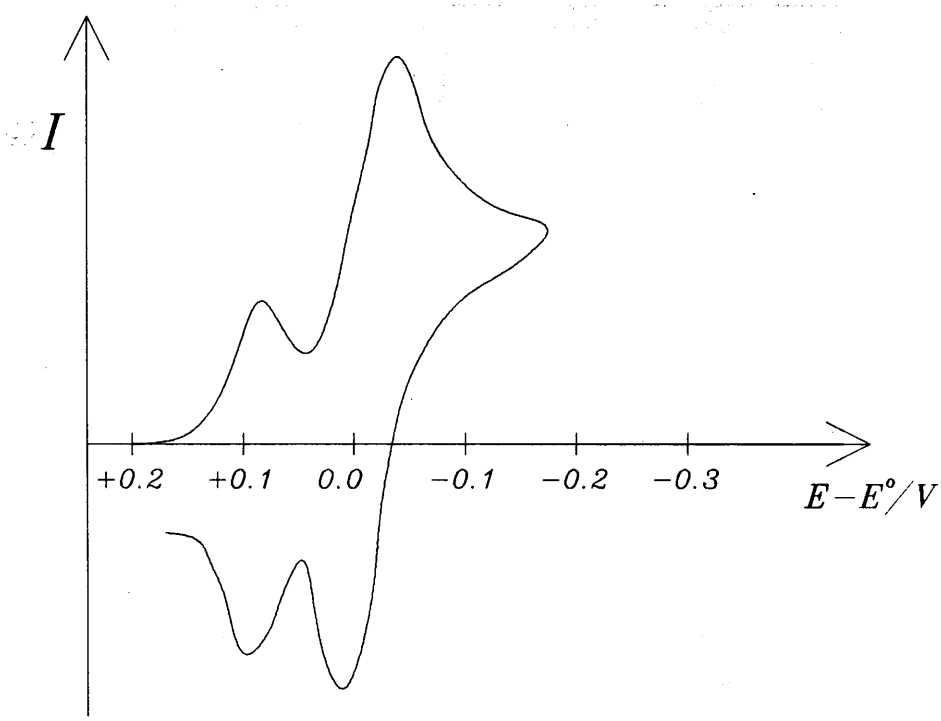

Figure 2.5: Cyclic voltammogram for the reversible reduction $O + e \longrightarrow R_{ads(strongly)}$

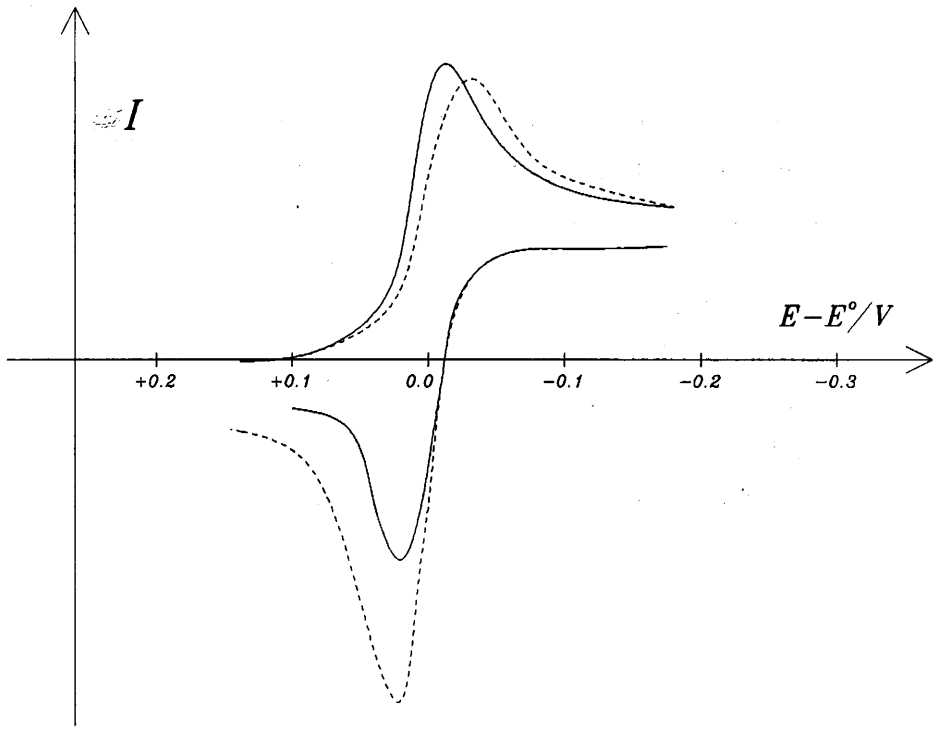

Figure 2.6: Cyclic voltammogram for the reversible reduction $O + e \longrightarrow R$ (solid) no adsorption, (dotted) weak adsorption of product.

2.12.3 Product R weakly adsorbed

When adsorption is weak the difference in energies for reduction of adsorbed and dissolved O is small, and a separate pre-wave is not observed. When R is weakly adsorbed, the forward cathodic current is only slightly altered but on reversal there is a contribution of adsorbed R as well as dissolved R to the anodic current (figure 2.6). The size of the anodic current increases with the sweep rate ν and is dependent on the switching potential E_λ. The effect of diffusion of adsorbed R away from the electrode becomes more accentuated as $\mid E^o - E_\lambda \mid$ increases and the anodic peak current will tend toward the diffusion current. In addition, the cathodic peak potential moves to slightly more positive potential with increasing sweep rate.

2.13 Instrumentation

When measuring the potential of an electrode versus a reference electrode, the voltage drop across the electrolyte solution, the IR_s drop, must be considered. This problem is compounded when using electrolyte solutions of high resistivity, a difficulty which is especially associated with aprotic solvents. To reduce the errors, the cell current and internal cell resistance must be kept as small as possible so that the reference electrode maintains a constant potential even if a small current passes through its surface. In order to minimise these difficulties a three electrode configuration is operated with which the current is passed between the working electrode and a third counter electrode. For this to work effectively, the area of the counter electrode should be much larger than that of the working electrode to prevent polarisation of the former. This was incorporated into the cell design by using a small micro-platinum working electrode consisting of three 500μm diameter platinum wires encased together in glass such that only the wire cross-sections were exposed, an area of approximately $6\text{x}10^{-7}\text{m}^2$.

The role of the reference electrode is to maintain a fixed invariable potential against which changes in the potential at the working electrode are monitored. By detecting the p.d. between the working and reference electrodes using a high input impedance device, an electrometer, the reference electrode draws a negligible current and its potential will remain constant. However, a good reference electrode should maintain a constant potential even if a few micro-amperes pass through it. Those reference electrodes most commonly used include the saturated calomel electrode (S.C.E.) and silver- silver halide electrodes. However, these external referencing methods are impossible to employ under anhydrous conditions in a vacuum apparatus as used in this work. Therefore an internal reference was used which is a compound whose reversible electrochemical behaviour has a fixed potential independent of the solvent, or a compound whose redox potentials are known versus an external reference in the solvent employed.

The prerequisites of an internal standard are :-

1. The electrochemical behaviour of the reference compound should not interfere with or mask the redox behaviour of the compound under investigation.

2. There should be no interaction between the reference compound and the compound under investigation.

In this thesis the ferrocene/ferricinium couple, $[FeCp_2]/[FeCp_2]^+$, was used as the internal standard, with previous referencing versus S.C.E. in methylene chloride, unless stated otherwise.

In respect of criterion 1) ferrocene proved excellent and no evidence for a specific interaction according to 2) was observed except in the presence of excess free bromine when the ferrocene/ferricinium couple was unresolvable.

In order to reference the redox potentials of a compound versus $[FeCp_2]/[FeCp_2]^+$, the voltammetric response is initially measured referred to the platinum-wire reference electrode inside the cell. When connected to an electrometer, a platinum wire will function satisfactorily as a quasi-reference electrode in solutions of high resistance [51], maintaining a moderately constant potential. For precise referencing, ferrocene is then added to the solution and subject to the satisfaction of criteria 1) and 2) above, the redox potentials of the compound under observation can then be compared with $[FeCp_2]/[FeCp_2]^+$.

Ideally, an $[MBr_6]^{n-}$ compound synthesized in this work would have made a suitable reference compound. Unfortunately the compounds synthesized were on the whole too unstable when oxidized to merit use. Unfortunately, the reference compound $[IrCl_6]^{2-}$ used by Klaus Moock [31] in his study of transition metal hexachlorometallates proved unsuitable because $[IrCl_6]^{2-}$ interacted with the hexabromometallates, probably becoming involved in halogen exchange.

All electrode potentials in this work are given in respect of the S.C.E. except those experiments where a Ag-0.1M $AgNO_3$(in CH_3CN) external reference electrode was used (chapter 4). Comparisons with electrochemical data obtained in aqueous solutions are based on the relation of the Standard Hydrogen Electrode (S.H.E.) to the S.C.E., which has been given as H_2/H^+ $E_{1/2}$ = -0.25V (vs. S.C.E.) in H_2O [33].

Table 2.1 shows the different reference systems in methylene chloride.

Table 2.1: The reference system in methylene chloride.

potential	reference
+0.48V	$[FeCp_2]/[FeCp_2]^+$
+0.38V[a]	Ag/Ag^+
0.00V	S.C.E.
-0.25V[b]	S.H.E.

[a] Ag-0.1M$AgNO_3$ (in CH_3CN) [b] potential measured in H_2O

The electrochemical cell apparatus used in this thesis, and the requirements of electrochemical solvents and background electrolytes are discussed under experimental procedures in chapter 6.

Chapter 3

3.1 Introduction

In this chapter the electrode potentials in methylene chloride of the second and third row transition metal hexabromometallates with the general formula $[Bu_4N]_n[MBr_6]$, (n=0,1,2 etc.), [M= Hf,Zr,Nb,Ta,Mo,W,Re,Ru,Os,Ir,Pt] are described. The electrode potentials presented are assumed to derive from addition or removal of an electron from the highest filled metal *d* orbitals. During the experiments it became apparent that almost all the compounds studied unexpectedly exhibited complicated electrochemical activity at potentials more positive than the relevant $[MBr_6]^{1-/2-}$ redox couple. This behaviour was initially attributed to a decomposition reaction and so therefore the electrochemistry of $[Bu_4N]Br$ alone in methylene chloride was also investigated because bromide or bromine were probable products of such a decomposition. The electrochemistry of $[Bu_4N]Br$ is described in Chapter 4 along with the chloride and iodide systems for comparison.

It should be noted that a limitation of the vacuum electrochemical cell used in these experiments (chapter 6), was that the solution temperature could only be measured approximately (ca.$\pm 5^o$). The nature of the electron transfer step of individual redox couples, as discussed in sections 2.3 and 2.6, is indicated by the labels reversible, quasi-reversible and irreversible. To differentiate an electrochemically irreversible couple (with large ΔE_p) from an electron transfer step which is followed by an irreversible chemical reaction (which has no return C.V. wave), the latter electron

transfer reaction is referred to as chemically irreversible.

All potentials were referred to the S.C.E. by using ferrocene as an internal standard (the procedure was described in chapter 2). Wherever possible, the electrode potentials obtained in this thesis have been compared with those obtained by previous workers using the re-referencing scheme in table 2.1.

3.2 The cyclic voltammetric study of bis tetra-n-butylammonium hexabromozirconate(IV) and bis tetra-n-butylammonium hexabromohafnate(IV)

3.2.1 Bis tetra-n-butylammonium hexabromozirconate(IV)

White $[Bu_4N]_2[ZrBr_6]$ has the electron configuration $4d^0$ and can therefore only undergo reduction. The reduction $[ZrBr_6]^{2-/3-}$, $4d^{0/1}$, was observed at $E_{1/2}$ = -1.82V (vs. S.C.E.) at -40°C in both the A.C. and D.C. modes. The reduction was quasi-reversible in both modes at -40°C, but when the solution was allowed to warm to room temperature the couple could not be detected and was also undetectable when the solution was re-cooled.

In fact, if the solution was not immediately cooled once the compound had been added to the solvent-electrolyte mixture (see experimental procedures chapter 6) then decomposition of the hexabromozirconate(IV) salt with what appeared to be the expulsion of bromide/bromine occurred. The presence of free bromide/bromine (see chapter 4) was suggested by a complex set of anodic waves centered around +0.9V (vs. S.C.E.). As the $[ZrBr_6]^{2-}$ complex was prepared in CH_2Cl_2 and characterized in CH_2Cl_2 solution without decomposition (chapter 6), it seems most likely that the $[ZrBr_6]^{2-}$ anion was hydrolysed by traces of moisture in the electrolyte, a reaction which was suppressed by immediately cooling the solution.

The reduction potential of $[ZrBr_6]^{2-/3-}$ at $E_{1/2}$ = -1.82V (vs. S.C.E.) indicates that $[ZrBr_6]^{3-}$ is a strong reducing agent. There are no electrochemical data for

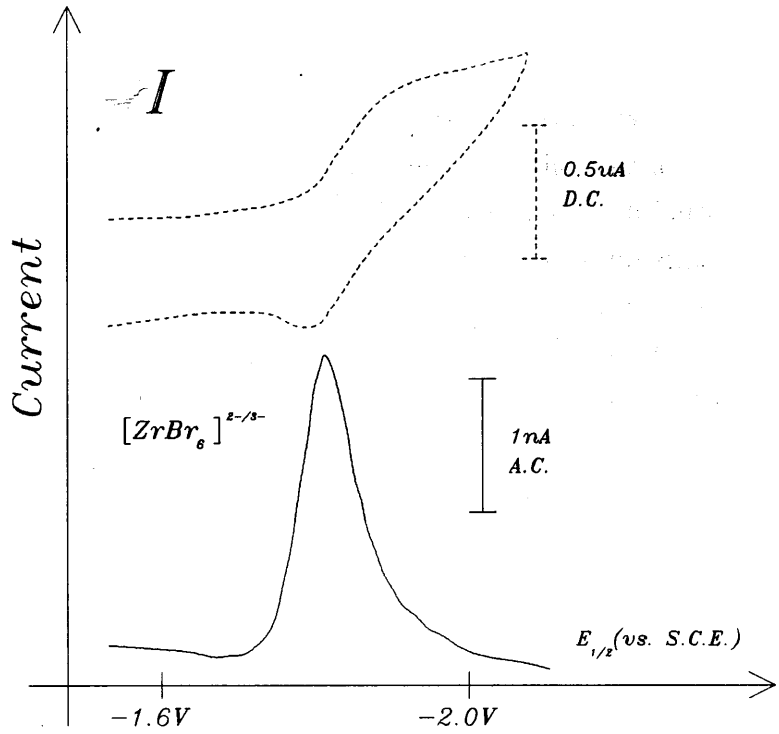

Figure 3.1: D.C. and A.C. cyclic voltammograms of $[Bu_4N]_2[ZrBr_6]$.
conditions: $[Bu_4N]PF_6$ (0.3M)/$[ZrBr_6]^{1-}$ (~0.005M) at micro-Pt electrode in CH_2Cl_2, temperature:-40°C, reference: ferrocene, sweep rate: 100mV/sec (D.C.), 20mV/sec (A.C.).

$[ZrBr_6]^{n-}$ complexes reported in the literature or any reference to a $[ZrBr_6]^{3-}$ compound. In fact the difficulties in obtaining any zirconium complex with an oxidation state less than four are well known [100], and so it is unsurprising that the $[ZrBr_6]^{2-/3-}$ couple is only quasi-reversible at -40°C.

Figure 3.1 shows the A.C. and D.C. cyclic voltammograms for the reduction :-

$$[ZrBr_6]^{2-} + e \rightleftharpoons [ZrBr_6]^{3-} \qquad , E_{1/2} = \text{-1.82V (vs. S.C.E.)} \qquad (3.1)$$

3.2.2 Bis(tetra-n-butylammonium hexabromohafnate(IV)

Analogously to the zirconium complex, white $[Bu_4N]_2[HfBr_6]$ reacted with the solvent-electrolyte medium at room temperature. Even when the reaction solution was immediately cooled to -40°C with a carbon dioxide-acetone slush bath, a large, broad anodic wave reminiscent of free bromide was observed at approximately +1.2V (vs. S.C.E.) in the D.C. and A.C. modes, indicating a decomposition had occurred. In the A.C. mode at -40°C a very small broad peak at $E_{1/2}$ = -1.90V (vs. S.C.E.) was also observed but was undetectable after the solution was allowed to warm to room temperature.

Chapter 5 discusses how various trends in the electrode potentials of a series of transition metal complexes allow other potentials in the same series to be predicted. The trend in the $[MBr_6]^{2-/3-}$ electrode potentials of the third row hexabromometallates predicts that the couple $[HfBr_6]^{2-/3-}$, $5d^{0/1}$, should occur around $E_{1/2}$ = -2.25V (vs. S.C.E.) in CH_2Cl_2. Therefore the A.C. signal observed at $E_{1/2}$ = -1.90V (vs. S.C.E.) cannot confidently be assigned to the $[HfBr_6]^{2-/3-}$ couple. Unfortunately, there are no data pertaining to the electrochemistry of $[HfBr_6]^{n-}$ complexes available in the literature for comparison.

Although the A.C. signal observed at -1.90V was very small, it is very unlikely that the signal was due to a trace of $[ZrBr_6]^{2-}$ contaminant ($[ZrBr_6]^{2-/3-}$, $E_{1/2}$ = -1.82V (vs. S.C.E.)) as $[Bu_4N]_2[ZrBr_6]$ is itself known to react with the solvent-electrolyte medium. It would be much more likely that the A.C. signal at -1.90V was the result of hydrolysis of $[HfBr_6]^{2-}$ by a trace of moisture in the solvent-electrolyte medium leading to an oxybromohafnate(IV) species.

Unfortunately, there are also no data pertaining to the electrode potentials of oxyhalohafnate complexes available in the literature for comparison.

3.3 The cyclic voltammetric study of tetra-n-butylammonium hexabromoniobate(V) and tetra-n-butylammonium hexabromotantalate(V)

3.3.1 Tetra-n-butylammonium hexabromoniobate(V)

Red-brown $[Bu_4N][NbBr_6]$ was prepared by the method of Dehnicke *et al* [105]. Infra-red and visible-ultra violet spectroscopy [106,107] indicated the sample was contaminated with an oxide, most probably $[Bu_4N]_2[NbOBr_5]$ or $[Bu_4N][NbOBr_4]$ (see chapter 6).

$[Bu_4N][NbBr_6]$ has the electron configuration $4d^0$ and will therefore only undergo reduction. At room temperature the complex exhibited a quasi-reversible reduction $[NbBr_6]^{1-/2-}$, $4d^{0/1}$, at $E_{1/2}$ = +0.30V (vs. S.C.E.) in both the A.C. and D.C. modes which became reversible when the solution was cooled to -40°C. A second reduction $[NbBr_6]^{2-/3-}$, $4d^{1/2}$, was observed at $E_{1/2}$ = -0.89V (vs. S.C.E.) and was chemically irreversible at room temperature but became quasi-reversible at -40°C. A third couple, which was not a daughter product (section 2.11), was assumed to be $[NbOBr_4]^{1-/2-}$ or $[NbOBr_5]^{2-/3-}$, $4d^{0/1}$, at $E_{1/2}$ = -0.04V (vs. S.C.E.) and was irreversible at room temperature and quasi-reversible at -40°C. The quasi-reversibility of the $[NbBr_6]^{1-/2-}$ couple at room temperature is surprising as stable hexabromoniobate(IV) compounds are well known [107,108]. The large half-width and ΔE_p of the couple in the A.C. and D.C. modes respectively might therefore originate from a large uncompensated IR-drop although the system was adjusted to minimise this problem.

The highly irreversible nature of the $[NbBr_6]^{2-/3-}$ couple at room temperature was expected as there are no reports of a hexabromoniobate(III) compound in the literature. Electrode potentials of $[NbBr_6]^{n-}$ complexes have not been previously reported in the literature.

The electrode potentials and the D.C. and A.C. cyclic voltammagrams in methylene chloride solution of $[Bu_4N][NbBr_6]$ are shown in table 3.1 and figure 3.2 respectively.

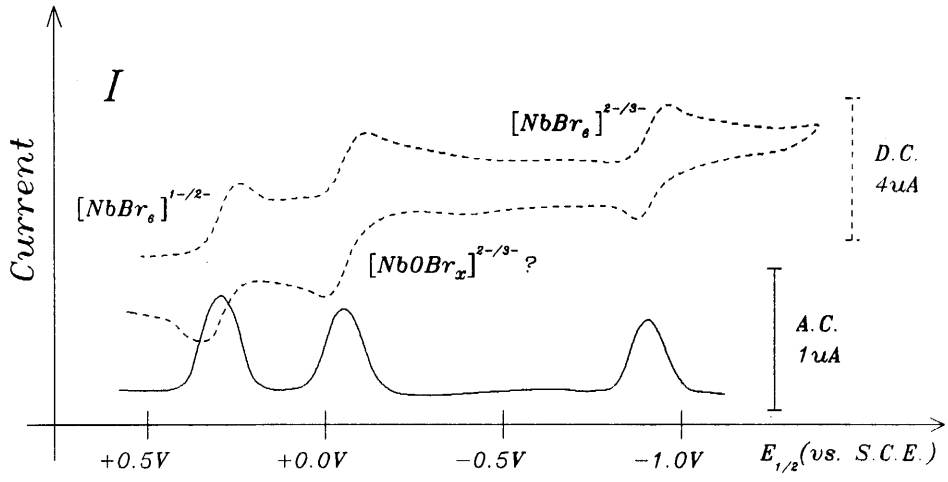

Figure 3.2: D.C. and A.C. cyclic voltammograms of $[Bu_4N][NbBr_6]$. conditions: $[Bu_4N]PF_6$ (0.3M)/$[NbBr_6]^{1-}$ (~0.005M) at micro-Pt electrode in CH_2Cl_2, temperature:-40°C, reference: ferrocene, sweep rate: 100mV/sec (D.C.), 20mV/sec (A.C.).

3.3.2 Tetra-n-butylammonium hexabromotantalate(V)

Yellow $[Bu_4N][TaBr_6]$ was prepared by the method of Dehnicke *et al* [105]. Infra-red and visible-ultra violet spectroscopy indicated that unlike the Nb compound (section 3.3.1) the Ta compound was not contaminated by any oxide . $[Bu_4N][TaBr_6]$ has the electron configuration $5d^0$ and will therefore only undergo reduction to Ta(IV), $5d^1$, and in principle to Ta(III), $5d^2$.

$[Bu_4N][TaBr_6]$ exhibited two reductions in CH_2Cl_2. The reduction $[TaBr_6]^{1-/2-}$, $5d^{0/1}$, at $E_{1/2}$ = -0.16V (vs. S.C.E.) was almost fully reversible in both the A.C. and D.C. modes at room temperature and was fully reversible at -40°C. The second reduction $[TaBr_6]^{2-/3-}$, $5d^{1/2}$, at $E_{1/2}$ = -1.35V (vs. S.C.E.) was chemically irreversible at room temperature but became quasi-reversible at -40°C (table 3.2).

The near fully-reversible nature of the $[TaBr_6]^{1-/2-}$ couple is consistent with the known existence of stable hexabromotantalate(IV) compounds [107]. As with $[NbBr_6]^{2-}$, the irreversibility of the $[TaBr_6]^{2-/3-}$ couple was expected as no $[TaBr_6]^{3-}$

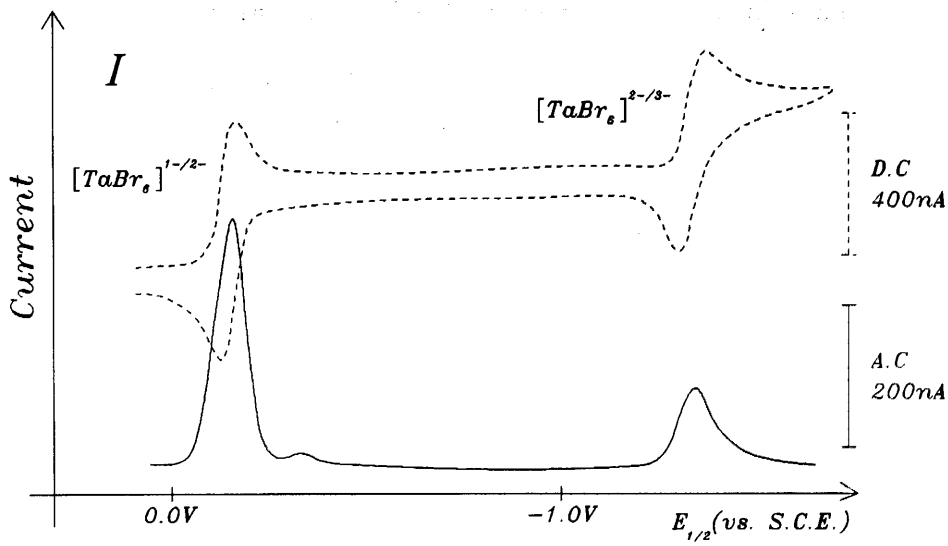

Figure 3.3: D.C. and A.C. cyclic voltammograms of $[Bu_4N][TaBr_6]$. conditions: $[Bu_4N]PF_6$ (0.3M)/$[TaBr_6]^{1-}$ (~0.005M) at micro-Pt electrode in CH_2Cl_2, temperature: -40 ^oC, reference: ferrocene, sweep rate: 100mV/sec (D.C.), 20mV/sec (A.C.).

complexes have been reported.

Lightner, Kirk and Katovic [187] have recently studied the cyclic voltammetry of $[Bu_4N][TaBr_6]$ in acetonitrile at -15°C versus a Normal Hydrogen Electrode (N.H.E.). They observed an almost reversible reduction $[TaBr_6]^{1-/2-}$ at $E_{1/2}$ = -0.29V (vs. N.H.E.) and an irreversible cathodic peak corresponding to the reduction $[TaBr_6]^{2-/3-}$ at E_p^c = -1.71V (vs. N.H.E.). Using the conversion factor $E_{1/2}$(ferricinium/ferrocene) = +0.400V (vs. N.H.E.) in CH_3CN [188] these two reductions can be re-referenced to -0.21V and -1.63V (vs. S.C.E.) in reasonable agreement with this thesis. (The large difference, *ca.* 0.3V, between the values of the two second reductions is attributable to the irreversibility of the $[TaBr_6]^{2-/3-}$ couple in CH_3CN at all temperatures).

The electrode potentials of $[Bu_4N][TaBr_6]$ are given in table 3.2 and the A.C. and D.C. cyclic voltammograms in methylene chloride are shown in figure 3.3.

Table 3.1: The electrode potentials of $[Bu_4N][NbBr_6]$.

D.C. mode					
temp. (^oC)	$E_{1/2}$ (V) (vs.S.C.E.)	ΔE_p (mV)	i_p^a/i_p^c	couple	electron confign.
+25	+0.30	100	1.0	V/IV	$5d^{0/1}$
-40	+0.30	70[a]	1.0	V/IV	$5d^{0/1}$
+25	irrev.	-	-	IV/III	$5d^{1/2}$
-40	-0.89	90	1.0	IV/III	$5d^{1/2}$

A.C. mode				
temp. (^oC)	$E_{1/2}$ (V) (vs.S.C.E.)	half-width (mV)	couple	electron confign.
+25	+0.30	150	V/IV	$5d^{0/1}$
-40	+0.30	120[a]	V/IV	$5d^{0/1}$
+25	-0.89	160	IV/III	$5d^{1/2}$
-40	-0.89	110	IV/III	$5d^{1/2}$

conditions: $[Bu_4N]PF_6$ (0.3M)/$[NbBr_6]^{1-}$ (~0.005M) at micro-Pt electrode in CH_2Cl_2, reference: ferrocene, sweep rate: 100mV/sec (D.C.), 20mV/sec (A.C.) , [a]not fully compensated.

Table 3.2: The electrode potentials of $[Bu_4N][TaBr_6]$.

D.C. mode					
temp. (^oC)	$E_{1/2}$ (V) (vs.S.C.E.)	ΔE_p (mV)	i_p^a/i_p^c	couple	electron confign.
+25	-0.16	75	1.0	V/IV	$5d^{0/1}$
-40	-0.16	60	1.0	V/IV	$5d^{0/1}$
+25	irrev.	-	-	IV/III	$5d^{1/2}$
-40	-1.35	70	1.0	IV/III	$5d^{1/2}$

A.C. mode				
temp. (^oC)	$E_{1/2}$ (V) (vs.S.C.E.)	half-width (mV)	couple	electron confign.
+25	-0.16	110	V/IV	$5d^{0/1}$
-40	-0.16	100	V/IV	$5d^{0/1}$
+25	-1.35	irrev.	IV/III	$5d^{1/2}$
-40	-1.35	130	IV/III	$5d^{1/2}$

conditions: $[Bu_4N]PF_6$ (0.3M)/$[TaBr_6]^{1-}$ (~0.005M) at micro-Pt electrode in CH_2Cl_2, reference: ferrocene, sweep rate: 100mV/sec (D.C.), 20mV/sec (A.C.)

3.4 The cyclic voltammetric study of bis tetra-n-butylammonium hexabromomolybdate(IV) and tetra-n-butylammomium oxytetrabromomolybdate(V)

3.4.1 Bis tetra-n-butylammonium hexabromomolybdate(IV)

Purple-black $[Bu_4N]_2[MoBr_6]$ was successfully prepared by reaction of molybdenum tetrabromide and tetra-n-butylammoniumbromide in methylene chloride (chapter 6). Recently, Dehnicke *et al* [58] have published the synthesis of $[PPh_3Me]_2[MoBr_6]$ using the same method as previously devised for this thesis.

At room temperature $[Bu_4N]_2[MoBr_6]$ exhibited complicated D.C. and A.C. cyclic voltammograms from which no specific redox couples were discernible. Once the experimental solution had been cooled to -40°C, by comparing the A.C. and D.C. cyclic voltammograms, five redox couples became apparent : $E_{1/2}$= +1.79V, +1.15V, +0.06V, -0.41V (all quasi-reversible) and (chemically irreversible) E_p^a = +1.6V (vs.S.C.E.). A pointed symmetrical cathodic peak at a potential more positive than the couple at +1.15V suggested an adsorbed species was a factor which should be considered (see figure 3.4).

The two quasi-reversible couples at +1.15V and +0.06V possessed approximately the same peak currents whilst the other three couples were smaller with similar currents. This suggested the two similar couples were the same species and also the species which was in most abundance. Therefore if the original compound had not decomposed, then the two couples at +1.15V and +0.06V must relate to the original compound, namely $[Bu_4N]_2[MoBr_6]$. The three smaller couples did not behave like daughter products (section 2.11) and were assumed to be an oxide contaminant. These assumptions were validated by the procedure in chapter 5 which predicted values of +1.10V and +0.05V (vs.S.C.E.) for the couples $[MoBr_6]^{1-/2-}$ and $[MoBr_6]^{2-/3-}$ respectively, in good agreement with the experimental values, while the remaining three couples were identified as a contaminant of oxide by comparison with the cyclic voltammogram of an authentic sample of $[Bu_4N][MoOBr_4]$ (see section 3.4.3).

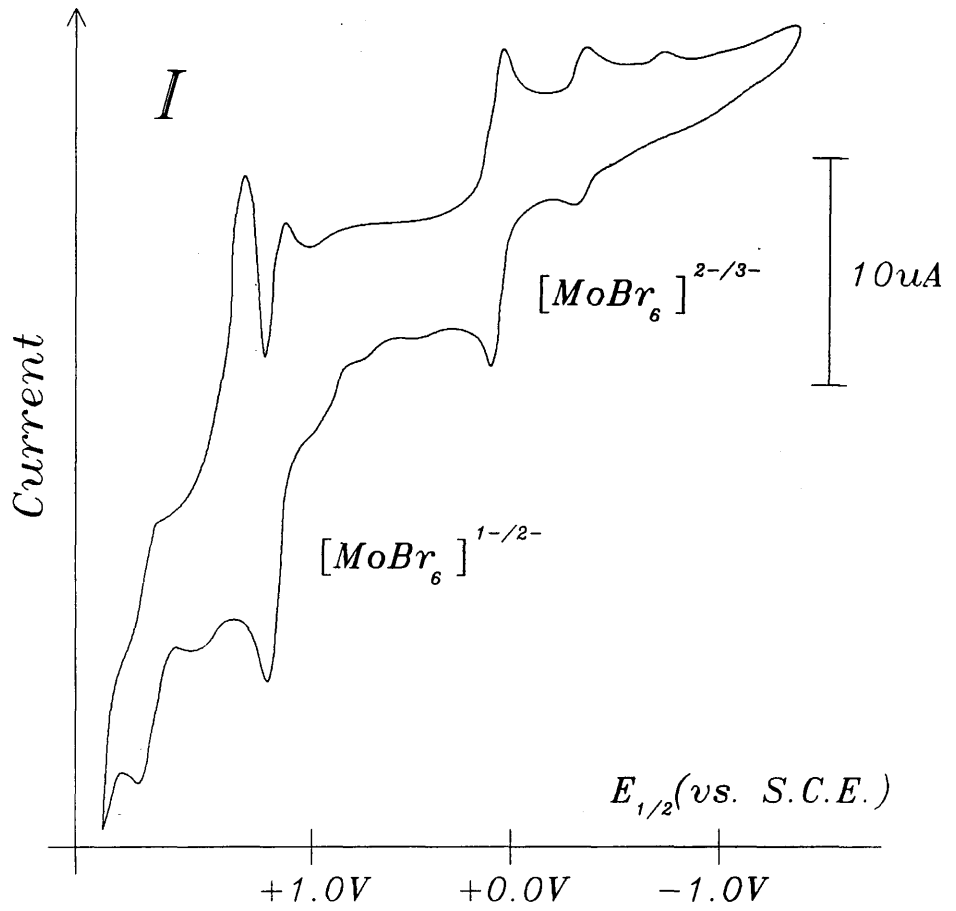

Figure 3.4: D.C. cyclic voltammogram of $[Bu_4N]_2[MoBr_6]$.
conditions: $[Bu_4N]PF_6$ (0.3M)/$[MoBr_6]^{2-}$ (~0.005M) at micro-Pt electrode in CH_2Cl_2, temperature:-40^oC, reference: ferrocene, sweep rate: 100mV/sec (D.C.).

The electrode potentials of bis(tetra-n-butylammonium) hexabromomolybdate(IV) are summarised in table 3.3: $[Bu_4N]_2[MoBr_6]$ exhibited two couples in methylene chloride which were both chemically irreversible at room temperature. When the solution was cooled to -40°C the couple $[MoBr_6]^{1-/2-}$, $4d^{1/2}$, at $E_{1/2}$ = +1.15V (vs.S.C.E.) became quasi-reversible and the couple $[MoBr_6]^{2-/3-}$, $4d^{2/3}$, at $E_{1/2}$ = +0.06V (vs.S.C.E.) became almost fully reversible. There are no previous reports of $[MoBr_6]^{n-}$ electrode potentials in the literature.

3.4.2 Discussion

The C.V. of $[Bu_4N]_2[MoBr_6]$ in CH_2Cl_2 at -40°C (figure 3.4) indicated that the oxidation $[MoBr_6]^{1-/2-}$ was followed by complicated electrochemical activity leading to the adsorption of a species on the electrode surface (indicated by the sharply pointed cathodic peak at c.a. +1.3V (vs.S.C.E.)). Similar observations were made with most of the hexabromometallates studied in this thesis ie: complicated redox processes occurred at potentials more positive than the $[MBr_6]^{1-/2-}$ couple, which at first suggested the most likely reaction was loss of bromide or bromine. Specifically for $[Bu_4N]_2[MoBr_6]$, the absence of a $[MoBr_6]^{1-}$ complex or a molybdenum bromide higher than $MoBr_4$ in the literature provided support for this argument. The potential of the pointed adsorption peak varied according to the identity of the metal complex and was therefore attributed to an adsorbed metal-bromide fragment. The situation is discussed further under bromide electrochemistry in section 4.2.

The irreversibility of the couple $[MoBr_6]^{2-/3-}$ at room temperature was unexpected because a number of hexabromomolybdate(III) compounds have been prepared previously by electrolytic reduction of Mo(VI) in concentrated HBr solution [56,57]. Previous workers have isolated the K^+, $[NH_4]^+$ and $[C_5H_5NH]^+$ salts of $[MoBr_6]^{3-}$ which were stable under anhydrous conditions but which could not be used in this thesis because they are insoluble in CH_2Cl_2. The $[Bu_4N]^+$ salt of $[MoBr_6]^{3-}$ should have been soluble in CH_2Cl_2 and easily prepared. But, in this work the compound $[Bu_4N]_3[MoBr_6]$ could not be isolated by the standard method, and in

fact the attempted synthesis resulted in the dimeric Mo(III) compound tris(tetra-n-butylammonium)nonabromodimolybdate(III) (see chapter 6). This result combined with the C.V. information indicates $[Bu_4N]_3[MoBr_6]$ is a thermodynamically unstable compound at room temperature in solution and readily decomposes to the dimeric complex, $[Mo_2Br_9]^{3-}$ ie:

$$2[Bu_4N]_3[MoBr_6] \rightleftharpoons [Bu_4N]_3[Mo_2Br_9] + 3[Bu_4N]Br \qquad (3.2)$$

This example of cation dependent stability was not the only isolated case encountered in this thesis- the same problem arose during the attempted syntheses of $[Bu_4N]_3[RhBr_6]$ and $[Bu_4N]_2[PdBr_6]$ (chapter 6). The reason why $[Bu_4N]^+$ cations have this effect is not clear although the large steric requirement of $[Bu_4N]^+$ cations is doubtlessly a contributing factor; even in solution the tetra-n-butylammonium cations and hexahalometallate anions are thought to stick closely together in large aggregates or micelles [192].

The cyclic voltammetry results indicated that equilibrium 3.2 could be shifted over to the left hand side by lowering the equilibrium temperature to -40°C.

Table 3.3: The electrode potentials of $[Bu_4N]_2[MoBr_6]$.

D.C. mode					
temp. (^oC)	$E_{1/2}$ (V) (vs.S.C.E.)	ΔE_p (mV)	i_p^a/i_p^c	couple	electron confign.
+25	irrev.	-	-	V/IV	$4d^{1/2}$
-40	+1.15	108	1.20	V/IV	$4d^{1/2}$
+25	irrev.	-	-	IV/III	$4d^{2/3}$
-40	+0.06	60	0.80	IV/III	$4d^{2/3}$

A.C. mode				
temp. (^oC)	$E_{1/2}$ (V) (vs.S.C.E.)	half-width (mV)	couple	electron confign.
+25	-	-	V/IV	$4d^{1/2}$
-40	+1.15	148	V/IV	$4d^{1/2}$
+25	-	-	IV/III	$4d^{2/3}$
-40	+0.06	106	IV/III	$4d^{2/3}$

conditions: $[Bu_4N]PF_6$ (0.3M)/$[MoBr_6]^{2-}$ (~0.005M) at micro-Pt electrode in CH_2Cl_2, reference: ferrocene, sweep rate: 100mV/sec (D.C.), 20mV/sec (A.C.)

3.4.3 tetra-n-butylammonium oxytetrabromomolybdate(V)

Ochre-yellow $[Bu_4N][MoOBr_4]$ was prepared by a variation of the method of Allen and Neumann [149] (chapter 6). The electrode potentials of $[Bu_4N][MoOBr_4]$ are summarised in table 3.4.

At -40°C $[Bu_4N][MoOBr_4]$ exhibited three chemically irreversible couples in the A.C. and D.C. modes at +1.80V, +1.63V and -0.38V (vs.S.C.E.). The contaminant present in the sample of $[Bu_4N]_2[MoBr_6]$ (section 3.4.1) exhibited a quasi-reversible couple at -0.41V (vs.S.C.E.) and two other couples of indeterminate reversibility at +1.79V and +1.6V (vs.S.C.E.).

Although the electrode potentials of the two compounds appear to match up the contrasting reversibility of the two couples at -0.38V and -0.41V requires some explanation. The answer may lie in the conditions at the electrode during the reduction $[MoBr_6]^{2-/3-}$. In section 3.4.1 it was pointed out that this reduction results in the formation of free bromide as a consequence of a dimerisation reaction. Under these conditions where there is an excess of free bromide at the electrode, a decomposition reaction of $[MoOBr_4]^{n-}$ at -0.38V involving loss of bromide would be suppressed, and a quasi- or fully reversible couple would be observed. In the absence of free bromide the same decomposition would result in an irreversible couple. The situation could therefore have been clarified by introducing excess bromide in the form of $[Bu_4N]Br$ to the solution of $[Bu_4N][MoOBr_4]$ in CH_2Cl_2 but, unfortunately this was not realised until after all the experiments in this thesis were completed. Nonetheless, in the light of the available data it is plausible to consider $[Bu_4N][MoOBr_4]$ and the contaminant mentioned in connection with $[Bu_4N]_2[MoBr_6]$ as one and the same compound.

The electrode potentials exhibited by $[Bu_4N][MoOBr_4]$ in CH_2Cl_2 solution are shown in table 3.4. Since the compound only exhibited chemically irreversible couples the individual cathodic and anodic peaks were not assigned to any specific $[MoOBr_4]^{n/n-1}$ redox couple.

Table 3.4: The electrode potentials of $[Bu_4N][MoOBr_4]$.

	A.C.mode		D.C.mode		
temp. (^oC)	$E_{1/2}$ (V) (vs.S.C.E.)	half-width (V)	$E_{1/2}$ (V) (vs.S.C.E.)	ΔE_p (mV)	i_p^a/i_p^c
+25	+1.10	190	-	-	-
+25	-0.41	110	-	-	-
-40	+1.80	110	irrev.	-	-
-40	+1.63	156	irrev.	-	-
-40	-0.38	112	irrev.	-	-

conditions: $[Bu_4N]PF_6$ (0.3M)/$[MoOBr_4]^{1-}$ (~0.005M) at micro-Pt electrode in CH_2Cl_2, reference: ferrocene, sweep rate: 100mV/sec (D.C.), 20mV/sec (A.C.)

3.5 The cyclic voltammetric study of tetra-n-butylammonium hexabromotungstate(V), bis tetra-n-butylammonium hexabromotungstate(IV) and tungsten hexabromide

The preparations of the three title compounds are described in chapter 6.

3.5.1 Tungsten hexabromide

The first compound prepared, green-black WBr_6 was almost totally insoluble in CH_2Cl_2 but, as there was a faint purple colouration evident in the solvent an electrochemical investigation was attempted. Surprisingly, the WBr_6 sample dissolved readily in the solvent/electrolyte medium of $CH_2Cl_2/[Bu_4N]PF_6$ producing a wine red solution.

The resultant wine red solution exhibited four reversible couples at -40^oC : $E_{1/2}$

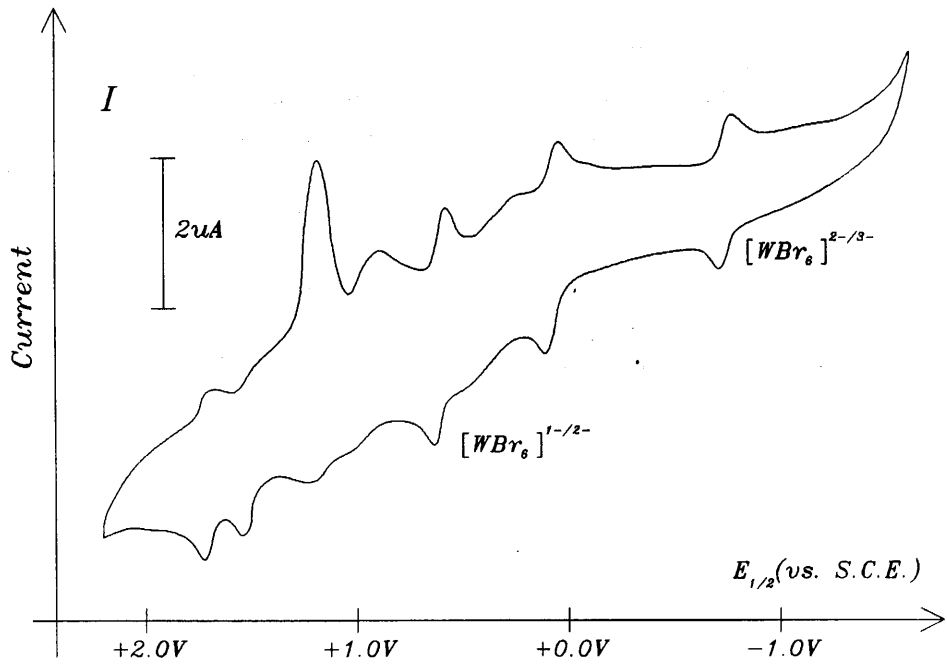

Figure 3.5: D.C. cyclic voltammogram of WBr_6.
Conditions: $[Bu_4N]PF_6$ (0.3M)/WBr_6 (~0.005M) at micro-Pt electrode in CH_2Cl_2, temperature:-40°C, reference: ferrocene, sweep rate: 100mV/sec (D.C.).

= -0.74V, +0.08V, +0.61V and +1.69V (vs.S.C.E.). In addition, significant electrochemical activity was observed at potentials more positive than the couple at +0.61V which was a common feature to most of the bromide complexes studied (figure 3.5 and see also sections 3.4 and 4.2). A strongly adsorbed species, indicated by a sharp, symmetrical peak, was observed during the cathodic scan at +1.18V (vs.S.C.E.) but was not observed with the Br_2/Br^- system (section 4.2), and was therefore provisionally attributed to an adsorbed W-Br fragment of unknown composition.

Obviously a reaction had occurred between $[Bu_4N]PF_6$ and WBr_6 but thus far the electrochemical data could provide little insight towards any specific reaction. As a preliminary experiment, the wine-red colouration of the $WBr_6/CH_2Cl_2/[Bu_4N]PF_6$ mixture was investigated. Figure 3.7 indicates how the visible-ultra violet spectrum of WBr_6 in CH_3CN solution changed over a period of 25 hours: The WBr_6 sample reacted gradually with CH_3CN until the final spectrum after 25 hours resembled that of $WBr_4.2CH_3CN$ obtained by previous workers from WBr_5 and CH_3CN [35] (table 3.5). Figure 3.6 shows the visible-ultra violet solution spectrum of WBr_6 in CH_2Cl_2 with/without added excess $[Bu_4N]PF_6$. Comparison of figures 3.6 and 3.7 indicated that the new compound produced by addition of excess $[Bu_4N]PF_6$ to WBr_6 in CH_2Cl_2 had the same spectrum as WBr_6 in CH_3CN after 1 hour. The same spectrum was produced by addition of excess $[Bu_4N]BF_4$ or $[Bu_4N]Br$ to WBr_6 in CH_2Cl_2. These spectra closely resembled the solution spectrum of $[Et_2NH_2][WBr_6]$ in CH_3CN obtained by previous workers [63] and $[Bu_4N][WBr_6]$ in CH_2Cl_2 obtained in this thesis (see table 3.5).

Therefore in summary, the visible-ultra violet spectroscopic data indicated that WBr_6 was reduced to $[WBr_6]^{1-}$ in CH_2Cl_2 solution in the presence of $[Bu_4N]PF_6$, $[Bu_4N]BF_4$ and $[Bu_4N]Br$. In order to verify this conclusion, the compounds $[Bu_4N][WBr_6]$ and $[Bu_4N]_2[WBr_6]$ were synthesised and investigated electrochemically (see section 3.5.2). The visible-ultra violet spectroscopic data also indicated that WBr_6 was reduced to $[WBr_6]^{1-}$ by CH_3CN over a period of approximately 1 hour and was subsequently reduced to $WBr_4.2CH_3CN$ over the following 24 hours. (Bromination of CH_3CN was discounted because it is known that there is little reaction between bromine and CH_3CN over 2-3 weeks [193]. The possibility of an initial reduction to

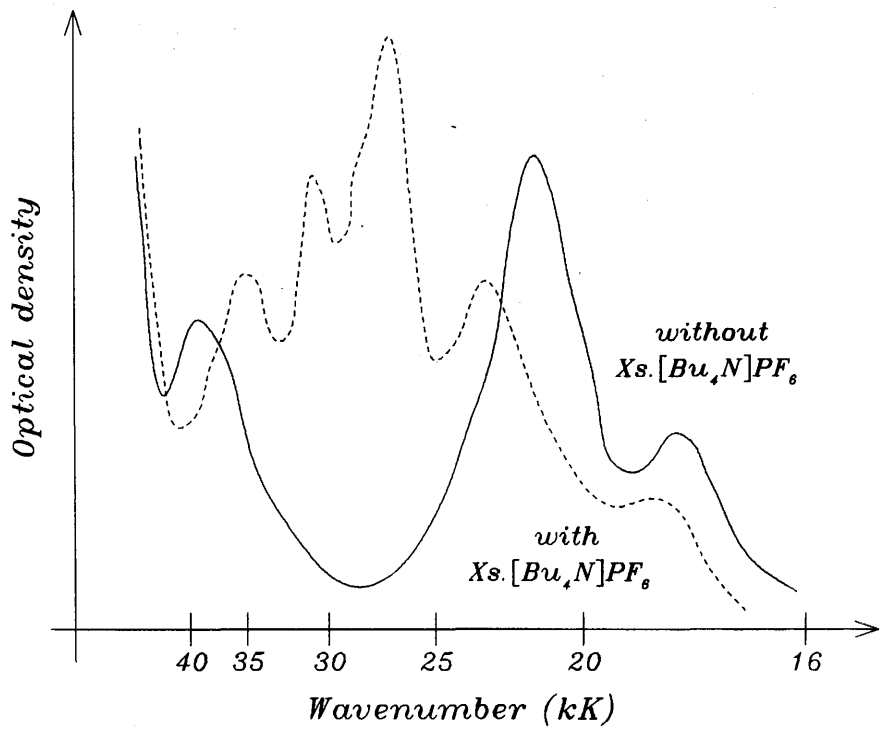

Figure 3.6: Solution spectrum of WBr_6 in CH_2Cl_2 with/without added excess $[Bu_4N]PF_6$.

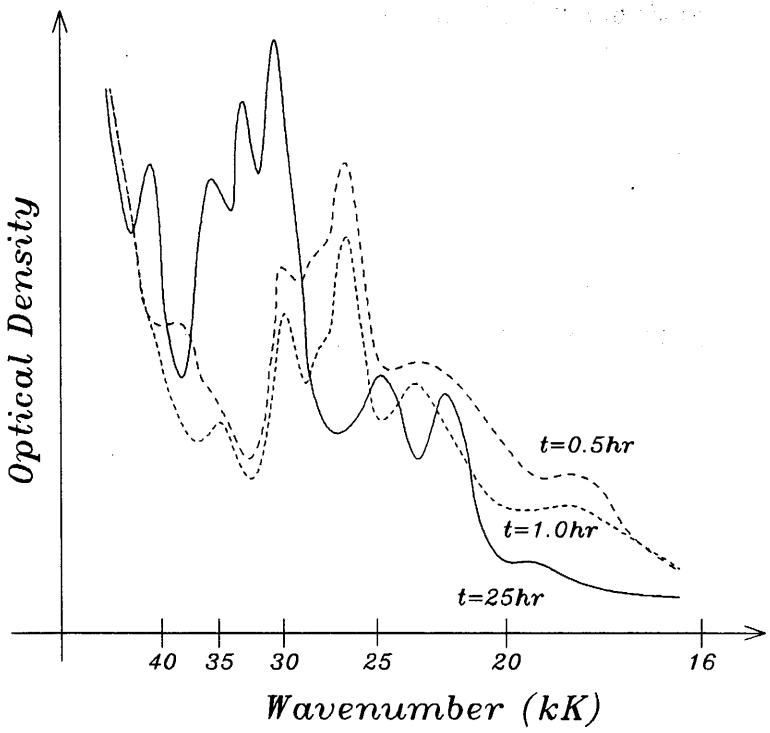

Figure 3.7: Solution spectrum of WBr_6 in CH_3CN after 0.5, 1.0 and 25.0 hours.

$WBr_5.CH_3CN$ cannot be discounted, however it is unlikely because the spectrum of WBr_6 in CH_3CN after 1 hour so closely resembled the spectrum of $[Bu_4N][WBr_6]$ in CH_2Cl_2 obtained in this thesis. The spectra should appear different if WBr_6 was initially reduced to $WBr_5.CH_3CN$.)

The argument favouring reduction of WBr_6 to $[WBr_6]^{1-}$ by CH_3CN is also favoured by the work of Brisdon *et al* [63] who noted that the spectrum of $[Et_2NH_2][WBr_6]$ in CH_3CN changed slowly over one day into the spectrum of $WBr_4.2CH_3CN$. The same behaviour was observed in this thesis with WBr_6 in CH_3CN and therefore the scheme 3.3 is proposed:-

$$WBr_6/Xs.CH_3CN \xrightarrow{1hr} [WBr_6]^{1-} \xrightarrow{24hr} WBr_4.2CH_3CN \qquad (3.3)$$

3.5.2 tetra-n-butylammonium hexabromotungstate(V) and bis tetra-n-butylammonium hexabromotungstate(IV)

The electrode potentials of $[Bu_4N][WBr_6]$ and $[Bu_4N]_2[WBr_6]$ are shown in tables 3.7 and 3.8. As expected, both compounds exhibited the same electrochemical behaviour : at -40°C, two reversible couples c.a. 1.35V apart with the $E_{1/2}$ values for both compounds agreeing to within 20mV. The couples $[WBr_6]^{1-/2-}$, $5d^{1/2}$, at $E_{1/2}$ = +0.59V (vs.S.C.E.) and $[WBr_6]^{2-/3-}$, $5d^{2/3}$, at $E_{1/2}$ = -0.75V (vs.S.C.E.) were both irreversible at room temperature but were reversible at -40°C.

The potentials of the two $[WBr_6]^{n/n-1}$ couples measured in this section coincide with those at $E_{1/2}$ = +0.60V and -0.74V (vs.S.C.E.) obtained with the $WBr_6/[Bu_4N]PF_6$ system investigated in section 3.5.1. Hence, in conjunction with the spectroscopic evidence already discussed, the electrochemical data in tables 3.7 and 3.8 provides clear evidence that the reaction of WBr_6 with the solvent/electrolyte medium resulted in the formation of $[WBr_6]^{1-}$.

The two remaining $WBr_6/[Bu_4N]PF_6$ couples at $E_{1/2}$ = +0.08V and +1.69V (vs.S.C.E.) were not observed with either $[Bu_4N][WBr_6]$ or $[Bu_4N]_2[WBr_6]$ and cannot therefore be attributed to $[WBr_6]^{n/n-1}$ redox couples. Intuitively one might suspect

that some oxide species were present although there was no evidence of this from the infra-red or visible- ultra violet spectra. Alternatively, that or those species which combined to reduce WBr_6 to $[WBr_6]^{1-}$ might have formed an oxidation product which was itself electroactive giving rise to the unassigned redox couples. Clearly some investigation of the first possibility should have been undertaken but the lack of spectroscopic evidence for any oxide was thought to be sufficient. (It transpired that a lack of spectroscopic evidence was not conclusive in the case of $[Bu_4N]_2[MoBr_6]$ (section 3.4) and the possibility of oxide contamination of WBr_6 should have been investigated further during this experiment.) The second alternative is discussed in the next section.

3.5.3 Discussion

The evidence outlined in sections 3.5.1 and 3.5.2 indicates that $[Bu_4N]PF_6$ or the combination of $[Bu_4N]PF_6$ and CH_2Cl_2 reduced WBr_6 to $[WBr_6]^{1-}$. Although $[Bu_4N]PF_6$ has not been reported to act as a reducing agent previously, this 'inert' electrolyte does undergo a number of reactions. For instance:-

- PF_6^-- anions undergo fluoride exchange with WF_6 or MoF_6 in CH_3CN [67]. eg:

$$WF_6 + [PF_5F^*]^{1-} \rightleftharpoons WF_6^* + [PF_6^*]^{1-} \tag{3.4}$$

- $[Bu_4N]PF_6$ attacks [31] niobium and tantalum pentachlorides (M_2Cl_{10}) in CH_2Cl_2 forming $[MF_6]^{1-}$ as one of the side products :-

$$M_2Cl_{10} + [Bu_4N]PF_6 \rightarrow [MCl_6]^{1-} + \text{small amounts of } [MF_6]^{1-},\ PF_5,\ PF_3,\ PCl_5 \text{ and } HF \tag{3.5}$$

- The tetra-n-butylammonium cation is also susceptible to degradation. For instance the instability of (tetra-n-butylammonium)fluoride, $[Bu_4N]F$, under anhydrous conditions was investigated by Sharma and Fry [68] who proposed the following reaction :-

$$2[Bu_4N]F \rightarrow [Bu_4N]^+[FHF]^- + Bu_3N + CH_3CH_2CH{=}CH_2 \qquad (3.6)$$

The strongly basic F^- ion is thought to cause a rapid E2 elimination which eventually results in the formation of the thermodynamically very stable bifluoride ion [69].

- Finally, Reeb *et al* [70] observed the rapid colour change of a THF solution of bis(pentamethylcyclopentadienyl)dichlorouranium(IV), (A), in the presence of $[Bu_4N]PF_6$. Also, the reduction potential of free A was shifted 0.4V cathodically due to the formation of a stable uranium(IV) adduct between A and $[PF_6]^{1-}$, although the authors did not identify the adduct.

The addition or exchange of a fluoride ion from the electrolyte with WBr_6 is unlikely because of the close similarity between the energies of the $WBr_6/[Bu_4N]PF_6$ electronic absorption spectrum and authentic $[WBr_6]^{1-}$ absorption spectra in CH_2Cl_2 and CH_3CN. This argument derives from the work of Rudzik and Preetz [65] who observed a hypsochromic shift of approximately 1.3kK in the absorption spectrum of $[ReBr_6]^{2-}$ when one Br^- ligand was replaced by a Cl^- ligand. According to Muller *et al* [66] this was due to the increase in the sum of the electronegativities of the ligands. If $[PF_6]^{1-}$ had exchanged a fluoride ligand with WBr_6 in a reduction reaction to form $[WBr_5F]^{1-}$ then a significant hypsochromic shift should have been observed because of the large electronegativity difference between Br^- and F^-.

Since both $[Bu_4N]BF_4$ and $[Bu_4N]Br$ also reacted with WBr_6 in CH_2Cl_2 to produce a wine red solution with the $[WBr_6]^{1-}$ absorption spectrum , if $[Bu_4N]PF_6$ does reduce WBr_6 in CH_2Cl_2 then the most likely reducing agent is the $[Bu_4N]^+$ cation. Quaternary ammonium compounds normally degrade by olefin-forming elimination mechanisms [71] such as 3.6 or more generally :-

$$B + H\text{-}C\text{-}C\text{-}X \longrightarrow BH + C{=}C + X \qquad (3.7)$$

where B is normally a basic, ie. nucleophilic, reagent and X separates with the electron pair which originally bound it to the carbon. In the case of $[Bu_4N]^+$, X

corresponds to tributylamine, Bu_3N: . Traces of bromine and/or bromide in the WBr_6 sample may have provided an indirect means by which a degradation could occur. For example, cerium(IV) and butadiene react in the presence of bromide ions by an additive dimerisation [72] :-

$$\begin{aligned} Ce(IV) + Br^- &\rightleftharpoons Ce(III) + Br^{\cdot} \\ Br^{\cdot} + \text{butadiene} &\rightleftharpoons BrC_4H_6^{\cdot} \\ 2BrC_4H_6^{\cdot} &\longrightarrow \text{Br-}C_4H_6 - C_4H_6\text{-Br} \quad (50\%) \end{aligned} \tag{3.8}$$

N.B. An added complication must also be considered: Couch *et al* [195] found WBr_6 lost bromine under vacuum at room temperature over several hours until the eventual stoichiometry of $WBr_{5.85}$ was reached. The same experimental conditions prevailed in this experiment also, hence the reacting species was probably not WBr_6 but $WBr_{5.85}$ which corresponds to a mixture of W(VI) and W(V) bromides.

It is known WBr_5 reacts with $[Bu_4N]Br$ in CH_2Cl_2 to form $[WBr_6]^{1-}$ therefore it would have been most beneficial to determine whether WBr_5 also reacted with $[Bu_4N]PF_6$ and $[Bu_4N]BF_4$ to produce a wine red solution with a '$[WBr_6]^{1-}$' spectrum.

Table 3.5 lists the electronic absorption maxima of a number of $[MBr_6]^{n-}$ salts. Extinction coefficients are not included because the weight of compound or volume of solution were not measurable with sufficient accuracy. However, all the transitions shown were very intense with ϵ values greater than 1000 $dm^3cm^{-2}mol^{-1}$ indicating they are most probably of a charge transfer nature. Tables 3.6, 3.7 and 3.8 list the electrode potentials of WBr_6, $[Bu_4N][WBr_6]$ and $[Bu_4N]_2[WBr_6]$ respectively while figure 3.5 shows a C.V. of WBr_6 in $CH_2Cl_2/[Bu_4N]PF_6$.

Table 3.5: Electronic absorption spectra of $[WBr_6]^{n-}$ complexes and related compounds (shoulders in parenthesis).

compound	reference	medium	absorption maxima (kK)[b]
WBr_6	[a]	CH_2Cl_2	17.9, 21.1, 37.2
WBr_6	[a]	CH_2Cl_2/ $[Bu_4N]PF_6$	18.4, 22.6, 26.2, (27.4), 29.5, 33.8
WBr_6	[a]	CH_3CN/ after 1hr	18.6, 23.4, 26.2, (27.5), 29.5, 34.0
$[Et_2NH_2]$/ $[WBr_6]$	63	CH_3CN	14.9, 18.9, 23.5, 26.3,(28.0), 29.6, 34.4,(39.0), 43.3
$[Bu_4N][WBr_6]$	[a]	CH_2Cl_2	18.3, 23.1, 26.1, 28.3, 30.7, 33.2
$[Bu_4N]_2[WBr_6]$	[a]	CH_2Cl_2	24.1, 28.1, 31.9, 34.9,37.8
$Cs_2[WBr_6]$	64	solid	23.3, 26.2, 29.0(br), 36.2, 44.6
WBr_6	[a]	CH_3CN/ after 25hr	22.2, 24.6, 29.8, 31.8, 34.4, 40.4
$WBr_4.2CH_3CN$	35	CH_3CN	22.1, 24.4, 29.8, 31.8, 34.5, 38.5
WBr_5	63	solid	~14.3, 19.6

[a] this thesis [b] 1kK = 1000cm^{-1}, br = broad

Table 3.6: The electrode potentials of tungsten hexabromide.

D.C. mode					
temp. (^oC)	$E_{1/2}$ (V) (vs.S.C.E.)	ΔE_p (mV)	i_p^a/i_p^c	couple[c]	electron confign.
-40	+0.60[a]	60	1.0	V/IV	$5d^{1/2}$
-40	-0.74	60	1.0	IV/III	$5d^{2/3}$

Table 3.7: The electrode potentials of $[Bu_4N][WBr_6]$.

D.C. mode					
temp. (^oC)	$E_{1/2}$ (V) (vs.S.C.E.)	ΔE_p (mV)	i_p^a/i_p^c	couple	electron confign.
+25	[b]	-	-	V/IV	$5d^{1/2}$
+25	irrev.		-	IV/III	$5d^{2/3}$
-40	+0.61	100[d]	1.0	V/IV	$5d^{1/2}$
-40	-0.75	110[d]	1.0	IV/III	$5d^{2/3}$

A.C. mode				
temp. (^oC)	$E_{1/2}$ (V) (vs.S.C.E.)	half-width (mV)	couple	electron confign.
+25	+0.74	150[d]	V/IV	$5d^{1/2}$
+25	-	-	IV/III	$5d^{2/3}$
-40	+0.61	100	V/IV	$5d^{1/2}$
-40	-0.74	90	IV/III	$5d^{2/3}$

Table 3.8: The electrode potentials of $[Bu_4N]_2[WBr_6]$.

D.C. mode					
temp. (^oC)	$E_{1/2}$ (V) (vs.S.C.E.)	ΔE_p (mV)	i_p^a/i_p^c	couple	electron confign.
+25	[b]	-	-	V/IV	$5d^{1/2}$
+25	irrev.	-	-	IV/III	$5d^{2/3}$
-40	+0.59	60	1.0	V/IV	$5d^{1/2}$
-40	-0.75	60	1.0	IV/III	$5d^{2/3}$

A.C. mode				
temp. (^oC)	$E_{1/2}$ (V) (vs.S.C.E.)	half-width (mV)	couple	electron confign.
+25	[b]	-	V/IV	$5d^{1/2}$
+25	-0.82	140[d]	IV/III	$5d^{2/3}$
-40	+0.59	100	V/IV	$5d^{1/2}$
-40	-0.75	90	IV/III	$5d^{2/3}$

Conditions: $[Bu_4N]PF_6$ (0.3M)/$[WBr_6]^{n-}$ (~0.005M) at micro-Pt electrode in CH_2Cl_2, reference: ferrocene, sweep rate: 100mV/sec (D.C.), 20mV/sec (A.C.) [a] referenced versus $[WBr_6]^{2-/3-}$ couple [b] couple not resolvable [c] couples also observed at +1.69V and +0.08V (see text) [d] not fully compensated

3.6 The cyclic voltammetric study of bis tetra-n-butylammonium hexabromorhenate(IV)

Yellow $[Bu_4N]_2[ReBr_6]$ was prepared by reduction of Re(VII) in the presence of bromide according to the method of Watt and Thompson [59] (chapter 6).

At room temperature, $[Bu_4N]_2[ReBr_6]$ exhibited one quasi-reversible couple, $E_{1/2}$ = +1.31V (vs.S.C.E.) and a chemically irreversible cathodic wave, E_p^c = -0.93V. The irreversible cathodic peak current was very large compared with that of the quasi-reversible couple and quickly moved off the scale of the chart recorder. But as the experimental solution was cooled to -40°C, the previously irreversible couple became increasingly quasi-reversible and exhibited an anodic return wave. At potentials more positive than the couple at +1.31V the compound exhibited a complex pattern of electrochemical activity analogous with the behavior of several of the hexabromometallates discussed in this chapter (see for example sections 3.4 and 3.5).

A previous electrochemical study [60] of $[Bu_4N]_2[ReBr_6]$ in CH_3CN solution at room temperature with $[Bu_4N][ClO_4]$ supporting electrolyte determined one fully reversible oxidation, $[ReBr_6]^{1-/2-}$ at $E_{1/2}$ = +1.18V (vs.S.C.E.) and an irreversible oxidation at E = +1.96V (vs.S.C.E.). Two irreversible reductions, $[ReBr_6]^{2-/3-}$ at E = -0.90V (vs.S.C.E.) and '$[ReBr_6]^{3-/4-}$' at E = -1.80V (vs.S.C.E.) were also observed.

Matching the CH_3CN data with the CH_2Cl_2 results obtained in this thesis indicates that in CH_2Cl_2 the couple $[ReBr_6]^{1-/2-}$, $5d^{2/3}$, at $E_{1/2}$ = +1.31V (vs.S.C.E.) is quasi-reversible at room temperature and nearly fully reversible at -40°C. The couple $[ReBr_6]^{2-/3-}$, $5d^{3/4}$, at $E_{1/2}$ = -0.89V (vs.S.C.E.) is chemically irreversible at room temperature and quasi- reversible at -40°C (see table 3.9).

The irreversibility of the $[ReBr_6]^{2-/3-}$ couple at room temperature is not surprising since there is no report of a stable hexahalorhenate(III) complex in the literature, although unsubstantiated reports of $[ReCl_6]^{3-}$ have been made [13]. The reduction observed at $E_{1/2}$ = -1.80V in CH_3CN by previous workers and assigned to the $[ReBr_6]^{3-/4-}$ couple is therefore almost certainly not a true $[ReBr_6]^{n/n-1}$ couple because $[ReBr_6]^{3-}$ is not stable at room temperature. At strongly reducing potentials

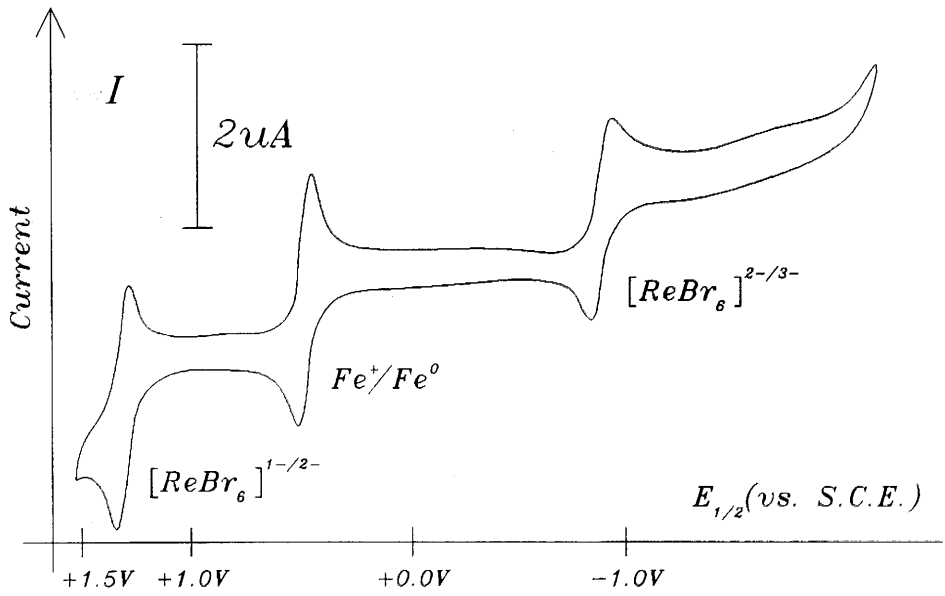

Figure 3.8: D.C. cyclic voltammogram of $[Bu_4N]_2[ReBr_6]$.
Conditions: $[Bu_4N]PF_6$ (0.3M)/$[ReBr_6]^{2-}$ (~0.005M) at micro-Pt electrode, temperature:--40°C, reference: ferrocene, sweep rate: 100mV/sec (D.C.).

Re(III) could be stabilised by expulsion of bromide followed by solvent coordination or, in a low dielectric constant solvent such as CH_2Cl_2 by dimerisation to the known [62] $[Re_2Br_8]^{2-}$ or $[Re_2Br_9]^{3-}$ eg.

$$2\ [ReBr_6]^{2-} \xrightarrow{+2e} [Re_2Br_9]^{3-} + 3Br^- \tag{3.9}$$

Although a dimerisation reaction of Re(III) similar to that of Mo(III) (section 3.4) is an attractive proposition, a major detraction is that there was no C.V. evidence for free Br^- in the customary region between +0.7V and +1.0V (vs.S.C.E.)(see section 4.2).

Since the $[ReBr_6]^{1-/2-}$ couple was not even fully reversible at -40°*C* in CH_2Cl_2 it is somewhat surprising that the same couple was reported to be fully reversible at room temperature in a strongly coordinating solvent like CH_3CN. The reverse behaviour is expected as with for example the couple $[TaBr_6]^{1-/2-}$ (section 3.3.2).

The electrochemical potentials of $[Bu_4N]_2[ReBr_6]$ are summarized in table 3.9. Figure 3.8 shows the D.C. cyclic voltammogram of the complex at -40°*C*.

Table 3.9: The electrode potentials of $[Bu_4N]_2[ReBr_6]$.

D.C. mode					
temp. (^oC)	$E_{1/2}$ (V) (vs.S.C.E.)	ΔE_p (mV)	i_p^a/i_p^c	couple	electron confign.
+25	+1.31	74	1.0	V/IV	$5d^{2/3}$
+25	irrev.	-	-	IV/III	$5d^{3/4}$
-40	+1.31	63	1.0	V/IV	$5d^{2/3}$
-40	-0.89	102	0.8	IV/III	$5d^{3/4}$

A.C. mode				
temp. (^oC)	$E_{1/2}$ (V) (vs.S.C.E.)	half-width (mV)	couple	electron confign.
+25	+1.31	200	V/IV	$5d^{2/3}$
+25	-0.93	[a]	IV/III	$5d^{3/4}$
-40	+1.31	[a]	V/IV	$5d^{2/3}$
-40	-0.89	139	IV/III	$5d^{3/4}$

Conditions: $[Bu_4N]PF_6$ (0.3M)/$[ReBr_6]^{2-}$ (~0.005M) at micro-Pt electrode, reference: ferrocene, sweep rate: 100mV/sec (D.C.), 20mV/sec (A.C.), [a] half-width not distinguishable

3.7 The cyclic voltammetric study of bis tetra-n-butylammonium hexabromoruthenate(IV)

Navy blue $[Bu_4N]_2[RuBr_6]$ did not exhibit any reversible couples at room temperature in CH_2Cl_2 but an anodic peak at $E_p^a = +1.52V$ (vs.S.C.E.) and a cathodic peak at $E_p^c = +0.09V$ (vs.S.C.E.) were detectable in the D.C. mode (only D.C. facilities were available at the time of experiment). When the experimental solution was cooled to -40°C three couples were detected : a chemically irreversible oxidation $[RuBr_6]^{1-/2-}$, $4d^{3/4}$, at $E_p^a = +1.52V$ (vs.S.C.E.), a quasi-reversible reduction $[RuBr_6]^{2-/3-}$, $4d^{4/5}$, at $E_{1/2} = +0.13V$ (vs.S.C.E.) and a chemically irreversible reduction $[RuBr_6]^{3-/4-}$, $4d^{5/6}$, at E_p^c = -1.7V (vs.S.C.E.).

Stephenson *et al* [109] have previously reported the redox potentials of $[PPh_3(CH_2Ph)]_2[RuBr_6]$ in CH_2Cl_2 at a Pt electrode. They observed a reduction $[RuBr_6]^{2-/3-}$ at $E_{1/2} = +0.13V$ (vs.S.C.E.) which was irreversible at +25°C but reversible at -40°C, and an oxidation $[RuBr_6]^{1-/2-}$ at E = +1.48V (vs.S.C.E.) which was irreversible at all temperatures. Both of these results are in good agreement with the values obtained in this thesis.

It was believed by the author that the room temperature reduction of $[RuBr_6]^{2-}$ at $E_{1/2} = +0.13V$ (vs.S.C.E.) was irreversible because the electron transfer was followed by Br^- expulsion and dimerisation of two Ru(III) fragments to form $[Ru_2Br_9]^{3-}$. ie:

$$2\ [RuBr_6]^{2-} + 2e \longrightarrow [Ru_2Br_9]^{3-} + 3Br^- \qquad (3.10)$$

To test this theory, a solution of $[Bu_4N]_2[RuBr_6]$ in CH_2Cl_2 at room temperature was electrolysed at a potential slightly less than the $[RuBr_6]^{2-/3-}$ couple until a mole equivalent of electrons had been passed. The electrolysed solution exhibited the distinctive anodic waves of a large amount of free Br^- (section 4.2) as well as a chemically irreversible reduction wave at E_p^c = -0.63V (vs.S.C.E.). (N.B. Free Br^- was not detected during conventional cyclic voltammetry.) Stephenson *et al* [109] determined the redox couples of $[Bu_4N]_3[Ru_2Br_9]$ in CH_2Cl_2 at room temperature and observed two reversible oxidations at $E_{1/2} = +0.83V$ and $E_{1/2} = +1.36V$ (vs.S.C.E.) and an

irreversible reduction at $E_{1/2}$ = -0.65V (vs.S.C.E.). The two sets of electrochemical results, electrolysed $[RuBr_6]^{2-}$ and $[Ru_2Br_9]^{3-}$ could represent the same compound if one assumes that the electrogenerated product exhibited redox couples at +0.83V and +1.36V but they were masked by the oxidation of free bromide. Unfortunately all attempts to precipitate the electrogenerated product in a pure form were unsuccessful.

Therefore, further evidence for a dimerisation was sought by spectro- electrochemical reduction of $[Bu_4N]_2[RuBr_6]$. By this technique, a solution of $[Bu_4N]_2[RuBr_6]$ in CH_2Cl_2 at room temperature was reduced at an optically transparent Pt-gauze electrode in a 1mm silica glass optical cell while the visible-ultra violet spectrum was continuously recorded. The spectrum of the electrogenerated product was very poor although possible absorptions were discernible at c.a. 19,000; 31,000 and 35000kK. Stephenson *et al* [109] listed the absorption maxima of $[Bu_4N]_3[Ru_2Br_9]$ at 34,720kK (ϵ=26,740dm^{3}mol^{-1}cm^{-2}), 30,960 (18,200); 23,360 (41,20); 19,720(6,050). The two spectra can only at best be described as similar, therefore, although circumstantial evidence exists, the product of the room temperature reduction $[RuBr_6]^{2-/3-}$ cannot be unequivocally identified as $[Ru_2Br_9]^{3-}$. (As with the couple $[ReBr_6]^{2-/3-}$, if dimerisation occurs then the absence of any evidence for Br^- during the conventional C.V. study of $[RuBr_6]^{2-}$ has yet to be adequately explained (see section 4.2).)

The electrochemistry of $[Bu_4N]_2[RuBr_6]$ in CH_2Cl_2 indicated that the oxidation state +IV is the only stable oxidation state of hexabromoruthenate complexes. This would appear to be correct as no stable $[RuBr_6]^{n-}$ compounds in either the +V or +III oxidation states have been reported in the literature [110] although Jørgensen has published [111] the electronic spectrum of an HBr solution claimed to contain $[RuBr_6]^{3-}$.

The electrode potentials of $[Bu_4N]_2[RuBr_6]$ in CH_2Cl_2 are listed in table 3.8 and the D.C. cyclic voltammogram of the compound is shown in figure 3.9.

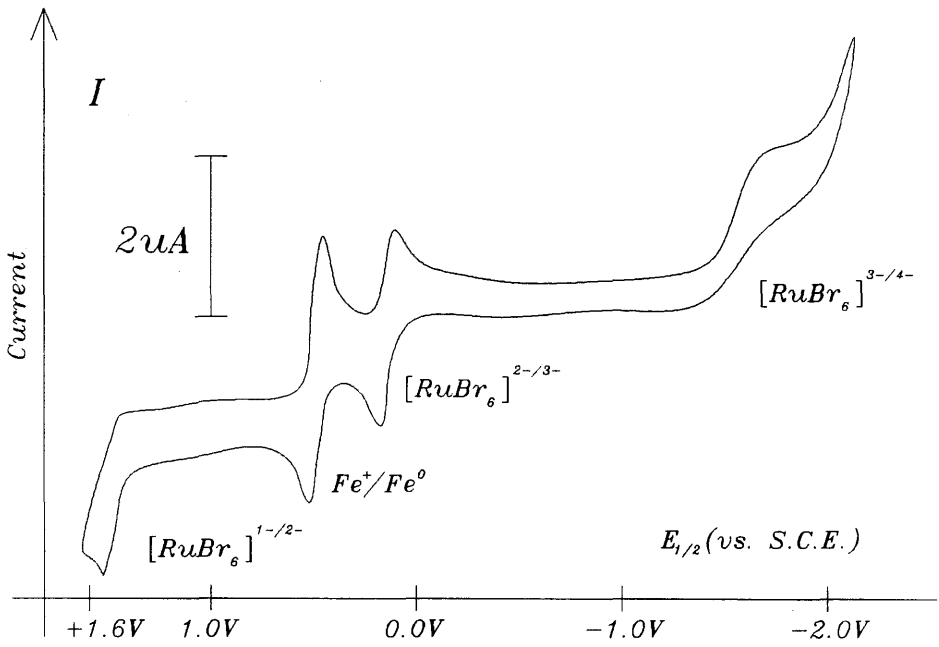

Figure 3.9: D.C. cyclic voltammogram of $[Bu_4N]_2[RuBr_6]$.
Conditions : $[Bu_4N]PF_6$ (0.3M)/$[RuBr_6]^{2-}$ (~0.005M) at micro-Pt electrode in CH_2Cl_2, temperature:-40°C: reference: ferrocene, sweep rate: 100mV/sec (D.C.).

Table 3.10: The electrode potentials of $[Bu_4N]_2[RuBr_6]$.

D.C. mode					
temp. (^oC)	$E_{1/2}$ (V) (vs.S.C.E.)	ΔE_p (mV)	i_p^a/i_p^c	couple	electron confign.
+25	+1.52[a]	irrev.	-	V/IV	$4d^{3/4}$
+25	+0.09[b]	irrev.	-	IV/III	$4d^{4/5}$
-40	+1.52[a]	irrev.	-	V/IV	$4d^{3/4}$
-40	+0.13	72	1.0	IV/III	$4d^{4/5}$
-40	-1.7[b]	irrev.	-	III/II	$4d^{5/6}$

Conditions : $[Bu_4N]PF_6$ (0.3M)/$[RuBr_6]^{2-}$ (~0.005M) at micro-Pt electrode in CH_2Cl_2, reference: ferrocene, sweep rate: 100mV/sec (D.C.), 20mV/sec (a.c.), [a] anodic peak potential [b] cathodic peak potential

3.8 The cyclic voltammetric study of bis tetra-n-butylammonium hexabromoosmate(IV)

Red-brown $[Bu_4N]_2[OsBr_6]$ exhibited three redox couples in CH_2Cl_2 at room temperature: $E_{1/2}$ = +1.24V, -0.55V and -0.79V (vs.S.C.E.). The two couples at +1.24V and -0.55V were approximately the same size and so were identified with successive couples of the same compound. The third couple at -0.79V was very much smaller and by varying the anodic switching potential was identified as a daughter product of the second couple (section 2.11).

The first couple, the oxidation $[OsBr_6]^{1-/2-}$, $5d^{3/4}$ at $E_{1/2}$ = +1.24V (vs.S.C.E.) was fully reversible at room temperature and -40^oC in the A.C. and D.C. modes. The second couple, the reduction $[OsBr_6]^{2-/3-}$, $5d^{4/5}$ at $E_{1/2}$ =-0.55V (vs.S.C.E.) was chemically irreversible at both room temperature and -40^oC with the peak current ratio, i_p^a/i_p^c, significantly less than 1.0. With the evidence for a daughter product at $E_{1/2}$ = -0.79V, this indicated that the reduction of $[OsBr_6]^{2-}$ to $[OsBr_6]^{3-}$ was

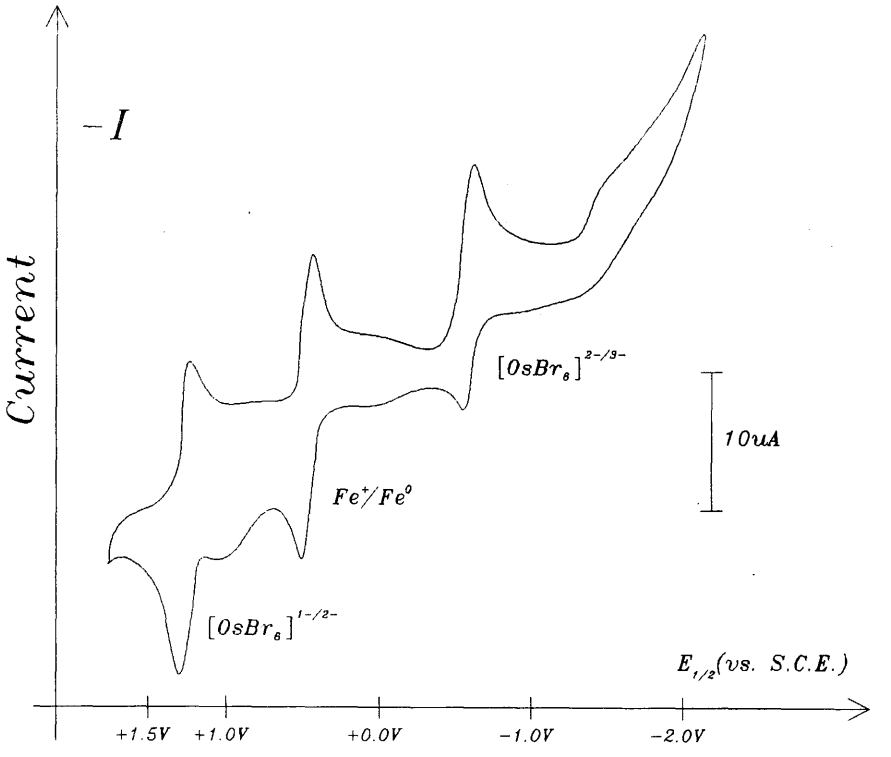

Figure 3.10: D.C. cyclic voltammogram of $[Bu_4N]_2[OsBr_6]$.
Conditions : $[Bu_4N]PF_6$ (0.3M)/$[OsBr_6]^{2-}$ (~0.005M) at micro-Pt electrode in CH_2Cl_2, temperature:0°C, reference: ferrocene, sweep rate: 100mV/sec (D.C.).

followed by an irreversible chemical reaction.

Dwyer, M^{c}Kenzie and Nyholm [88] studied the redox couples $[OsBr_6]^{2-/3-}$ in aqueous HBr and $[OsCl_6]^{2-/3-}$ in aqueous HCl. At zero acid strength the value of both couples extrapolated to the same value, -0.45V (vs.S.H.E.). The authors suggested that at low $[H^+]$, the complex halides hydrolysed to form $[OsO]^+$ and $[OsO]^{2+}$. Mertes, Crowell and Brinton [98] made cell measurements using concentrated HBr solutions (2-4M) and reported the couple $[OsBr_6]^{2-/3-}$ at E^o = -0.349V (vs.S.H.E.) in 2.1M HBr. Re-referencing (table 2.1) estimates the couple $[OsBr_6]^{2-/3-}$ at E^o = -0.60V (vs.S.C.E.) in 2.1M HBr which agrees with the value of -0.55V obtained in this thesis allowing for the very different solvents.

During a study of hexabromoosmate(V) compounds, Magnusson [73] determined the electrode potentials of $[Et_4N]_2[OsBr_6]$ in CH_3CN with $[Et_4N]ClO_4$ as background

electrolyte. Magnusson found a nearly reversible oxidation $[OsBr_6]^{1-/2-}$ at $E_{1/2}$ = +1.20V (vs.S.C.E.) and a totally irreversible reduction $[OsBr_6]^{2-/3-}$ with a cathodic peak potential at E_p^c = -0.55V (vs.S.C.E.).

The potentials observed by Magnusson are in very good agreement numerically with those observed in this thesis, the very slight differences probably being attributable to effects arising from the differing dielectric constants of the solvents CH_3CN and CH_2Cl_2. The reversibility of the $[OsBr_6]^{n/n-1}$ redox couples in CH_3CN reflect a general trend already observed with hexabromotungstates and hexabromoniobate(V), as well as with hexachlorometallates [31]. That is, hexahalometallates in the high oxidation states +VI and +V and the lower oxidation state +III react with CH_3CN to form adducts while hexahalometallates in CH_2Cl_2 appear to be more stable.

Table 3.9 shows the electrode potentials of $[Bu_4N]_2[OsBr_6]$ and figure 3.10 shows the D.C. cyclic voltammogram of $[Bu_4N]_2[OsBr_6]$ at 0^oC.

Table 3.11: The electrode potentials of $[Bu_4N]_2[OsBr_6]$.

D.C. mode					
temp. (^oC)	$E_{1/2}$ (V) (vs.S.C.E.)	ΔE_p (mV)	i_p^a/i_p^c	couple	electron confign.
+25	+1.24	80[a]	1.0	V/IV	$5d^{3/4}$
-40	+1.24	70[a]	1.0	V/IV	$5d^{3/4}$
+25	-0.55	71	0.5	IV/III	$5d^{4/5}$
-40	-0.55	70	0.6	IV/III	$5d^{4/5}$

A.C. mode				
temp. (^oC)	$E_{1/2}$ (V) (vs.S.C.E.)	half-width (mV)	couple	electron confign.
+25	+1.24	120[a]	V/IV	$5d^{3/4}$
-40	+1.24	120[a]	V/IV	$5d^{3/4}$
+25	-0.55	130	IV/III	$5d^{4/5}$
-40	-0.55	130	IV/III	$5d^{4/5}$

Conditions : $[Bu_4N]PF_6$ (0.3M)/$[OsBr_6]^{2-}$ (~0.005M) at micro-Pt electrode in CH_2Cl_2, reference: ferrocene, sweep rate: 100mV/sec (D.C.), 20mV/sec (a.c.), [a] not fully compensated

3.9 The cyclic votammetric study of tris tetra-n-butylammonium hexabromorhodate(III) and bis tetra-n-butylammmonium hexabromoiridate(IV)

3.9.1 Tris tetra-n-butylammonium hexabromorhodate(III)

Green $K_3[RhBr_6]$ was prepared by the method of Robb and Bekker [102] (chapter 6). All attempts to prepare $[Bu_4N]_3[RhBr_6]$ using cation exchange methods were unsuccessful and the only isolatable product was $[Bu_4N]_3[Rh_2Br_9]$.

Fergusson and Sherlock [103] found the nature of the halogenorhodate(III) species isolated was dependent on the size of the counter ion and the concentration of the halide ion in solution. It has also been reported [104] that with very large cations, halogen bridged species such as $[Rh_2Cl_9]^{3-}$ are obtained from Rh(III) chloride solutions. Therefore the difficulties encountered during this attempt to isolate the monomeric compound $[Bu_4N]_3[RhBr_6]$ were not unexpected. Analogous problems were encountered elsewhere in this thesis during the attempted preparations of $[Bu_4N]_3[MoBr_6]$ (section 3.4) and $[Bu_4N]_2[PdBr_6]$ (section 3.10).

Electrode potentials of $[RhBr_6]^{n-}$ compounds have not been previously reported in the literature.

3.9.2 Bis tetra-n-butylammonium hexabromoiridate(IV)

Navy-blue $[Bu_4N]_2[IrBr_6]$ has a $5d^5$ d-electron configuration. Using D.C. cyclic voltammetry in CH_2Cl_2 solution, two chemically irreversible oxidations and a chemically irreversible reduction were observed at +1.57V, +0.59V and +0.12V (vs.S.C.E.) respectively (table 3.10). When the solution was cooled to -40^oC, only two processes were observed : a chemically irreversible oxidation $[IrBr_6]^{1-/2-}$, $5d^{4/5}$, at E_p^a = +1.63V (vs.S.C.E.) and a fully reversible reduction $[IrBr_6]^{2-/3-}$, $5d^{5/6}$, at $E_{1/2}$ = +0.12V (vs.S.C.E.). The equipment necessary to study the A.C. cyclic voltammetry of $[Bu_4N]_2[IrBr_6]$ was not available at the time of the experiment.

During a previous study, Dwyer, Mckenzie and Nyholm [89] observed the reduction $[IrBr_6]^{2-/3-}$ at E^o = +0.99V (vs.S.H.E.) in aqueous acid solution, extrapolated to infinite dilution. Preetz and Steinebach [90] observed the same reduction in aqueous solution at E^o = +0.908V (vs.S.H.E.) in good agreement.

Preetz and Steinebach also observed the reduction $[IrBr_6]^{2-/3-}$ in CH_2Cl_2 at $E_{1/2}$ = +0.095V (vs.S.C.E. re-referenced), in good agreement with the value of $E_{1/2}$ = +0.12V obtained in this thesis. However, the text of their paper is a little confusing. On the one hand they stated "...the trivalent octahedral (halide) complexes are unstable in organic solvents due to their large negative charge and by ligand extraction (form) bridged dimers." ie.

$$2[Bu_4N]_3[IrX_6] \overset{CH_2Cl_2}{\rightarrow} [Bu_4N]_3[Ir_2X_9] + 3[Bu_4N]X, \qquad (X= Cl, Br) \qquad (3.11)$$

This would imply a certain degree of irreversibility of the $[IrBr_6]^{2-/3-}$ couple at the sweep rates employed (10-500 mV/sec). But, on the other hand Preetz and Steinebach reported that the couple $[IrBr_6]^{2-/3-}$, at $E_{1/2}$ = +0.095V, was fully reversible and that the temperature dependence of the reversibility "was insignificant".

These contradictory remarks would appear to be an oversight because in this thesis the reduction $[IrBr_6]^{2-/3-}$ was totally irreversible at room temperature although it became fully reversible when the solution was cooled to -40^oC. In CH_2Cl_2 at room temperature, $[Bu_4N]_3[IrBr_6]$ most probably decomposes according to equation 3.11 to form the well known [91] $[Ir_2Br_9]^{3-}$ compound. But, in common with the decomposition of rhenium and ruthenium hexabromometallates discussed previously (sections 3.6 and 3.7), free Br^- was not observed during cyclic voltammetry. The anodic peak observed at +0.59V at room temperature was only observed when the potential sweep was reversed at potentials more negative than the $[IrBr_6]^{2-/3-}$ couple at E_p^c= +0.12V. This behavior indicated the anodic peak at +0.59V was a daughter product of the irreversible reduction $[IrBr_6]^{2-/3-}$ at +0.12V.

Table 3.10 shows the electrode potentials of $[Bu_4N]_2[IrBr_6]$ and figure 3.11 shows the D.C. cyclic voltammograms obtained at room temperature and -40^oC in CH_2Cl_2.

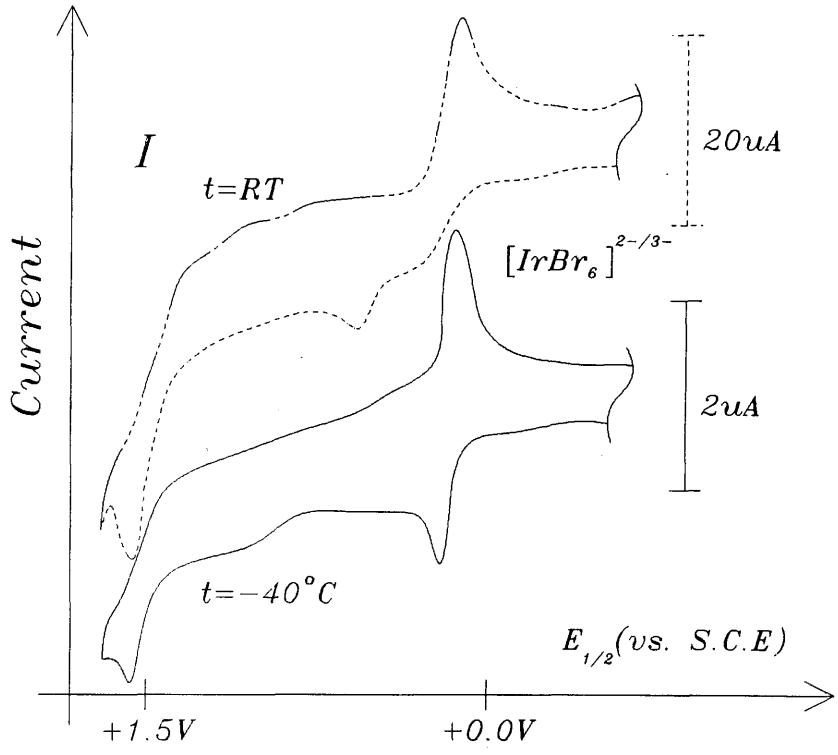

Figure 3.11: D.C. cyclic voltammogram of $[Bu_4N]_2[IrBr_6]$.
Conditions: $[Bu_4N]PF_6$ (0.3M)/$[IrBr_6]^{2-}$ (0.005M) at micro-Pt electrode in CH_2Cl_2, reference: ferrocene, sweep rate: 100mV/sec.

Table 3.12: The electrode potentials of $[Bu_4N]_2[IrBr_6]$.

D.C. mode					
temp. (^oC)	$E_{1/2}$ (V) (vs.S.C.E.)	ΔE_p (mV)	i_p^a/i_p^c	couple	electron confign.
+25	$+1.57^a$	-	-	V/IV	$5d^{4/5}$
+25	$+0.12^b$	-	-	IV/III	$5d^{5/6}$
-40	$+1.63^a$	-	-	V/IV	$5d^{4/5}$
-40	+0.15	59	1.0	IV/III	$5d^{5/6}$

Conditions: $[Bu_4N]PF_6$ (0.3M)/$[IrBr_6]^{2-}$ (0.005M) at micro-Pt electrode in CH_2Cl_2, reference: ferrocene, sweep rate: 100mV/sec, ^{a} anodic peak potential ^{b} cathodic peak potential

3.10 The cyclic voltammetric study of bis tetra-n-butylammonium hexabromopalladate(IV) and bis tetra-n-butylammonium hexabromoplatinate(IV)

3.10.1 Bis tetra-n-butylammonium hexabromopalladate(IV)

A.Gutbier and co-workers have prepared a large number of hexabromopalladate(IV) salts. Gutbier and Fellner [189] have described the preparation of, among others, bis(tetra-ethylammonium)hexabromopalladate(IV) and bis(tri-iso-butylammonium)-hexabromopalladate(IV). It appears they did not attempt to, or could not, prepare a tetrabutylammonium salt of hexabromopalladate(IV).

In this thesis, black $K_2[PdBr_6]$ was prepared by the method of Gutbier and Krell [101] (chapter 6). All attempts to isolate $[Bu_4N]_2[PdBr_6]$ using cation exchange methods in HBr or organic solvents were unsuccessful. The only compound which could be isolated was identified by infra-red spectroscopy as the Pd(II) compound

$[Bu_4N]_2[Pd_2Br_6]$. This unusual result suggests that the introduction of a large tetra-n-butylammonium counter cation resulted in the reduction of Pd(IV) to Pd(II) (presumably with the expulsion of Br_2). (The hexabromopalladate(IV) salt was synthesised in low yield using the smaller tetraethylammonium cation but the resulting compound $[Et_4N]_2[PdBr_6]$ was not soluble in CH_2Cl_2 (section 6.20)). Similar problems involving dimerisation have been encountered previously in this thesis with Mo and Rh hexabromometallates(III) (sections 3.4 and 3.9), but in those instances the metal ions did not alter their formal oxidation states.

It is often energetic considerations which govern the outcome of a chemical reaction. In aqueous solution the formation energies of tetrabromopalladate(II) and hexabromopalladate(IV) are :-

compound	ΔG_f (Kcal/mol)
$[PdBr_4]^{2-}$(aq)	-77
$[PdBr_6]^{2-}$(aq)	-81

And because Pd(IV) and Pd(II) bromometallates have similar formation energies, they are relatively easy to interchange. Thus, the $[PdBr_6]^{2-}$(aq) anion is thermally unstable in acidic solution and can be reduced to $[PdBr_4]^{2-}$(aq) by gentle heating. When this occurs, the small overall energy gain incurred by breaking two Pd-Br bonds may be compensated for by the Pd complex adopting the more energetically favourable Pd(II), d^8 square planar stereochemistry. By the same reasoning, the steric requirement of the $[Bu_4N]^+$ cation must inhibit the precipitation of $[PdBr_6]^{2-}$ such that it is more energetically preferable for $[PdBr_6]^{2-}$ to dimerize and precipitate as $[Bu_4N]_2[Pd_2Br_6]$ with square planar Pd(II) metal ions. ie :-

$$2[Bu_4N]^+ + 2[PdBr_6]^{2-} \rightarrow [Bu_4N]_2[Pd_2Br_6] + 2Br^- + 2Br_2 \qquad (3.12)$$

$[PdBr_6]^{2-}$(aq) has previously been reported [190] to undergo a two electron reduction to $[PdBr_4]^{2-}$(aq) in 1M KBr solution at E = -0.99V (vs.S.H.E.). ie.

$$[PdBr_6]^{2-}(aq) + 2e \longrightarrow [PdBr_4]^{2-}(aq) + 2Br^- \qquad (3.13)$$

3.10.2 Bis tetra-n-butylammonium hexabromoplatinate(IV)

Dark-red $[Bu_4N]_2[PtBr_6]$ was prepared by a similar method to that of Swihart and Mason [92] (chapter 6). The complex has a $5d^6$ electron configuration and exhibited two redox processes in CH_2Cl_2 : a chemically irreversible oxidation wave at E_p^a = +2.02V (vs.S.C.E.) and a larger chemically irreversible reduction wave at E_p^c = -0.80V (vs.S.C.E.) (table 3.11). No return waves in the D.C. mode were observed on an oscilloscope for either the oxidation or the reduction at room temperature or -40°C with sweep rates up to 200V/sec.

A coulometric analysis of the reduction wave was not performed although it would have determined the exact number of electrons transferred. However, the reduction of the analogous compound $[Bu_4N]_2[PtCl_6]$ in CH_2Cl_2 has been investigated by Moock [31]. Using coulometric analysis, Moock found $[PtCl_6]^{2-}$ exhibited an irreversible 2e reduction, $[PtCl_6]^{2-}/[PtCl_4]^{2-}$ at -0.87V (vs.S.C.E.) with the loss of two chloride ions, and an irreversible oxidation, $[PtCl_6]^{1-/2-}$ at E_p^a= +2.30V (vs.S.C.E.). In this thesis, the reduction wave of $[Bu_4N]_2[PtBr_6]$ was approximately twice the size of the oxidation wave and a small amount of free Br^- in solution was indicated by a broad anodic peak at +0.98V (vs.S.C.E.) in both the A.C. and D.C. modes. Therefore, by comparison with the behaviour of $[Bu_4N]_2[PtCl_6]$, the irreversible oxidation of $[Bu_4N]_2[PtBr_6]$ at E_p^a = +2.02V (vs.S.C.E.) was assigned to the couple $[PtBr_6]^{1-/2-}$ and the irreversible reduction at E_p^c = -0.80V (vs.S.C.E.) was assigned to the two electron reduction $[PtBr_6]^{2-}/[PtBr_4]^{2-}$ ie.

$$[PtBr_6]^{2-} + 2e \longrightarrow [PtBr_4]^{2-} + 2Br^- \tag{3.14}$$

Goldberg and Hepler [99] reported the $[PtBr_6]^{2-}/[PtBr_4]^{2-}$ couple in 1M NaBr at E = -0.89V (vs.S.C.E. re-referenced v. the S.H.E.) in good agreement with the value obtained in this thesis in CH_2Cl_2 solution. Hubbard and Anson [93] reported the same couple in 1F NaBr solution at approximately +0.30V (vs.S.C.E.) which appears to be incorrect.

The possible one electron reduction $[PtBr_6]^{2-/3-}$, $5d^{6/7}$, was not observed even at

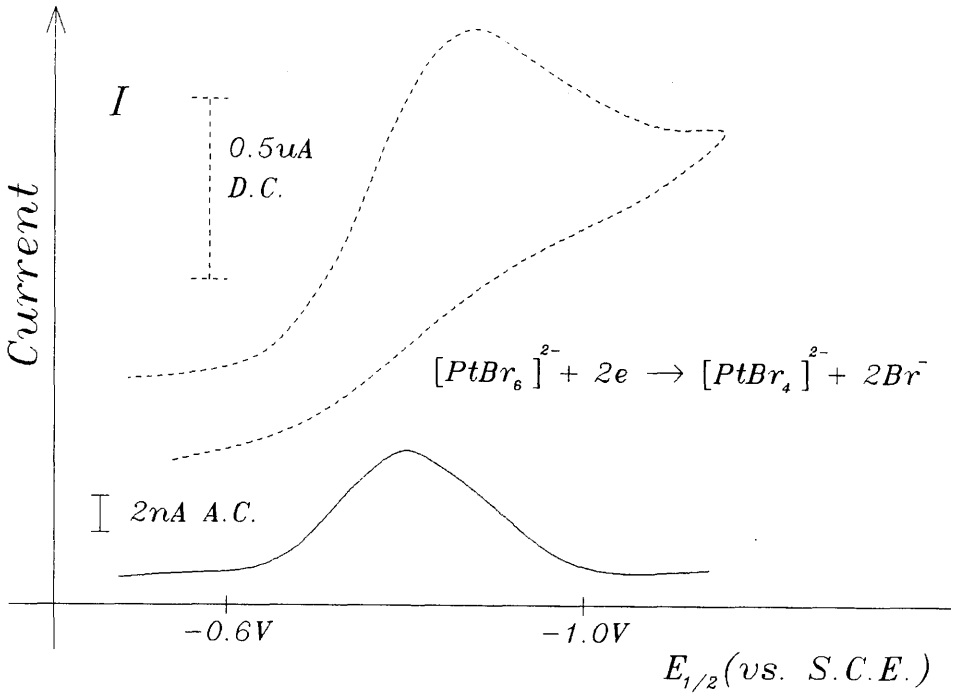

Figure 3.12: D.C. A.C. cyclic voltammograms of the reduction $[PtBr_6]^{2-}/[PtBr_4]^{2-}$. Conditions: $[Bu_4N]PF_6$ (0.3M)/$[PtBr_6]^{2-}$ (0.005M) at micro-Pt electrode in CH_2Cl_2, temperature:-40°C, reference: ferrocene, sweep rate: 100mV/sec (D.C.), 20mV/sec (A.C.),

very fast sweep rates because of the unfavourable ligand field stabilisation energy of a Pt(III) ion surrounded by an octahedral ligand field compared with a Pt(II) ion, $5d^8$, surrounded by a square planar ligand field. Instead, octahedral hexabromoplatinate(IV) undergoes a fast two electron reduction to Pt(II), $5d^8$, accompanied by the expulsion of two Br^- ions in order to adopt a square planar stereochemistry. The complex thereby maximises the available L.F.S.E. at the expense of two platinum-bromine bonds. The exact mechanism by which the reduction of $[PtBr_6]^{2-}$ occurs is not known but it is thought to be quite complex.

Table 3.11 lists the electrode potentials of $[Bu_4N]_2[PtBr_6]$ and figure 3.12 shows the A.C. and D.C. cyclic voltammograms of the reduction $[PtBr_6]^{2-}/[PtBr_4]^{2-}$ in CH_2Cl_2 at -40°C.

Table 3.13: The electrode potentials of $[Bu_4N]_2[PtBr_6]$.

D.C. mode					
temp. (^oC)	$E_{1/2}$ (V) (vs.S.C.E.)	ΔE_p (mV)	i_p^a/i_p^c	couple	electron confign.
+25	+2.0[a]	-	-	V/IV	$5d^{5/6}$
+25	-0.86[b]	-	-	IV/II	$5d^{6/8}$
-40	+2.02[a]	-	-	V/IV	$5d^{5/6}$
-40	-0.86[b]	-	-	IV/II	$5d^{6/8}$

A.C. mode				
temp. (^oC)	$E_{1/2}$ (V) (vs.S.C.E.)	half-width (mV)	couple	electron confign.
+25	[d]	-	V/IV	$5d^{5/6}$
+25	-0.80	>200	IV/II	$5d^{6/8}$
-40	+2.02	[c]	V/IV	$5d^{5/6}$
-40	-0.80	190	IV/II	$5d^{6/8}$

Conditions: $[Bu_4N]PF_6$ (0.3M)/$[PtBr_6]^{2-}$ (0.005M) at micro-Pt electrode in CH_2Cl_2, reference: ferrocene, sweep rate: 100mV/sec (D.C.), 20mV/sec (A.C.), [a] anodic peak potential [b] cathodic peak potential [c] half-width unmeasurable [d] not observed

Chapter 4

4.1 The cyclic voltammetric study of tetra-n-butylammonium chloride in methylene chloride solution at a platinum electrode

4.1.1 Results

In this thesis, $[Bu_4N]Cl$ exhibited one oxidation wave at $E_p^a = +1.44V$ (vs.S.C.E.) in methylene chloride solution at a micro-platinum electrode. The oxidation was totally irreversible at room temperature and -40^oC (figure 4.1). The anodic peak current of the oxidation was approximately twice the anodic peak current of an equimolar sample of ferrocene added to the solution, indicating the oxidation was a 2e process.

Several groups of workers have previously studied the oxidation of chloride ion in nitromethane and acetonitrile solution. Marchon and Lambling [174] reported that Cl^- exhibited a 2e oxidation at E = +1.38V (vs.Ag/AgCl) in CH_3NO_2 solution at a rotating platinum microelectrode (equivalent to E = +1.03V (vs.S.C.E.) using the re-referencing scheme E(Ag/AgCl) = -0.35V (vs.S.C.E.) [175]). They also found the electron transfer was kinetically slow at a polished platinum electrode but was quasi-rapid at a platinised platinum or activated platinum electrode. Marchon and Lambling postulated the simple chloride oxidation mechanism :-

$$2Cl^- - 2e \longrightarrow Cl_2 \tag{4.1}$$

Mastragostino *et al* [176] also observed the oxidation of Cl^- at $\Delta E_p \simeq +1.0V$ (vs.S.C.E.) in CH_3NO_2 solution although they found that the oxidation wave was only poorly reproducible. Their coulometric experiments indicated that a primary oxidation product was formed initially involving the transfer of 2e, then a secondary product was formed by a chemical reaction after a given time. They thought the most probable primary product was Cl_3^- which then slowly disproportionated to Cl_2 and Cl^- in the bulk solution. ie:

$$\begin{array}{lcl} 3Cl^- & \longrightarrow & Cl_3^- + 2e \\ Cl_3^- & \overset{slow,k}{\longrightarrow} & Cl_2 + Cl^- \end{array} \tag{4.2}$$

This mechanism was supported by the work of Nelson and Iwamoto [49] who previously estimated the formation constant of Cl_3^- in CH_3CN solution to be around 10^{10}. Mastragostino *et al* calculated that the rate constant k for the disproportionation was $7x10^{-4}s^{-1}$ (at $-10°C$).

A third explanation of the oxidation of chloride ions in CH_3NO_2 solution has been put forward by Novak and Visy [180]. They found the anodic oxidation of Cl^- ions at a rotating platinum electrode in CH_3NO_2 solution could be characterised by the assumption of reversible (2e) charge transfer followed by an irreversible recombination and that a weak positive interaction acts between the adsorbed species. ie:

$$\begin{array}{lcl} 2Cl^- & \rightleftharpoons & 2Cl\cdot + 2e \\ 2Cl\cdot & \longrightarrow & Cl_2 \end{array} \tag{4.3}$$

The electrochemical experiments conducted by previous workers in CH_3CN solution provided even more ambiguous results. Sereno *et al* [177] examined the electrochemistry of Cl^- ions in CH_3CN solution at a rotating platinum disk electrode and observed an irreversible 2e oxidation process at $E \simeq 20mV$ (vs. Ag/AgCl= +0.37V (vs.S.C.E.)). Anderson [178] used C.V. in CH_3CN solution at a platinum electrode to

study tetraethylammoniumchloride which exhibited an anodic and a cathodic wave, $E_{1/2} = +0.98V$ (vs.S.C.E.), $\Delta E_p = 450mV$. Kolthoff and Coetzee [74] observed two anodic oxidation waves at +1.1V and +1.7V (vs.S.C.E.) with LiCl in CH_3CN at a rotating platinum micro-electrode. The first wave was twice the size of the second wave hence they postulated the following oxidation mechanism :-

$$\begin{aligned} 6Cl^- &\longrightarrow 2Cl_3^- + 4e \\ 2Cl_3^- &\longrightarrow 3Cl_2 + 2e \end{aligned} \tag{4.4}$$

4.1.2 Discussion

For the equilibrium

$$X_3^- \rightleftharpoons X^- + X_2 \tag{4.5}$$

Marchon [179] was able to determine pK values of 7.4 and 7.0 for I_3^- and Br_3^- respectively in both CH_3CN and CH_3NO_2, but Cl_3^- was too unstable to determine its pK value. This is in agreement with the electrochemical results but contradicts the pK value of 10^{10} for Cl_3^- previously obtained by Nelson and Iwamoto [49]. However, since Sereno *et al* [177] have reported $pK(Cl_3^-) = 2.0$, the combined evidence strongly suggests Nelson and Iwamoto were wrong and that Cl_3^- is unstable in CH_3CN and CH_3NO_2 and therefore mechanism 4.2 must be incorrect. Similarly, one must consider mechanism 4.4 incorrect for the same reason, especially considering there was already some doubt because only one oxidation wave was ever observed by other workers.

Mechanisms 4.1 and 4.3 would appear to be very similar because although Marchon and Lambling [174] did not explicitly postulate adsorbed chlorine radicals they mentioned the rate of electron transfer was affected by the nature of the platinum electrode surface. All the available results suggest (with the exception of Anderson [178] and Kolthoff and Coetzee [74]) that in CH_3NO_2, CH_3CN and CH_2Cl_2, Cl^- exhibits only one irreversible oxidation wave which corresponds to a 2e oxidation of Cl^- to Cl_2 and which can be best described by mechanism 4.3. Hence in this thesis, the

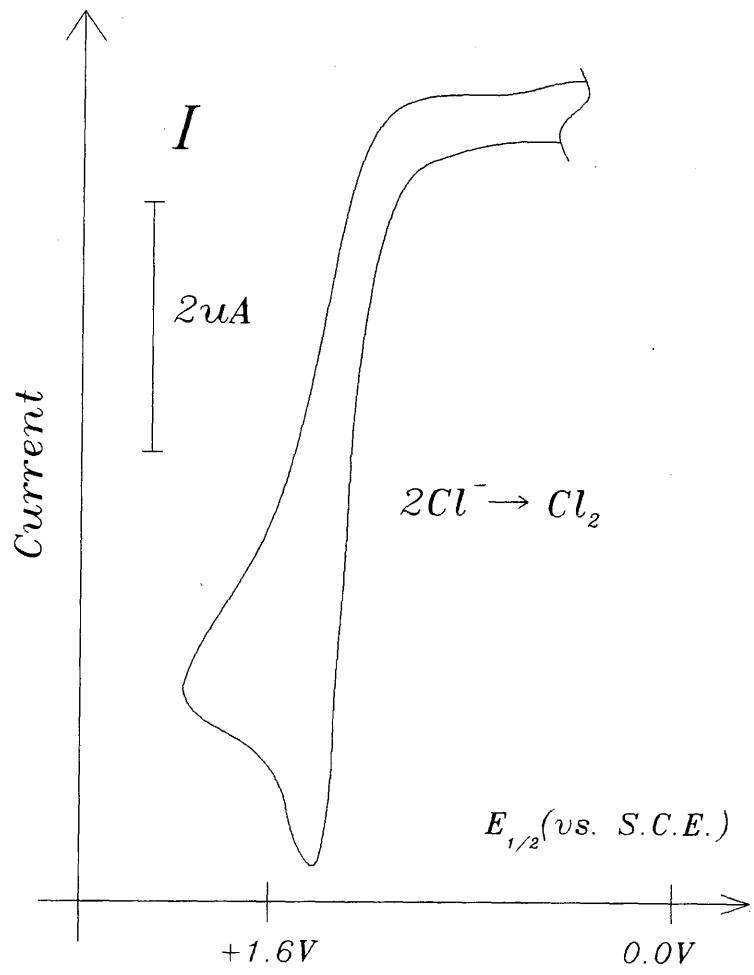

Figure 4.1: D.C. cyclic voltammogram of $[Bu_4N]Cl$.
Conditions; $[Bu_4N]PF_6$ (0.3M)/$[Cl^-]$ (0.005M) at micro-Pt electrode in CH_2Cl_2 solution, temperature:-40°C, reference; ferrocene, sweep rate; 100mV/sec (D.C.).

irreversible oxidation Cl^-/Cl_2 was observed at $E_p^a = +1.44V$ (vs.S.C.E.) in CH_2Cl_2 at -40°C. The D.C. cyclic voltammogram of $[Bu_4N]Cl$ in CH_2Cl_2 at -40°C is shown in figure 4.1.

[Note: Mechanism 4.4 proposed by Kolthoff and Coetzee is intriguing because it conforms to the accepted mechanism of Br^- and I^- oxidation in non-aqueous solvents (sections 4.2 and 4.3). It could be that initial oxidation of Cl^- does produce Cl_3^-, but that Cl_3^- immediately disproportionates to Cl^- and Cl_2 according to equilibrium 4.5. The reaction is then essentially the same as 4.3 with the oxidation of two moles of Cl^- to form one mole of Cl_2 with the passage of 2e. Since free Cl^+ is not known in solution (except as Cl_3^+ in super-acid media [194]) the second wave observed by Kolthoff and Coetzee must then be assigned to an impurity or possibly an oxychloro species formed between chlorine/chloride and adsorbed oxygen.]

4.2 The cyclic voltammetric study of the bromide-bromine system in methylene chloride at a platinum electrode

4.2.1 Results

Tetra-n-butylammoniumbromide, $[Bu_4N]Br$, exhibited two distinct electrochemical processes in CH_2Cl_2 solution at both room temperature and -40°C in both the A.C. and D.C. cyclic voltammetry modes (table 4.2). In the D.C. mode the first process, wave I, an anodic wave at $E_p^a = +0.79V$ (vs.S.C.E.) was totally irreversible at both room temperature and -40°C. In the A.C. mode, wave I was very broad at room temperature and was too broad to distinguish from wave II at -40°C. When Br_2 was added to the solution of Br^- in CH_2Cl_2, wave I was no longer visible in either the A.C. or D.C. modes.

In the D.C. mode the second process, wave II at $E_{1/2} = +1.05V$ (vs.S.C.E.) was quasi-reversible at room temperature and -40°C. The peak separation ΔE_p was markedly dependent on the sweep rate, varying between 100mV and 200mV at 100mV/sec and 500mV/sec respectively. In the A.C. mode, wave II was very broad at

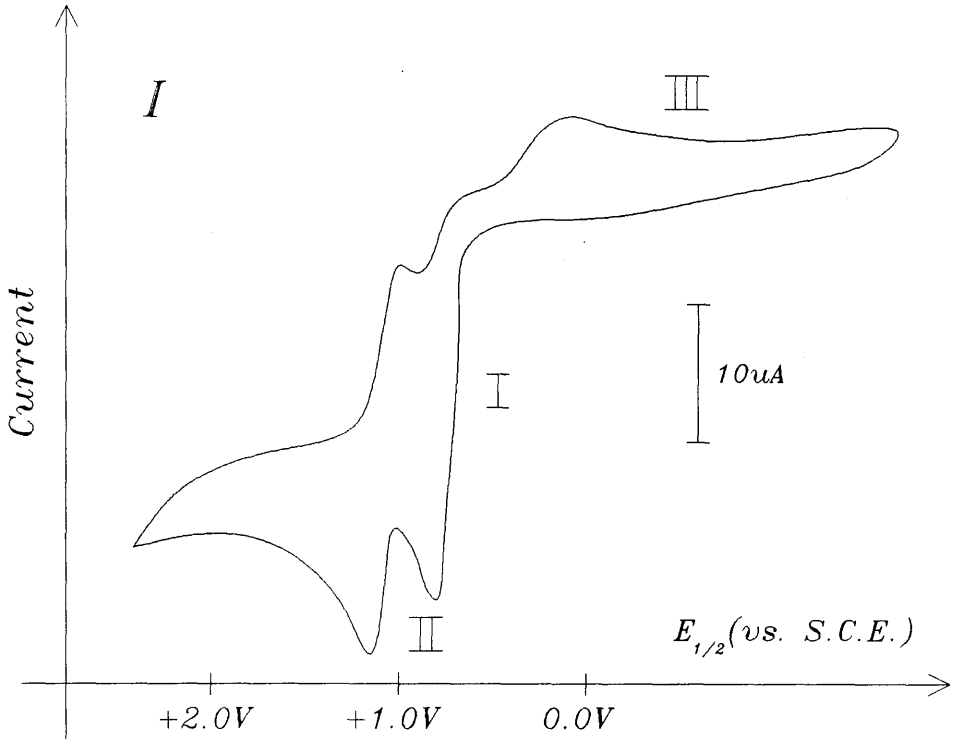

Figure 4.2: D.C. cyclic voltammogram of [Bu_4N]Br.
Conditions; [Bu_4N]PF_6 (0.3M)/[Br^-] (0.005M) at micro-Pt electrode in CH_2Cl_2 solution, temperature:room temp., reference; ferrocene, sweep rate; 100mV/sec (D.C.).

room temperature with a half-width of 210mV. When the temperature was lowered to -40°C, the half- width of wave II was unobtainable because the broadness of wave I made waves I and II almost indistinguishable.

In the D.C. mode, if the anodic potential sweep was reversed at a potential $\geq$ +0.79V (the peak potential of wave I), then a broad cathodic wave, wave III, was observed between +0.16 and +0.30V (vs.S.C.E.)(figure 4.2). Wave III was not observed in the A.C. mode at either room temperature or -40°C indicating a high degree of irreversibility.

4.2.2 Discussion

Mastragostino *et al* [46] have previously studied the electrochemistry of the Br_3^-/Br_2 system in CH_2Cl_2 at a platinum electrode. Using periodic renewal of the diffusion layer voltammetry (P.R.D.L.V.) and a 5.25mM solution of tetrabutylammoniumbromide in CH_2Cl_2 they observed two irreversible oxidation waves; wave I at $E_{1/2}$ = +0.75V (vs. S.C.E.) and wave II at $E_{1/2}$ = +1.06V (vs.S.C.E.) in good agreement with this thesis. Mastragostino *et al* observed positive and negative potential shifts of waves I and II respectively with decreasing concentration of bromide. By coulometry they calculated the number of moles of electrons exchanged per mole of Br^- for processes I and II were 2/3 and 1/3 respectively, which led them to postulate the following general mechanism for the bromide/bromine couple:-

$$\begin{aligned} 3Br^- &\rightleftharpoons Br_3^- + 2e \quad (I) \\ 2Br_3^- &\rightleftharpoons 3Br_2 + 2e \quad (II) \end{aligned} \tag{4.6}$$

The results obtained in this thesis from the cyclic voltammetric study of $[Bu_4N]Br$ in CH_2Cl_2 are consistent with mechanism 4.6 ; the ratio of anodic peak currents, $i_p^a(I)$: $i_p^a(II)$, was approximately 2:1, indicating twice as many electrons per mole of bromide were involved in wave I compared with wave II (figure 4.2); and when Br_2 was added to the solution of Br^-, wave I was no longer observable.

The significance of the latter observation can be explained as follows : for the equilibrium

$$Br_2 + Br^- \rightleftharpoons Br_3^- \tag{4.7}$$

the stability constant of the tribromide ion is given by

$$\beta(Br_3^-) = \frac{[Br_3^-]}{[Br_2][Br^-]} \tag{4.8}$$

In non-aqueous solutions the stability constant of Br_3^- is increased dramatically

with respect to an aqueous environment [85] (table 4.1).

Table 4.1: The stability constant of the Br_3^- ion in various solvents.

solvent	$\log_{10}(\beta)$	reference
acetone	9.00	85
nitromethane	7.00	85
acetonitrile	7	85
water	1.23	87

Although the value of $\beta(Br_3^-)$ is not known for CH_2Cl_2 solution, the Br_3^- ion is expected to be much more stable in CH_2Cl_2 than in H_2O. In this thesis, when Br_2 was added to the solution of Br^- in CH_2Cl_2, according to equilibrium 4.7 the Br^- ions were converted into Br_3^- and so in agreement with mechanism 4.6 it was no longer possible to observe wave I.

Table 4.2 shows the electrode potentials of $[Bu_4N]Br$ obtained in CH_2Cl_2 in this thesis and figure 4.2 shows the D.C. cyclic voltammogram of $[Bu_4N]Br$ in CH_2Cl_2 at room temperature.

4.2.3 The cyclic voltammetric study of hexabromometallate complexes

In chapter three it was remarked upon, on several occasions, that the exposure of hexabromometallate complexes to potentials more positive than the relevant $[MBr_6]^{1-/2-}$ redox couple resulted in complicated electrochemical activity at those potentials. Adsorbed species were believed to be a product of this process because a 'pointed' symmetrical cathodic peak (see for example figure 3.5), which are strongly suggestive of adsorbed species (section 2.12), were recorded on the D.C. cyclic voltammograms of the complexes under consideration. The presence of adsorbed species has been considered by previous workers to be an integral process of bromide electrochemistry in both aqueous [43,44,78] and non-aqueous [46] solution which therefore suggested some form of degradation reaction of the hexabromometallate complexes with expulsion of Br^- or Br_2 was occurring. However, degradation must be discounted for two

Table 4.2: The electrode potentials of $[Bu_4N]Br$

D.C. mode				
temp. (^oC)	$E_{1/2}$ (V) (vs.S.C.E.)	ΔE_p (mV)	i_p^a/i_p^c	couple
+25	+0.79[a]	irrev.	-	Br^-/Br_3^-
+25	+1.05	100	1.0	Br_3^-/Br_2
-40	+0.79[a]	irrev.	-	Br^-/Br_2
-40	+1.05	170	1.0	Br_3^-/Br_2

A.C. mode			
temp. (^oC)	$E_{1/2}$ (V) (vs.S.C.E.)	half-width (mV)	couple
+25	+0.78	>220	Br^-/Br_3^-
+25	+1.05	210	Br_3^-/Br_2
-40	-	-	Br^-/Br_3^-
-40	+1.05	-	Br_3^-/Br_2

Conditions; $[Bu_4N]PF_6$ (0.3M)/$[Br^-]$ (0.005M) at micro-Pt electrode in CH_2Cl_2 solution,reference; ferrocene, sweep rate; 100mV/sec (D.C.), 20mV/sec (A.C.), [a] anodic peak potential

reasons:-

1. The distinctive appearance of bromide electrochemical activity between +0.8V and +1.1V (vs.S.C.E.) was only once observed (with $[Bu_4N]_2[PtBr_6]$) during the cyclic voltammetric studies of second and third row transition metal hexabromometallates.

2. When the anodic potential sweep was reversed at +2.0V say, the relevant $[MBr_6]^{1-/2-}$ couple still appeared as a quasi- if not fully reversible couple when the whole potential cycle was completed . If the complexes did break up with the expulsion of Br^- or Br_2 after oxidation to $[MBr_6]^{1-}$ then with an anodic switching potential much more positive than the relevant $[MBr_6]^{1-/2-}$ redox potential, a cathodic return wave corresponding to the reduction $[MBr_6]^{1-} \rightarrow [MBr_6]^{2-}$, should not have been observed.

Indeed, at more and more positive electrochemical potentials, the central transition metal ions would try to retain as much electron density around them as possible. The electrode reactions in these examples are evidently complicated and there is not enough information with which to specify the precise nature of the processes occurring. Nevertheless, the fact that the potential of the 'pointed' cathodic peak was variable and dependent on the identity of the metal complex does indicate the existence of some form of adsorbed metal-bromide species at strongly oxidizing potentials during the cyclic voltammetric studies of hexabromometallates. Given that no degradation reaction occurred but that complicated redox activity was detected, then the adsorbed species might possibly be linked with the uncharged $[MBr_6]^0$ compound.

The cyclic voltammetric study at room temperature of $[Bu_4N]_2[RuBr_6]$ (section 3.7) strongly suggested $[RuBr_6]^{3-}$ readily dimerized to $[Ru_2Br_9]^{3-}$ yet the resulting three mole equivalents of Br^- expected were not detected by cyclic voltammetry. This indicates either a) Br^- and/or Br_2 were not a factor during the investigation and the proposed reaction is wrong, or b) under the experimental conditions ie: in the presence of hexabromometallate complex, Br^- and/or Br_2 were not electroactive. It is very probable that the solvent- electrolyte system and/or the nature of the electrode

play an important role under the same conditions. The cyclic voltammetric study of hexabromotungstates (section 3.5) showed so called 'inert' background electrolytes like $[Bu_4N]PF_6$ and $[Bu_4N]BF_4$ are not strictly unreactive. And it might be of considerable benefit towards the understanding of hexabromometallate electrochemistry if the investigations in this thesis were repeated using alternative electrode materials such as graphite or carbon paste because as with the case of iodide (section 4.3), it may be possible for Br^- to be adsorbed onto platinum electrodes in a non-electroactive state.

4.3 The cyclic voltammetric study of the iodide-iodine system in methylene chloride at a platinum electrode

All potentials in this section are referenced versus the Ag-0.1M $AgNO_3$(in CH_3CN) reference electrode (equivalent to +0.38V vs.S.C.E.).

4.3.1 Tetra-n-butylammoniumiodide

$[Bu_4N]I$ exhibited two anodic processes in CH_2Cl_2: wave I at $E_p^a = +0.03V$ (vs.Ag/Ag^+) and wave II at $E_p^a = +0.42V$ (vs.Ag/Ag^+). Both processes appeared irreversible at both room temperature and -40°C. (Wave II showed some evidence of a cathodic return wave but the cyclic voltammogram was very poorly resolved and only the anodic wave could be confidently distinguished).

Biserni and Mastragostino [81] also investigated the electrochemistry of tetrabutylammoniumiodide in CH_2Cl_2 at a platinum micro-electrode by the method of linear sweep voltammetry with periodic renewal of the diffusion layer (P.R.D.L.V.). For a 3.3mM solution of I^- they observed two oxidation waves: wave I at $E_{1/2}$ = -0.06V and wave II at $E_{1/2} = +0.33V$ (vs.Ag/Ag^+). The degree of separation of the two oxidation waves was found to increase with increasing I^- concentration. Their coulometric measurements showed that the proportions of the number of moles of electrons exchanged for each mole of I^- were respectively 2/3 and 1/3 for the first and second

processes. By combining these results with their studies using P.R.D.L.V. on I_2 and I_3^- in CH_2Cl_2, (and in agreement with previous workers [76-80]), Biserni and Mastragostino concluded the mechanism of iodide oxidation in solvents stabilizing the trihalogenide ion (ie. non-aqueous solvents) was the following:-

$$\begin{aligned} 3I^- &\longrightarrow I_3^- + 2e \quad (I) \\ 2I_3^- &\longrightarrow 3I_2 + 2e \quad (II) \end{aligned} \tag{4.9}$$

Biserni and Mastragostino concluded that electrode reactions I and II were reversible in methylene chloride. Experimenting with a solution of I^- in acetonitrile, Popov and Geske [75] observed two oxidation waves by linear sweep voltammetry and although deviations from ideally reversible behaviour were observed, these were considered to arise from electrode surface effects and Popov and Geske concluded that both oxidation processes were electrochemically reversible. However, analysis of ΔE_p from cyclic voltammetry of I^- in CH_3CN solution by Hinman *et al* [79] and of I^- in propylene carbonate by Hanson and Tobias [80] concluded process I was irreversible and process II was, at best, quasi-reversible.

The cyclic voltammograms of I^- in CH_3CN solution and propylene carbonate obtained by previous workers exhibited two processes with both anodic waves and cathodic return waves. For example, Song [82] determined the electrochemistry of 1,1'-dimethyl-2,2' -bipyridiniumdiiodide in CH_3CN solution at a platinum electrode. The compound exhibited two distinguishable iodide couples: couple I at $E_{1/2}$ = -0.09V (vs.Ag/Ag^+), ΔE_p = 171mV and couple II at $E_{1/2}$ = +0.35V (vs.Ag/Ag^+), ΔE_p = 153mV.

Hence, although there is a consensus of opinion favouring mechanism 4.9, the kinetic natures of reactions I and II have not been agreed. Unfortunately, because the cyclic voltammogram of I^- in CH_2Cl_2 obtained in this thesis was not clearly resolved, the kinetic nature of processes I and II could not be specified precisely from the results of I^- electrochemistry. However, the cyclic voltammetric study of I_2 in CH_2Cl_2 discussed in the next section (4.3.2) indicated that electrode reactions I and II were both irreversible.

The electrode potentials of I^- obtained by cyclic voltammetry in CH_2Cl_2 in this thesis are shown in table 4.3 along with those obtained by other workers in CH_2Cl_2 and CH_3CN. It was noticeable that while Dryhurst and Elving [77] reported a third anodic wave for I^- in CH_3CN solution at +1.15V, a third anodic wave was not observed in CH_2Cl_2 either in this thesis or by Biserni and Mastragostino [81]. Dryhurst and Elving assigned wave III to a cationic iodine species which agrees with the known ability [84] of CH_3CN to stabilise I(1+). Since CH_2Cl_2 is a poorer donor solvent than CH_3CN it is likely that cationic iodine species are too unstable in CH_2Cl_2 to be observed by cyclic voltammetry under normal conditions.

Table 4.3: Electrode potentials[a] of iodide in non-aqueous solvents at a platinum micro-electrode.

solvent	E(I)/(V)	E(II)/(V)	E(III)/(V)	ref.
CH_3CN[b]	+0.04	+0.37	+1.15	77
CH_3CN	-0.09	+0.35	-	82
CH_2Cl_2	+0.03	+0.42	-	this work
CH_2Cl_2[c]	-0.06	+0.33	-	81

[a] electrode potentials referenced vs. $Ag/AgNO_3$(in CH_3CN) [b] pyrolytic graphite electrode [c] re-referenced using $E(Ag/Ag^+)$ = +0.38V (vs.S.C.E.)

4.3.2 Iodine

In contrast with $[Bu_4N]I$, the room temperature cyclic voltammogram of I_2 in CH_2Cl_2 at a platinum electrode obtained in this thesis exhibited two well defined redox couples with both cathodic and anodic waves which were distinguishable at sweep rates in excess of 50mV/sec (figure 4.3). As the electrochemical reactions of I_2 and I^- are expected to follow the same mechanism, with reference to mechanism 4.9 the two iodine redox couples were assigned as follows : couple I at $E_{1/2}$ = -0.12V (vs.Ag/Ag^+) was assigned to the electrode reaction I and couple II at $E_{1/2}$ = +0.42V (vs.Ag/Ag^+)

was assigned to electrode reaction II. Both iodine couples were electrochemically irreversible at room temperature with large ΔE_p's and peak current ratio's i_p^a/i_p^c greater than 1.0 for sweep rates in the range 50-100mV/sec (D.C.). The electrode potentials of I_2 in CH_2Cl_2 obtained in this thesis are shown in table 4.4.

Table 4.4: The electrode potentials of I_2 in CH_2Cl_2

	wave I			wave II		
sweep rate (mV/sec)	$E_{1/2}$ (V)	ΔE_p (mV)	i_p^a/i_p^c	$E_{1/2}$ (V)	ΔE_p (mV)	i_p^a/i_p^c
50	-0.13	233	1.33	+0.40	217	1.27
100	-0.12	249	1.19	+0.41	202	1.09
200	-0.12	295	1.17	+0.42	194	1.07

Conditions: $[Bu_4N]PF_6$ (0.3M)/I_2 (0.005M) at a micro-Pt electrode in CH_2Cl_2, reference; Ag/0.1M $AgNO_3$ (in CH_3CN), temperature; $+25°C$.

Biserni and Mastragostino [81] observed two iodine couples using P.R.D.L.V. with a 1.5mM solution of I_2 in CH_2Cl_2 at $E_{1/2}$ = -0.19V (vs.Ag/Ag^+) and $E_{1/2}$ = +0.35V (vs.Ag/Ag^+). The ca. 0.07V increase in $E_{1/2}$ of reactions I and II between the results of Biserni and Mastragostino and the $E_{1/2}$ values obtained in this thesis can be attributed to the different concentrations of I_2 in CH_2Cl_2 used (table 4.5). Popov and Geske [75] have previously noted that $E_{1/2}$ for electrode reactions I and II shifted to more positive potential when the concentration of I_2 in CH_3CN solution was increased. These results indicate that in non aqueous solvents in the I_2 concentration range 1-5mM, couples I and II become more thermodynamically stable with increasing I_2 concentration.

4.3.3 Discussion

Table 4.5 compares the electrode potentials of iodine obtained in this thesis with those obtained by previous workers. Ideally the ratio of anodic currents should equal

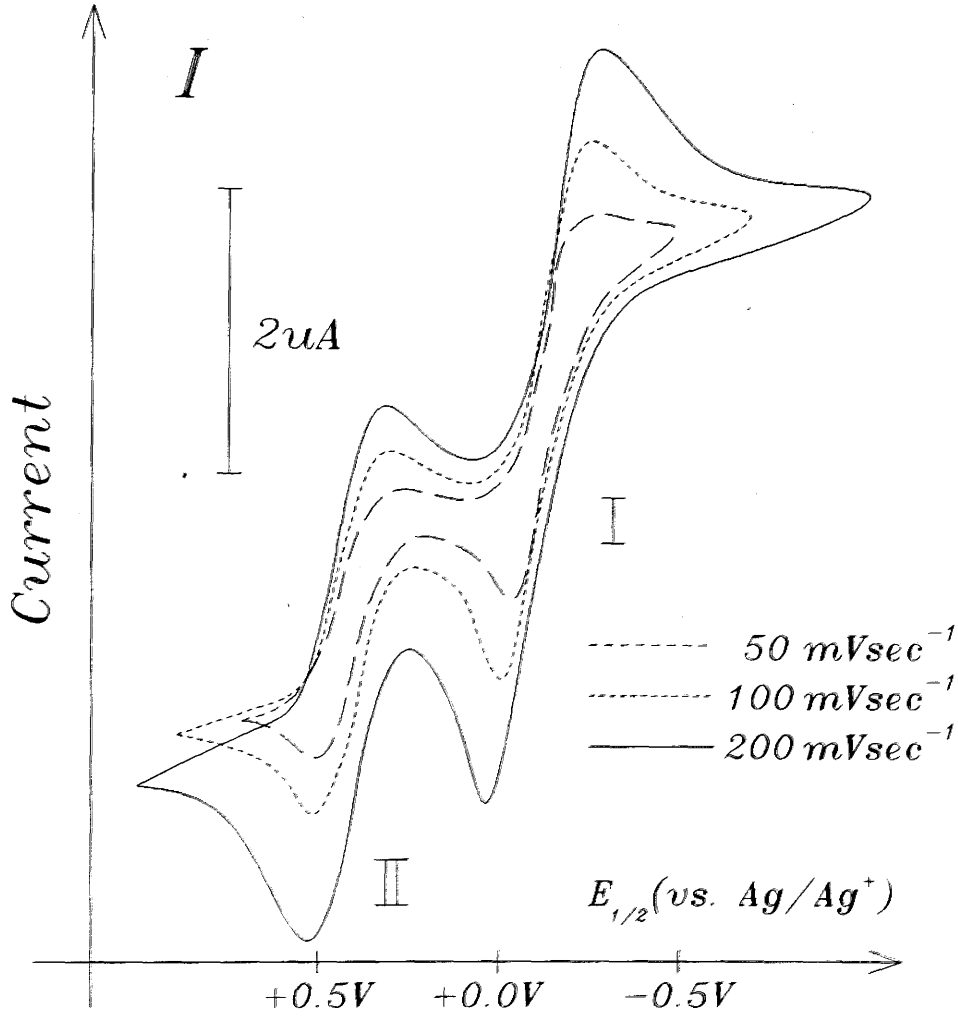

Figure 4.3: D.C. cyclic voltammogram of I_2.
Conditions; $[Bu_4N]PF_6$ (0.3M)/I_2 (0.005M) at micro-Pt electrode in CH_2Cl_2 solution, temperature:room temp., reference: ferrocene.

Table 4.5: Comparison of the electrode potentials of I_2

solvent	I_2 conc. (mM)	$E_{1/2}$ (I) (V)	$E_{1/2}$ (II) (V)	i(I)/i(II)	ref.
CH_3CN	1.0	-0.16	+0.32	1.55[a]	[75]
CH_2Cl_2[b]	1.5	-0.19	+0.35	1.60[a]	[81]
CH_2Cl_2	5.0	-0.12	+0.42	1.50[c]	[d]

[a] ratio of the limiting currents of processes I and II [b] potentials re-referenced using $Ag/(0.1M)AgNO_3$ = +0.38V vs S.C.E. [c] ratio of the anodic peak currents $i_p^a(I)/i_p^a(II)$ [d] This work

2.0 according to reaction scheme 4.7. However, the current ratio i(I)/i(II) was substantially less than 2.0 when iodine was the only species initially present. Biserni and Mastragostino [81] found the ratio i^I/i^{II} was approximately 2.0 when either I^- or I_3^- was the initial reactant in solution but could not explain the anomalous behaviour of I_2.

A possible explanation can be deduced from the thin-layer electrochemical experiments of Hubbard and Osteryoung [83] who studied the adsorption of iodide and iodine at platinum electrodes in acid solution. They found approximately $2x10^{-9}$ $molcm^{-2}$ of I^- ion or $2x10^{-9}$ $molcm^{-2}$ I_2 was adsorbed in a non-electroactive state and an additional $1x10^{-9}$ $molcm^{-2}$ I_2, but not I^- was adsorbed in an electroactive state. Popov and Geske [75] observed that it was the increase in the current constant for wave II that was responsible for the decrease of the ratio i(I)/i(II) below 2.0. The increased current constant of the reaction

$$2I_3^- \longrightarrow 3I_2 + 2e \qquad (II) \tag{4.10}$$

when I_2 was the initial reactant present in solution can then be explained by the presence of weakly adsorbed, electroactive I_2 on the platinum electrode. The

anodic peak current of reaction II, i_p^a(II), was thereby enhanced by a contribution from electroactive weakly pre-adsorbed I_2 in addition to the normal diffusion current.

Hanson and Tobias [80] found that although the anodic peak separation E_p^a(II)-E_p^a(I) remained constant at 440mV in propylene carbonate (cf. 470mV in CH_2Cl_2 in this thesis) the separation between the corresponding cathodic peaks, E_p^c(II) -E_p^c(I) was dependent on the history of the potential scan (ie. the switching potential) and the sweep rate. The same dependency was observed in this thesis with I_2 in CH_2Cl_2 solution. When the anodic potential sweep was reversed at potentials progressively greater than +1.4V then the cathodic peaks of processes I and II were shifted to progressively more negative potential. Eventually a situation occurred where the anodic and cathodic sweeps crossed one another , a phenomenon which is associated with deposition of metals onto electrodes [27]. The expected enhancement of anodic current i_p^a(I) due to a deposition process on the cathodic sweep was not observed and so the most appropriate conclusion would be that the oxidation of I_2 at large positive potentials alters the nature of the electrode surface, possibly due to formation of species with cationic iodine.

4.3.4 The triiodide-iodine equilibrium

For the equilibrium

$$I_2 + I^- \rightleftharpoons I_3^- \tag{4.11}$$

the stability constant β of the triiodide ion is given by

$$\beta\,(I_3^-) = \frac{[I_3^-]}{[I_2]\,[I^-]} \tag{4.12}$$

A characteristic feature of polyhalide solutions [85] in most non-aqueous solvents is a dramatic increase in the stability constant of the polyhalide ions with respect to aqueous solution (table 4.6).

Table 4.6: The stability constant of the I_3^- ion in various solvents.

solvent	$\log_{10}(\beta)$	reference
dichlorobenzene	8.80	[86]
acetone	8.3	[49]
dichloromethane	~8.00	[81]
tetramethylsulpholane	7.49	[86]
dichloroethane	7.20	[86]
nitromethane	6.7	[49]
acetonitrile	6.6	[49]
methanol	4.20	[86]
water	2.85	[87]

The large value of $\beta(I_3^-)$ in non-aqueous solvents has a marked effect on the electrochemistry of iodide in the presence of iodine. Previous workers investigated the oxidation of iodide in CH_3CN and CH_3NO_2 using linear sweep voltammetry [74,76] and observed that addition of sufficient iodine to the solution of iodide prevented the observation of a wave corresponding to process I. Using cyclic voltammetry to study an equimolar solution of I^- and I_2 in CH_3CN, Dryhurst and Elving [77] could only observe a well formed wave I at higher sweep rates (160mV/sec) although at slower sweep rates (16mV/sec) an anodic process corresponding to wave I was observed indistinctly. A similar behaviour was observed in this thesis with the C.V. of an equimolar solution of I^- and I_2 in CH_2Cl_2 down to 50mV/sec sweep rate.

When a large excess of I^- had been added, the cyclic voltammogram of I^-/I_2 in CH_2Cl_2 (figure 4.4) began to resemble the cyclic voltammogram of Br^- in CH_2Cl_2 (section 4.2). If the experimental results are interpolated further, then at even greater I^- concentration, effectively I^- and a trace of I_2, a similar C.V. to that of Br^- would possibly have been observed.

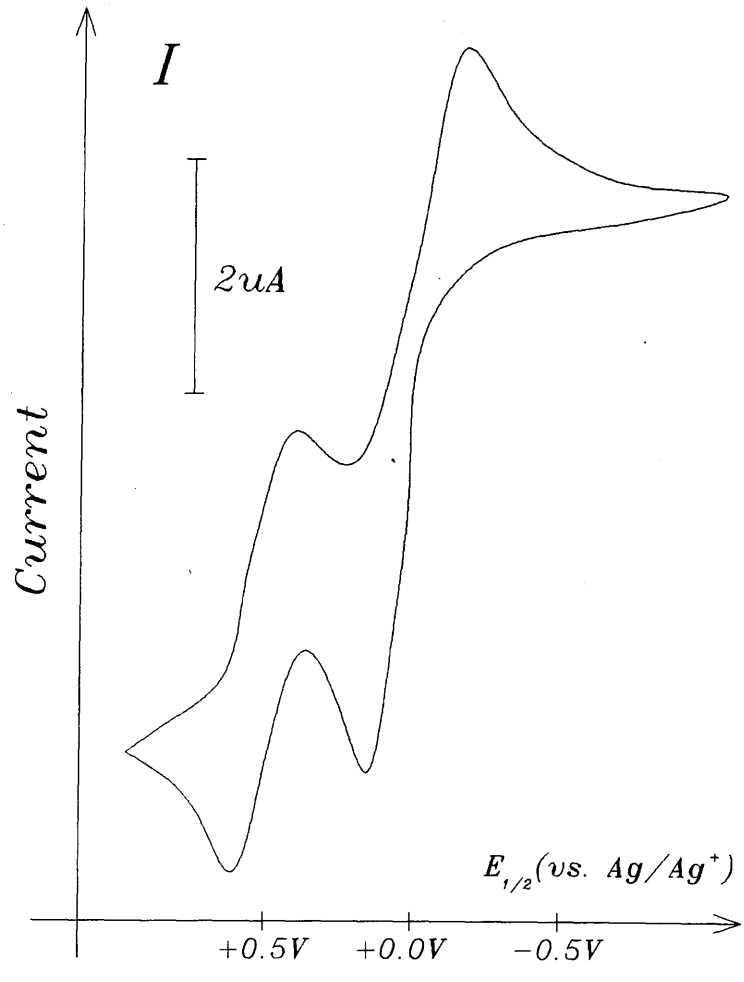

Figure 4.4: D.C. cyclic voltammogram of I_2 (with excess I^-.
Conditions; $[Bu_4N]PF_6$ (0.3M)/I_2 (0.005M) at micro-Pt electrode in CH_2Cl_2 solution, temperature:room temp., reference: ferrocene, sweep rate: 200mVsec^{-1} (D.C.).

Chapter 5

5.1 Introduction

The standard electrode potentials [116] of the first row transition metal hexaaquo - cations , $[M(H_2O)_6]^{2+}$, are listed in table 5.1. Previous authors [113,115, 116] have described the general trend of figure 5.1, a generally increasing potential across the period with a discontinuation between Mn(II) and Fe(II), in terms of ligand field effects and ionisation potentials.

Table 5.1: Standard electrode potentials of first row transition metal $[M(H_2O)_6]^{2+}$ (figures in brackets are estimates only).

metal	$E^{\circ}(M^{3+}/M^{2+})/V$	metal	$E^{\circ}(M^{3+}/M^{2+})/V$
Sc	(-2.6)	Fe	0.771
Ti	(-1.1)	Co	1.93
V	-0.26	Ni	(4.2)
Cr	-0.41	Cu	(4.6)
Mn	1.60	Zn	(7.0)

The redox potentials of second and third row transition metal hexahalometallates exhibit the same general trend as the first row transition metal hexaaquocations. In this chapter the trends exhibited are discussed in relation to the energy difference between different d^n configurations and the intrinsic differences between second and third row, and F^-, Cl^- and Br^-. The arguments expressed by Johnson [116] and Van

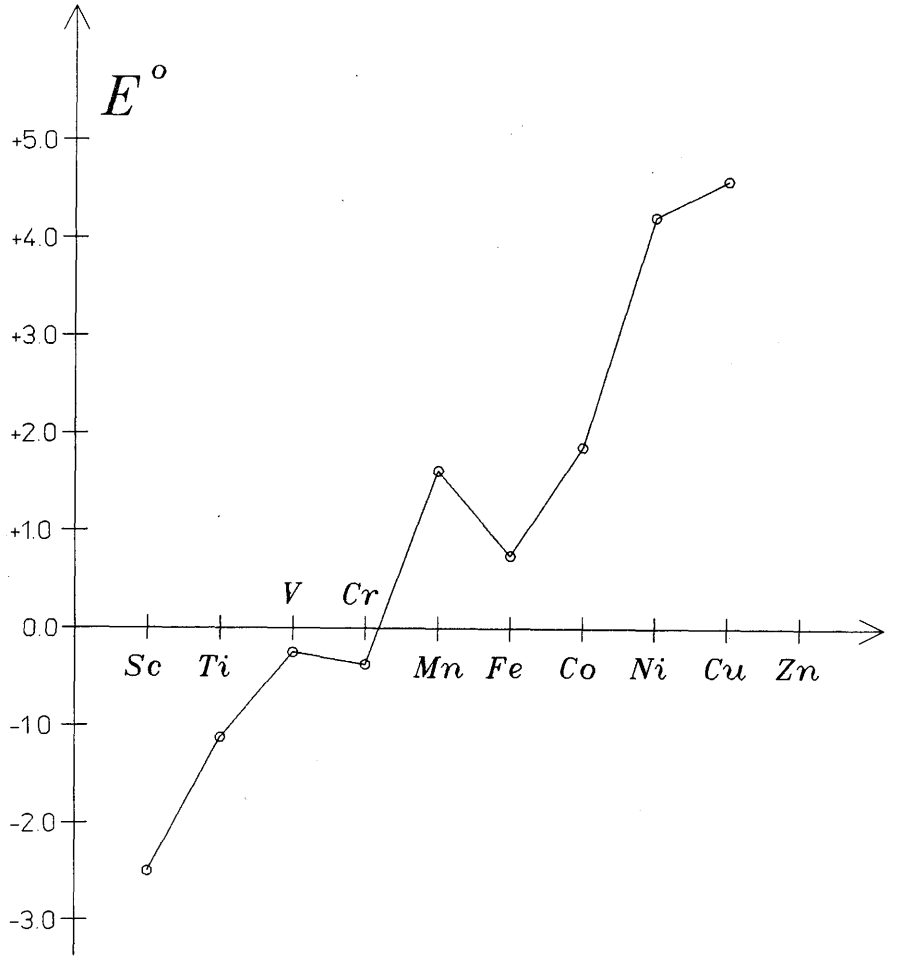

Figure 5.1: The standard electrode potentials of first row $[M(H_2O)_6]^{2+}$.

Gaal and Van der Linden [114] as well as Moock [31] were found to be most useful in this respect.

As in the previous chapters the couples $[MX_6]^{z/z-1}$ refer to :- M = Zr, Nb, Mo, (Tc), Ru, Rh, Pd, Hf, Ta, W, Re, Os, Ir and Pt; X = F^-, Cl^- and Br^-; z = 1-, 2-, 3- etc. The electrode potentials of the hexafluorometallates and hexachlorometallates (tables 5.2 and 5.3) are taken from references 55 and 41. Table 5.4 lists the redox potentials of the hexabromometallates obtained in this thesis.

Table 5.2: The electrode potentials of $[MF_6]^{z/z-1}$, $E_{1/2}$ in V (vs.S.C.E.) in CH_3CN (z = 0,-1,-2).

	oxidation state of the metal		
metal (M)	VI/V	V/IV	IV/III
Nb	-	-1.17	-
Mo	+2.08	+0.03	-1.87
(Tc)	-	+1.2[a]	-1.8[a]
Ru	-	+1.23	-0.87
Ta	-	-2.17	-
W	+1.08	-0.92	-
Re	+2.38	+0.18	-
Os	+3.28	+0.63	-1.92
Ir	-	+1.23[b]	-1.48[b]

[a]interpolated potential ; [b]CH_2Cl_2 solution

Table 5.3: The electrode potentials of $[MCl_6]^{z/z-1}$, $E_{1/2}$ in V (vs.S.C.E.) in CH_2Cl_2 (z = 0,-1,-2,-3).

	oxidation state of the metal			
metal (M)	VI/V	V/IV	IV/III	III/II
Zr	-	-	-2.53	-
Nb	-	+0.08	-1.32	-
Mo	+2.20	+1.05	-0.28	-
(Tc)	-	+2.0[a]	-0.8[a]	-
Ru	-	+1.61	-0.05	-1.6
Rh	-	+2.43	+0.72	-
Pd	-	+2.91	-	-
(Hf)	-	-	-3.1[b]	-
Ta	-	-0.55	-2.05	-
W	+1.59	+0.40	-1.15	-
Re	+2.35	+1.33	-1.12	-
Os	-	+1.28	-0.64	-2.0
Ir	-	+1.74	-0.02	-
Pt	-	+2.30	-	-

[a] interpolated potential [b] extrapolated potential; outside solvent range

Table 5.4: The electrode potentials of $[MBr_6]^{z/z-1}$, $E_{1/2}$ in V (vs.S.C.E.) in CH_2Cl_2 (z = -1,-2).

	oxidation state of the metal	
metal (M)	V/IV	IV/III
Zr	-	-1.82
Nb	+0.30	-0.89
Mo	+1.15	+0.06
(Tc)	+2.0[a]	-0.4[a]
Ru	+1.52[b]	+0.13
Ta	-0.16	-1.35
W	+0.59	-0.75
Re	+1.31	-0.89
Os	+1.24	-0.55
Ir	+1.63[b]	+0.15
Pt	+2.02[b]	-

[a]interpolated potential; [b]irreversible

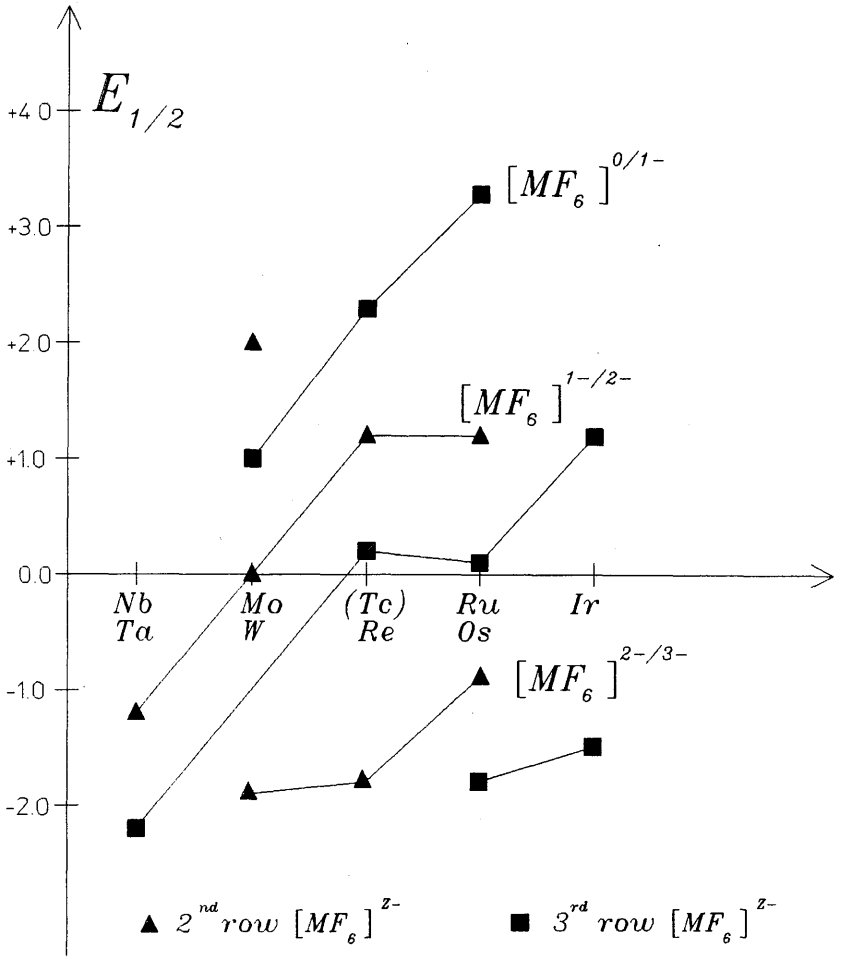

Figure 5.2: $E_{1/2}$(vs.S.C.E.) of second and third row transition metal $[MF_6]^z$ in CH_3CN.

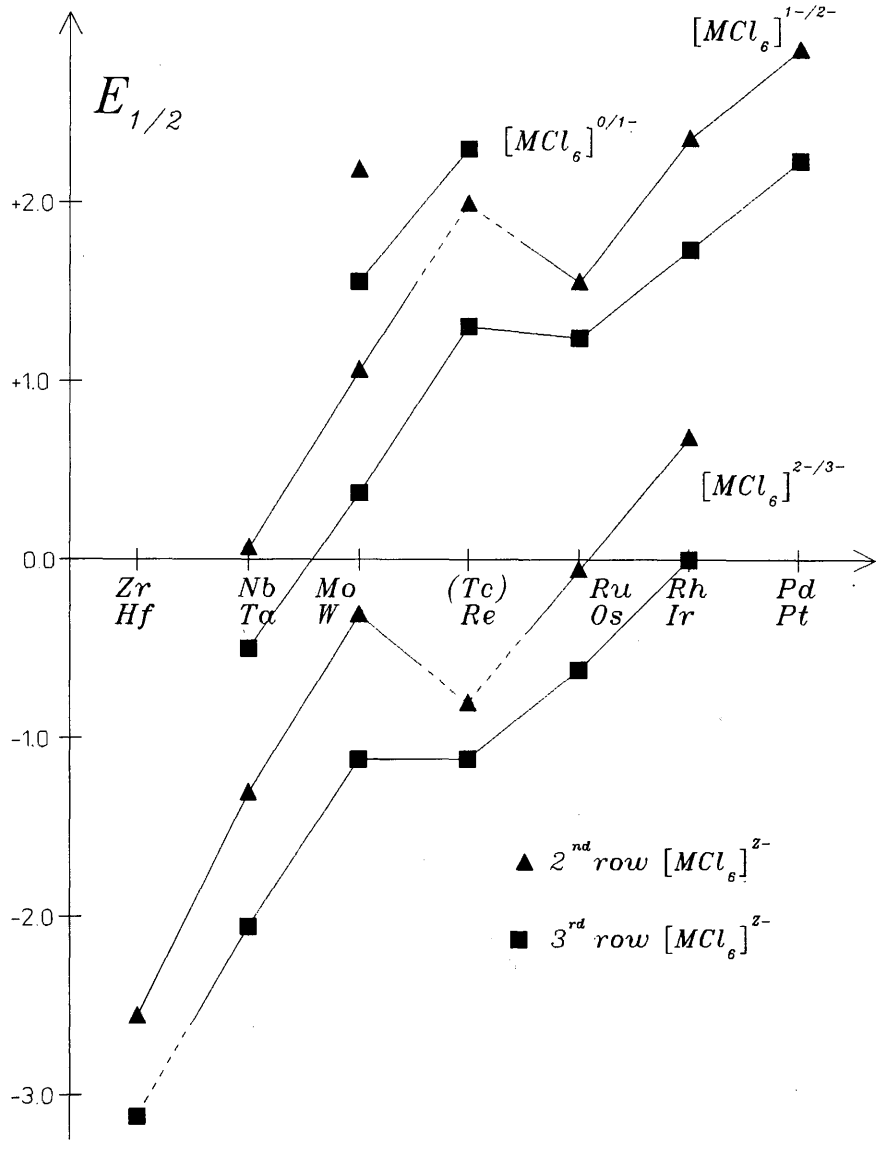

Figure 5.3: $E_{1/2}$(vs.S.C.E.) of second and third row transition metal $[MCl_6]^z$ in CH_2Cl_2.

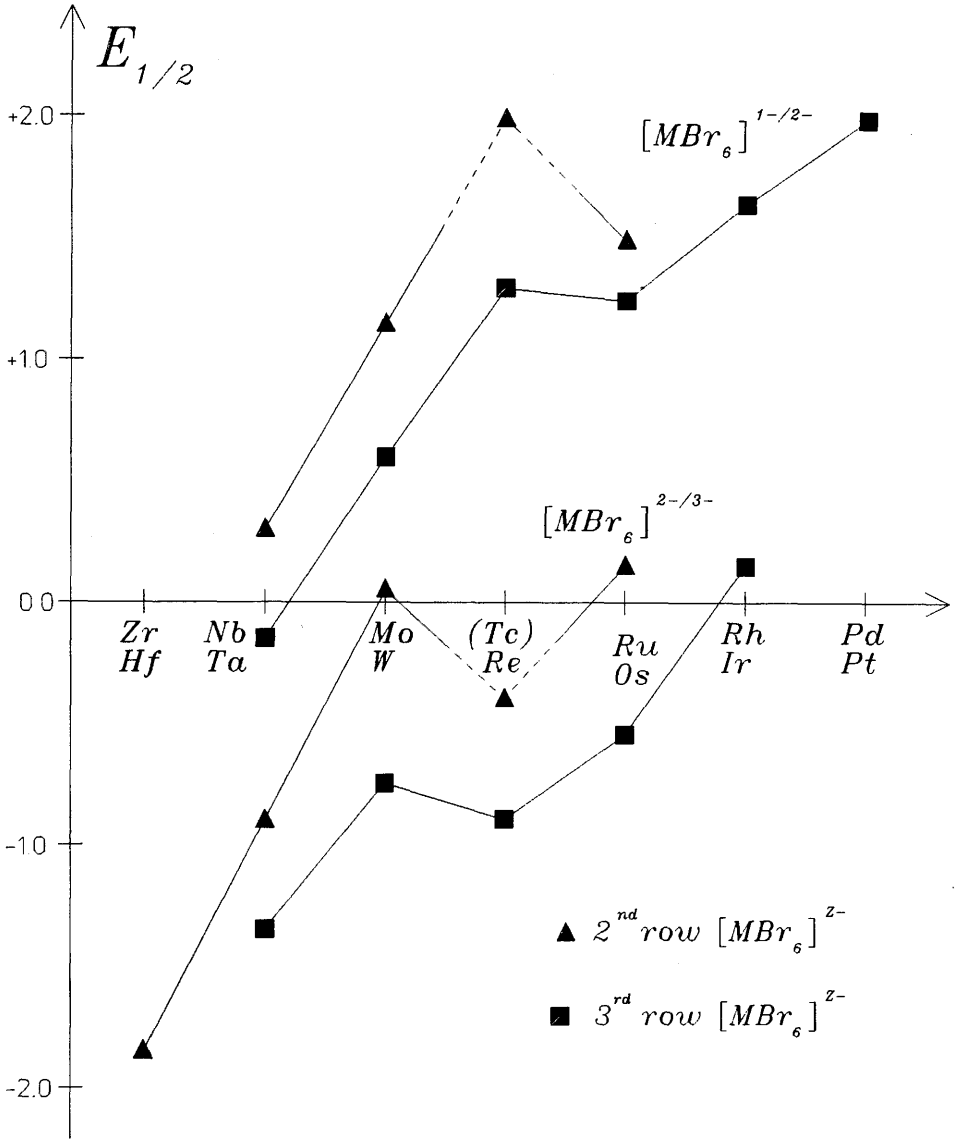

Figure 5.4: $E_{1/2}$(vs.S.C.E.) of second and third row transition metal $[MBr_6]^z$ in CH_2Cl_2.

5.2 The redox potentials of $[MF_6]^{z/z-1}$

As noted in section 5.1 the redox potentials of the hexafluorometallates of the second and third row transition metals have been studied by G.A. Heath, D.W.A.Sharp and their co-workers [55,117]. All the potentials given in table 5.2 were obtained in acetonitrile solution except the $[IrF_6]^{z/z-1}$ couples which were obtained in CH_2Cl_2 solution [31]. In figure 5.2 the electrode potentials of the second and third row hexafluorometallates are plotted versus atomic number.

5.3 The redox potentials of $[MCl_6]^{z/z-1}$

Taken from references [41] and [31] the electrode potentials of second and third row hexachlorometallates in CH_2Cl_2 are listed in table 5.3. In figure 5.3 the corresponding electrode potentials are plotted versus atomic number.

5.4 The redox potentials of $[MBr_6]^{z/z-1}$

The measurement of all the $[MBr_6]^{z/z-1}$ electrode potentials were described in chapter 3. The potentials are listed in table 5.4 and are plotted versus atomic number in figure 5.4.

5.5 Comparison of the redox potentials of second and third row transition metal hexahalometallates

Comparison of figures 5.2, 5.3 and 5.4 indicates that a number of similarities exist between the hexahalometallate redox systems:

5.5.1

The electrode potentials of isovalent hexahalometallate couples $[MX_6]^{z/z-1}$ increase regularly with increasing atomic number, except for a discontinuity at the $d^{3/4}$ couple. For the hexafluorometallates the electrode potentials increase in the order:-

$$nd^{0/1} \ll nd^{1/2} \ll nd^{2/3} < nd^{3/4} < nd^{4/5} \tag{5.1}$$

whereas for the hexachloro- and hexabromometallates the electrode potentials increase in the order:-

$$nd^{0/1} \ll nd^{1/2} \ll nd^{2/3} \geq nd^{3/4} < nd^{4/5} < nd^{5/6} \tag{5.2}$$

5.5.2

$[MX_6]^z$ ions become more oxidizing with increasing oxidation state of the metal. Hence for a given metal M and halogen X, the value of the couple $[MX_6]^{z/z-1}$ is always greater (more +ve) than the value of the couple $[MX_6]^{z-1/z-2}$ ie;

$$E_{1/2}\left([MX_6]^{z/z-1} \right) > E_{1/2}\left([MX_6]^{z-1/z-2} \right) \tag{5.3}$$

for given M and X.

5.5.3

Third row transition metal hexahalometallate ions are more reducing than their isoelectronic second row counterparts. eg:

$[RuBr_6]^{2-/3-}$ at $E_{1/2}$= +0.13V (vs.S.C.E.)
$[OsBr_6]^{2-/3-}$ at $E_{1/2}$= -0.55V (vs.S.C.E.)

Figures 5.5 and 5.6 show the isovalent series of $[MX_6]^{1-/2-}$ and $[MX_6]^{2-/3-}$ electrode potentials superimposed on one another for the second and third row transition metals respectively. A number of features are apparent which, with reference to the generalized scheme ABCD are :-

5.5.4

Although slight deviations from ideally straight lines occur, the average gradient of section AB is greater than the average gradient of section CD. Hence the average difference in value between adjacent redox couples of an isovalent series is greater between $d^{0/1}$ and $d^{2/3}$ than between $d^{3/4}$ and $d^{5/6}$.

5.5.5

Comparing between the isovalent hexahalometallate series $[MX_6]^{z/z-1}$, the overall slope dE/dn increases in the sense :

$$[MF_6]^{z/z-1} \gg [MCl_6]^{z/z-1} > [MBr_6]^{z/z-1} \qquad (5.4)$$

5.5.6

The discontinuity occurring between $d^{2/3}$ and $d^{3/4}$ is more pronounced ie; P is greater. for second row than third row transition metal hexahalometallates.

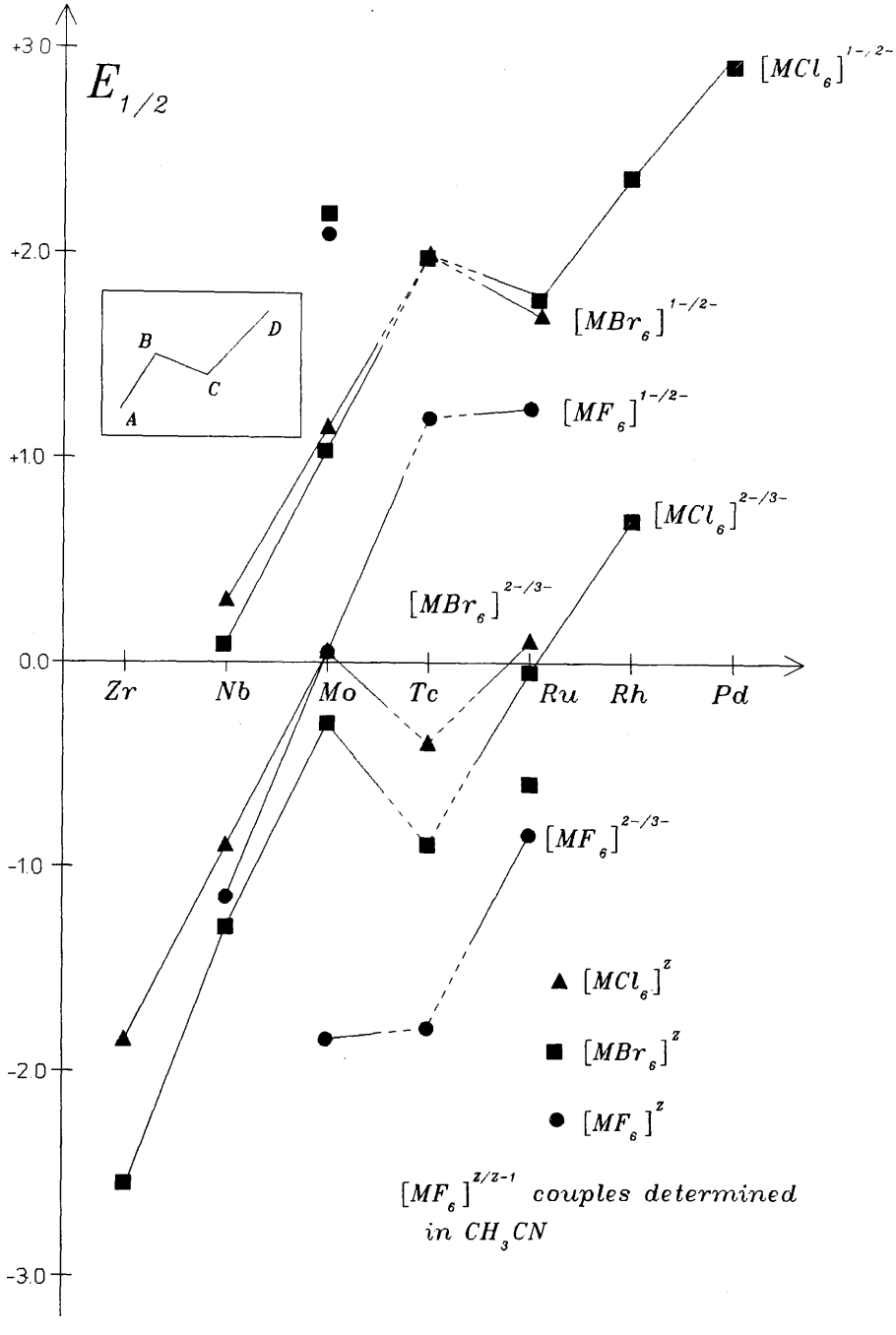

Figure 5.5: $E_{1/2}$(vs.S.C.E.) of second row transition metal $[MX_6]^z$ in CH_2Cl_2.

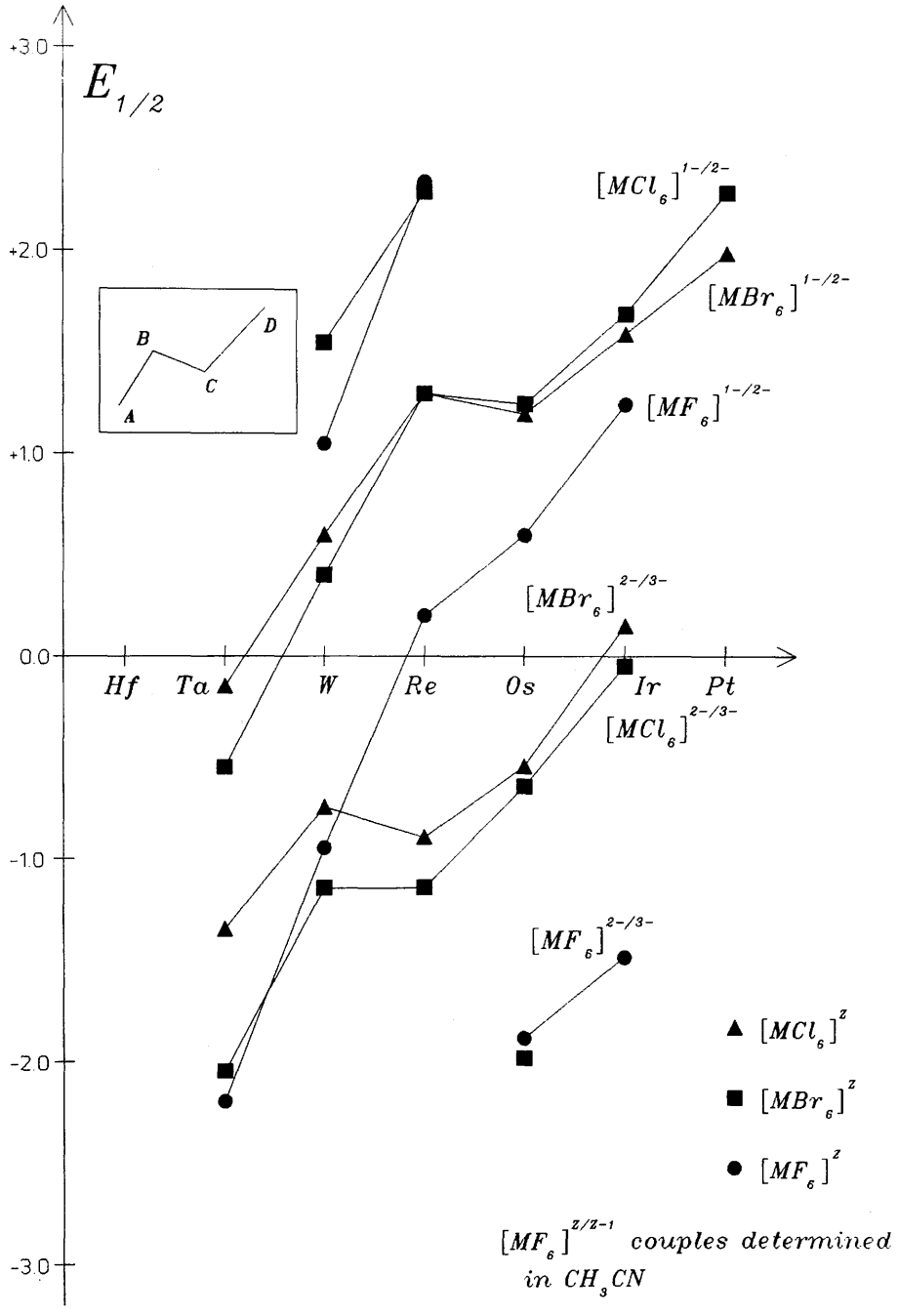

Figure 5.6: $E_{1/2}$(vs.S.C.E.) of third row transition metal $[MX_6]^z$ in CH_2Cl_2.

5.6 Reversible (equilibrium) potentials

For the reversible redox couple

$$[MX_6]^z + e \rightleftharpoons [MX_6]^{z-1} \tag{5.5}$$

the standard free energy change of the reaction ΔG^o, and the reversible electrode potential E^o are related to the equilibrium constant K by :-

$$\Delta G^o = -RT \ln K \tag{5.6}$$

and

$$E^o = \frac{RT}{nF} \ln K \tag{5.7}$$

combining 5.6 and 5.7 gives

$$\Delta G^o = -nFE^o \tag{5.8}$$

Strictly speaking, the redox potential is a measure of the free energy difference between the reduced and the oxidized species in equation 5.5 including solvent effects and other variables, ie;

$$E^o \propto \sum \text{free energies } [MX_6]^{z-1} - \sum \text{free energies } [MX_6]^z \tag{5.9}$$

However, the free energy change involved in reaction 5.5 is also a function of enthalpy, entropy and temperature from

$$\Delta G = \Delta H - T\Delta S \tag{5.10}$$

Therefore equation 5.9 can be re-written as :-

$$E^{o} \propto \sum(H[MX_6]^{z-1} - H[MX_6]^{z}) - T\sum(S[MX_6]^{z-1} - S[MX_6]^{z}) \qquad (5.11)$$

(M = metal; X = F, Cl, Br; z = 0,-1,-2,-3)

Hence the dependence of the electrode potential on the free energy difference between the reduced and the oxidized species (equation 5.5) is composed of two separate contributions: the enthalpy change and the entropy change of the reaction. The separate contributions are discussed independently in the following sections.

5.7 The effect of the entropy term on the electrode potential

The entropy contribution to the redox potential of the reversible electron transfer between the platinum electrode and hexahalometallate ion is a measure of the change in disorder of the system. As the octahedral structure of each hexahalometallate ion is maintained during reversible electron transfer, significant entropy changes only arise from changes in the structure of the solvation shell surrounding the ion.

The surrounding solvation shell or secondary solvation sphere [120] contains partly oriented solvent molecules which have some translational freedom, unlike the molecules in the bulk solvent which have both random orientation and translational freedom. Reversible electron transfer to or from the central metal ion in hexahalometallate ions affects the secondary solvation sphere in two ways:-

1. Changes in the metal-halogen bond length require an alteration to the volume of the solvation sphere.

2. Electrostatic considerations imply that an increase in the overall charge of a complex ion produces an increase or decrease in the ordering of surrounding solvent molecules and hence a decrease or increase in the reaction entropy.

5.7.1 The Born approximation

One of the simplest quantitative treatments of the solvent-solute interaction is to regard the solvent as a dielectric, situated in the field of complex ions which are considered as electrically charged spheres. The free energy change associated with solvation of one mole of ions can then be estimated by the Born expression [121] :-

$$\Delta G_{I-S} = \text{-L}\frac{(\text{z}_i\text{e}_o)^2}{8\pi\epsilon_o \text{r}_i}\left(1 - \frac{1}{\text{D}}\right) \tag{5.12}$$

ΔG_{I-S}= free energy of ion solvation in solvent s; L = Avogadro's constant; z_i = charge on ion; e_o = electronic charge; r_i = radius of ion; D = solvent dielectric constant; ϵ_o = vacuum permittivity (= $8.854\text{x}10^{-12}\text{Fm}^{-1}$).

Then that part of the free energy change during reaction 5.5 which arises from the rearrangement of the secondary solvation sphere can be approximated by :-

$$\Delta G_{I-S} = \frac{\text{-Le}_o^2}{8\pi\epsilon_o}\left(1 - \frac{1}{\text{D}}\right)\left(\frac{\text{z}_{red}^2}{\text{r}_{red}} - \frac{\text{z}_{ox}^2}{\text{r}_{ox}}\right) \tag{5.13}$$

differentiating equation 5.10 with respect to temperature

$$\left(\frac{\partial \Delta G}{\partial \text{T}}\right)_p = -\Delta S \tag{5.14}$$

Therefore the Born entropy change arising from the rearrangement of the secondary solvation sphere (and hence the entropy contribution to the overall free energy change) is approximated by :-

$$(\Delta S)_{Born} = \frac{\text{Le}_o^2}{8\pi\epsilon_o \text{D}^2}\left(\frac{\partial \text{D}}{\partial \text{T}}\right)\left(\frac{\text{z}_{red}^2}{\text{r}_{red}} - \frac{\text{z}_{ox}^2}{\text{r}_{ox}}\right) \tag{5.15}$$

Finally, that part of the enthalpy change during reaction 5.5 arising from the rearrangement of the solvation sphere can be approximated by

$$(\Delta H)_{Born} = \frac{-\,Le_o^2}{8\pi\epsilon_o}\left(1 - \frac{1}{D} - \frac{T}{D^2}\frac{\partial D}{\partial T}\right)\left(\frac{z_{red}^2}{r_{red}} - \frac{z_{ox}^2}{r_{ox}}\right) \qquad (5.16)$$

Given that [122]; $D_{CH_2Cl_2}$= 9.08 at 293K ; r_{red}=r_{ox}=$r_{average}$= 0.45nm ; and $D_{CH_2Cl_2}$= (3320/T)-2.24. Then for the reversible electrode reaction 5.5 with z_{red}=3 and z_{ox}=2, equation 5.13 predicts that the free energy change arising from the rearrangement of the solvation sphere is $(\Delta G)_{Born} \approx$ -687KJmol^{-1}. For the same reaction, equation 5.16 predicts that the enthalpy change arising from the rearrangement of the solvation sphere is $(\Delta H)_{Born} \approx$ -793KJmol^{-1}. And finally, for the same reaction, equation 5.15 predicts the entropy change arising from the rearrangement of the solvation sphere is $(\Delta S)_{Born} \approx$ -362JK^{-1}mol^{-1}. From equation 5.10 the entropy contribution to the Born free energy change is then -T$(\Delta S)_{Born} \approx$ -293 x -362 $\approx$ +106KJmol^{-1} (which is only roughly 15% of $(\Delta G)_{Born}$).

The magnitude of $(\Delta G)_{Born}$ and therefore also $(\Delta S)_{Born}$ would be reduced with z_{red}=1 and z_{ox}=0 (by a factor of 5 neglecting changes in the radii) but significantly, $(\Delta G)_{Born}$ would still be dominated by the contribution of $(\Delta H)_{Born}$. It should be recognised that the Born theory only provides a rough approximation as the solvent cannot be regarded as a continuous dielectric in the vicinity of the ions [123] and the complex radii are not known in solution. Nevertheless, it would appear that the effect of the entropy term in equation 5.11 on the electrode potential of hexahalometallate complexes is likely to be small.

N.B. With regard to the systematic trends exhibited by hexahalometallate redox couples outlined in section 5.5, it is reasonable to assume that a series of isovalent hexahalometallate redox couples undergo very similar solvation effects given the similar sizes of isovalent transition metal ions across a period. Therefore, ignoring the possibility of a Jahn-Teller distortion (chapter 1), the entropy contribution to the electrode potential is likely to be very similar for each isovalent hexahalometallate couple within the same period. Therefore the systematic trends exhibited by the redox potentials of hexahalometallate ions will be independent of any entropy contribution because each redox couple in an isovalent series involves approximately the same entropy change.

5.8 The effect of the enthalpy term on the electrode potential

In the previous section the effect of the entropy term, -TΔS, on the systematic variation of isovalent hexahalometallate electrode potentials across a period was considered to be small. From equation 5.11 the enthalpy changes occurring in hexahalometallate redox systems are therefore responsible for the systematic trends exhibited by hexahalometallate redox potentials (section 5.5).

The enthalpy or heat of reaction 5.5 is related to the energy of the redox electron in the reduced molecule and hence to the ionization energy of the reduced molecule. When comparing values of E^o the energy of the redox electron can be approximated by the energy of the redox orbital including electron pairing energy when required, $\mathcal{E}$(redox) [114]. Consequently the enthalpy change is influenced by those factors governing $\mathcal{E}$(redox), namely ; the metal (M), the number of redox electrons (n), the ligand (L) and the solvent (S).

The following sections will examine the contributions of each factor towards the general similarities between the redox potentials of the hexahalometallates as described in section 5.5. The differences between the redox potentials of hexafluoro-, hexachloro- and hexabromometallates, shown in figures 5.5 and 5.6, will be discussed within the context of the influence of the different ligands.

5.9 The influence of the metal on ε(redox)

As already noted above, the redox potentials of the hexahalometallate complexes are influenced by the ionization enthalpies of the monatomic gas atoms [87,113,116], especially for the higher oxidation states where the (n+1)s electrons have been removed. Unfortunately there are no comprehensive data concerning the third, fourth and fifth ionization enthalpies of the second and third row transition elements - the states which are chemically relevant to this thesis (table 5.5). Even then a direct comparison could not be possible because the gaseous ions possess a five-fold degenerate

d-orbital manifold whereas the hexahalometallate d-orbital manifold degeneracy is split between e_g and t_{2g} orbitals (chapter 1). However, the first and second ionization enthalpies do show some phenomena which can be related to the electrode potentials of the $[MX_6]^z$ complexes.

5.9.1 Periodic variation of ionization enthalpies

The lower ionization enthalpies of the transition metals increase progressively across the second and third periods as a consequence of the increasing effective nuclear charge ie: in the sequence

Zr < Nb < Mo < Tc < Ru < Rh < Pd
Hf < Ta < W > Re < Os < Ir > Pt

This is reflected by the isovalent hexahalometallate redox couples which generally increase across a period, indicating an increasing reluctance to release an electron. N.B. The steady increase of the third ionization enthalpies of the second row transition metals (and therefore removal of a d-electron) has a discontinuity at Ru(III)-$4d^5$. This is due to the removal of a spin-paired d-electron from the gaseous Ru(II) ion-$4d^6$. This important effect also concerns $[MX_6]^z$ electrode potentials and is discussed in section 5.10.

5.9.2 Comparison of second and third row

The increased ionization enthalpies observed when progressing from second to third row transition metals are traditionally explained by the increased nuclear charge of the 5d elements and the poor screening ability of their filled 4f shell. This would suggest that third row hexahalometallates should be harder to oxidize than their isoelectronic second row $[MX_6]^z$ counterparts, which is the opposite of the observed effect (criterion 5.5.3). It is unfortunate that a more extensive range of third row transition metal ionization enthalpies is not available because it is not certain that the same trend

is obeyed when the 5d electrons are removed. In fact, relativistic explanations of d-orbital energies [124] indicate that the orbital energies of the 5d-metals are above those of the 4d-metals of the previous row. This suggests 5d electrons are more available for redox processes than 4d electrons which is consistent with the greater reducing ability of 5d hexahalometallates than their 4d isoelectronic counterparts, as observed in this thesis. The relativistic interpretation also postulates a contraction of the 6s and 6p orbitals inside the 5s and 5p orbitals which would explain the larger first and second ionization enthalpies of the third row transition elements.

5.9.3 The oxidation state of the metal

The successive ionization enthalpies of a metal increase progressively as the effective nuclear charge increases. Similarly, the electrode potential of a hexahalometallate complex increases with increasing oxidation state of the metal (criterion 5.5.2).

5.10 The influence of the d^n configuration

The influence of the d^n configuration can be assessed by calculating the electrostatic interactions between electrons within an ion. It is not within the scope of this thesis to quantitatively calculate interelectronic correlation energies [2] but fortunately a qualitative approach can be used to explain the observed results. In order to simplify the analysis further we shall assume the $[MX_6]^z$ complexes adopt a regular octahedral symmetry and that effects such as Jahn-Teller distortions do not occur.

When the d-orbital manifold is split according to the ligand field theory (chapter 1), the e_g-t_{2g} energy separation of second and third row transition metals is sufficiently large that spin-pairing in the t_{2g} orbitals becomes more energetically favourable than maximising the multiplicity within the d manifold. Hence it is the filling of the t_{2g} d-orbital manifold which is of most concern in this thesis. The d^n configuration plays an important role in determining $\mathcal{E}$(redox) as the redox processes of hexahalometallates are assumed to be metal based.

Table 5.5: The successive ionization enthalpies of the second and third row transition metals [126], $\Delta H_{298}/\mathrm{MJmol}^{-1}$.

metal	I	II	III	IV	V
Zr	0.666	1.273	2.224	3.319	7.87
Nb	0.670	1.388	2.422	3.70	4.884
Mo	0.691	1.564	2.627	4.48	5.91
Tc	0.708	1.478	2.856		
Ru	0.717	1.623	2.753		
Rh	0.726	1.751	3.003		
Pd	0.811	1.881	3.183		
Hf	0.68	1.44	2.25	3.22	
Ta	0.767				
W	0.776				
Re	0.766				
Os	0.85				
Ir	0.88				
Pt	0.87	1.797			

5.10.1 Discontinuities and the d^n configuration

The concept of $\mathcal{E}$(redox) will be discussed in section 5.10.3 using the concepts of M.O. theory but to explain the discontinuities observed in the series of isovalent $[MX_6]^{z/z-1}$ couples a crystal field approach is more appropriate: The energy of the nd shell is divided into two components ; the coulombic attraction which the positively charged inert gas core has on the nd electrons contributing -nU to ΔH and the interaction energies between the nd electrons. The energy processes arising from electron-electron interaction are [125] :-

1. The exchange energy (parallel spins, $\uparrow\uparrow$), k.
   This is the energetic origin of Hund's rule and is roughly proportional to the number of pairs of parallel spins. Addition of an electron with a parallel spin within the d-t_{2g} manifold exerts a stabilizing influence on the ion of -ΔH and vice versa.

2. The repulsion energy (parallel spins, $\uparrow\uparrow$), r.
   The coulombic repulsion between all pairs of parallel spin electrons within the d-t_{2g} manifold exerts a destabilizing influence on the ion of +ΔH and is roughly proportional to the number of pairs of parallel spins.

3. The repulsion energy (spin pairing, $\uparrow\downarrow$), R.
   When two electrons occupy the same orbital within the d-t_{2g} manifold, the coulombic repulsion energy between them destabilizes the ion by an energy +ΔH.

Neglecting ligand and solvation effects the energy of the d-shell, $\mathcal{E}(d^n)$ is then approximately given by

$$\mathcal{E}(d^n) = \text{-nU} + \text{a(k)} + \text{b(r)} + \text{c(R)} \tag{5.17}$$

the energy change when one electron is removed is then

$$\mathcal{E}(d^{n-1}) - \mathcal{E}(d^n) = \text{U} + \Delta\ \text{a(k)} + \Delta\ \text{b(r)} + \Delta\ \text{c(R)} \qquad (5.18)$$

The individual contributions of k, r and R identified as a, b and c can be easily calculated for each $d^n(t_{2g})$ configuration and they are listed in table 5.6. The relative $E_{1/2}$ values are then the difference between successive d^n configurations, $\mathcal{E}(d^{n-1})$-$\mathcal{E}(d^n)$, with an arbitrary zero point at the $d^{0/1}$ couple (having the energy U).

Table 5.6: Interelectronic correlation terms of k, r and R for $[MX_6]^z$ complexes.

t_{2g} config.	core attraction	exchange energy,k	repulsion (↑↑), r	repulsion (↑↓), R		$E_{1/2}$	$\Delta\mathcal{E}$
d^0	0	0	0	0			
					} d^0/d^1	U	
d^1	-U	0	0	0			} k+r
					} d^1/d^2	U-k-r	
d^2	-2U	k	r	0			} k+r
					} d^2/d^3	U-2k-2r	
d^3	-3U	3k	3r	0			} 3R-2k-2r
					} d^3/d^4	U-3R	
d^4	-4U	3k	3r	3R			} k+r
					} d^4/d^5	U-k-r-3R	
d^5	-5U	4k	4r	6R			} k+r
					} d^5/d^6	U-2k-2r-3R	
d^6	-6U	6k	6r	9R			

The $\Delta\mathcal{E}$ terms refer to the energy differences between successive couples. Referring to figures 5.5 and 5.6, it is clear from table 5.6 that the prevailing slope and the discontinuities observed in the electrode potentials of isovalent hexahalometallate couples are determined by the enthalpy contributions of the interelectronic repulsion terms (k+r) and (3R-2k-2r). Furthermore, the abrupt discontinuity between the $d^{2/3}$ and $d^{3/4}$ couples is a consequence of there being no appreciable difference in the exchange energy and the parallel repulsion energy between low spin nd^3 and nd^4 ions.

However, a general gradient (k+r) does not satisfy the observation that the linear progression of redox potentials is smaller for the $d^{3/4}$, $d^{4/5}$, $d^{5/6}$ series than the $d^{0/1}$,

$d^{1/2}$, $d^{2/3}$ series (criterion 5.5.4). This inaccuracy can be explained in two ways : Either the interelectronic repulsion energies are significantly altered when spin pairing occurs or, by the introduction of a fourth repulsion parameter K which acts between spin paired orbitals in the d-t_{2g} manifold destabilizing the ion with and enthalpy $+\Delta H$.

Table 5.7: Interelectronic correlation terms of k, K, r and R for $[MX_6]^z$ complexes.

t_{2g} config.	core attraction	exchange energy,k	repulsion (↑↑), r	repulsion (↑↓), R	repulsion K		$E_{1/2}$	$\Delta\mathcal{E}$
d^0	0	0	0	0	0			
						} d^0/d^1	U	
d^1	-U	0	0	0	0			} k+r
						} d^1/d^2	U-k-r	
d^2	-2U	k	r	0	0			} k+r
						} d^2/d^3	U-2k-2r	
d^3	-3U	3k	3r	0	0			} 3R-2k-2r
						} d^3/d^4	U-3R	
d^4	-4U	3k	3r	3R	0			} k+K+r
						} d^4/d^5	U-k-K	
d^5	-5U	4k	4r	6R	K		-r-3R	} k+K+r
						} d^5/d^6	U-2k-2K	
d^6	-6U	6k	6r	9R	3K		-2r-3R	

The new interelectronic correlation terms with the parameter K included are shown in table 5.7. According to the $\Delta\mathcal{E}$ terms, the differing gradients and the discontinuity between $d^{2/3}$ and $d^{3/4}$ represented in the schematic figures by AB, CD and BC can now be attributed to the energies (k+r), (k+K+r) and (3R-2k-2r).

The same procedure was repeated but with the Racah parameters for the ground state electrostatic energies of the various ions instead of k, K, r and R. (The repulsion energies for the various d^n configurations were listed previously by J.S.Griffith [2] who utilized the Racah parameters A,B and C). A new parameter D was introduced in this work to account for the differing gradients observed (see table 5.8). The $d^{0/1}$ couple was again given the arbitrary value of zero and the $\Delta\mathcal{E}$ terms indicated the slope

gradients corresponded to the energies A-5B and A-5B+D with the discontinuity amounting to an energy of A+10B+5C. Hence:-

$$\begin{aligned} k+r &\simeq A - 5B \\ R &\simeq A + 5/3C \\ K &\simeq D \end{aligned} \tag{5.19}$$

Table 5.8: Interelectronic correlation terms for $[MX_6]^z$ using the Racah parameters A, B, C and D.

t_{2g} config.	correlation energy	$E_{1/2}$	$\Delta\varepsilon$
d^0	0		
		}0	
d^1	0		}A-5B
		}5B-A	
d^2	A-5B		}A-5B
		}10B-2A	
d^3	3A-15B		}A+10B+5C
		}-5C-3A	
d^4	6A-15B+5C		}A-5B+D
		}5B-5C-D-4A	
d^5	10A-20B+10C+D		}A-5B+D
		}10B-5A-5C-2D	
d^6	15A-30B+15C+3D		

5.10.2 The interelectronic repulsion parameters

From the experimental values of the electrode potentials given in tables 5.2, 5.3 and 5.4 the three gradients (k+r), (k+K+r) and (3R-2k-2r) can be given numerical values x, y and z ie:

$$\begin{aligned} k + r &= x \\ k + K + r &= y \\ 3R - 2k - 2r &= z \end{aligned} \tag{5.20}$$

Straightforward calculations can then derive values for the relative energies of the repulsion energy $(\uparrow\downarrow)R$, the repulsion between spin paired orbitals K and the combination (k+r), the exchange and repulsion energies $(\uparrow\uparrow)$. The values determined for the isovalent series $[MX_6]^{z/z-1}$ are listed in table 5.9 while the relevant calculations are outlined in Appendix A.

Table 5.9: The relative energies of the interelectronic correlation terms (k+r), K and R for hexahalometallate complexes.

	Second row transition metal hexahalometallates					
	$[MF_6]^{1-/2-}$	$[MF_6]^{2-/3-}$	$[MCl_6]^{1-/2-}$	$[MCl_6]^{2-/3-}$	$[MBr_6]^{1-/2-}$	$[MBr_6]^{2-/3-}$
(k+r)	+1.21	-	+0.96	+1.12	+0.85	+0.95
K	-	-	-0.31	-0.36	-	-0.42
R	+0.80	-	+0.51	+0.57	+0.41	+0.48

	Third row transition metal hexahalometallates					
	$[MF_6]^{1-/2-}$	$[MF_6]^{2-/3-}$	$[MCl_6]^{1-/2-}$	$[MCl_6]^{2-/3-}$	$[MBr_6]^{1-/2-}$	$[MBr_6]^{2-/3-}$
(k+r)	+1.18	-	+0.94	+0.98	+0.74	+0.60
K	-0.58	-	-0.43	-0.43	-0.11	-0.08
R	+0.93	-	+0.61	+0.66	+0.47	+0.35

Table 5.10 summarizes the values in table 5.9 by indicating whether the values (r+k), K and R increase or decrease in the order

$$[MF_6]^z : [MCl_6]^z : [MBr_6]^z \tag{5.21}$$

Where values in table 5.9 were absent, the underlying trend was interpreted from the remaining two values in 5.21. The important features of table 5.10 are :-

a) The repulsion energies, R, between two electrons paired in a d-t_{2g} orbital decrease within the same period in the order:

Table 5.10: Relative trends of the interelectronic repulsion energies between isovalent hexahalometallate series in the sequence $[MF_6]^{z/z-1}$: $[MCl_6]^{z/z-1}$: $[MBr_6]^{z/z-1}$

	(k+r)	K	R
second row $[MX_6]^{1-/2-}$	decreasing	-	decreasing
second row $[MX_6]^{2-/3-}$	decreasing	(decreasing)	decreasing
third row $[MX_6]^{1-/2-}$	decreasing	increasing	decreasing
third row $[MX_6]^{2-/3-}$	decreasing	increasing	decreasing

$$R[MF_6]^z > R[MCl_6]^z > R[MBr_6]^z \tag{5.22}$$

This order reflects the nephelauxetic effect of the ligands (section 1.3) as one might expect because the nephelauxetic ratio β is a function of the Racah repulsion parameter B, and decreases with decreasing interelectronic repulsion in the complex ion. The d-t_{2g} electrons, which are formally located on the metal in hexahalometallate complexes therefore experience less interelectronic repulsion when surrounded by chloride and bromide ligands than when surrounded by fluoride ligands. Such a result is consistent with the greater delocalization and hence greater covalency of M-Cl and M-Br bonds (section 1.7).

b) For third row hexahalometallates the repulsion between spin paired orbitals, K, appears to increase in the sense

$$K[MF_6]^z < K[MCl_6]^z < K[MBr_6] \tag{5.23}$$

Owing to the greater delocalization within M-Cl and M-Br bonds the reverse trend was expected and there appears to be no logical explanation of this phenomenon. The expected trend in K was observed with the second row isovalent series $[MX_6]^{2-/3-}$, although the accuracy of the values calculated are dependent on the $[TcBr_6]^{2-/3-}$ electrode potential which was predicted to be -0.4V (table 5.4),(close to the value of -0.34V obtained by previous workers [60] in HBr solution), but which may be inaccurate.

N.B. The unexpected order of 5.23 indicates that linking K with spin-paired orbital repulsion energy is incorrect and a different interpretation leading to the same result is required.

c) Within the same period, the values of the energy (k+r) decrease according to

$$[MF_6]^z > [MCl_6]^z > [MBr_6]^z \tag{5.24}$$

According to 5.10.2a) the repulsion energy r(↑↑) decreases in the order 5.24 because of the ligand nephelauxetic effect. Therefore either: 1) the exchange energy k also decreases but the ensuing destabilization is less than the loss of repulsion energy 2) the exchange energy is the same for $[MF_6]^z$, $[MCl_6]^z$ and $[MBr_6]^z$ or 3) the exchange energy increases according to the ligand sequence F < Cl < Br.

N.B. The interpretation of the results obtained are best confined to the relative values between isovalent hexahalometallate series within a given period and not to the actual numerical values. Inspection of table 5.9 indicates that R energies of second row hexahalometallates are less than those of the corresponding third row complexes conflicting with the greater size of 5d compared with 4d orbitals. Indeed the analysis assumes that values of k, K, r and R remain constant across a period within the same isovalent series. In fact the values of the repulsion energies B and C, and hence k, r and R appear to generally increase across a period [2] although data are only available for M(I) and M(II) ions.

5.10.3 The energy of the redox orbital, ε(redox)

The crystal field interpretation of the series of isovalent $[MX_6]^{z/z-1}$ redox couples is very successful when describing the origin of the discontinuity between $nd^{2/3}$ and $nd^{3/4}$ (criterion 5.5.1). To explain how the different halide ligands effect the isovalent $[MX_6]^{z/z-1}$ redox series an alternative approach based on molecular orbital methods will be used here:

The energy of the redox orbital, $\mathcal{E}$(redox), [114], is written as the summation of

two terms: a) the energy of the lowest-lying d-orbital in the d-manifold, $\mathcal{E}(t_{2g})$, and b) the difference in energy between this orbital and the redox orbital. In the context of low-spin hexahalometallate complexes (with no Jahn-Teller distortion) this energy difference is equivalent to the spin-pairing energy P.

In M.O. theory $\mathcal{E}(t_{2g})$ is defined as the sum of two components :-

1. The valence state ionization energy (VSIE) of the d-orbital of the metal M with effective charge q, $VSIE_m^q$. (This is the application of Koopman's theorem which approximates the orbital energy of the metal as the negative of the ionization potential for the removal of an electron from that orbital [127]). Plus
2. A π-covalency contribution,Δ_π, which is positive for a π-donor ligand and negative for a π-acceptor ligand.

Thus

$$\mathcal{E}(t_{2g}) = -VSIE_m^q + \Delta_\pi \tag{5.25}$$

As the VSIE is charge dependent, it can be represented by

$$VSIE_m^q = \alpha_m + k\beta_m q \tag{5.26}$$

α_m and β_m are constants of the metal and kq, $(0 < k < 1)$, represents the effective charge of the metal which is less than the charge of the free ion because of the charge transfer contribution from the ligands. After correction for electron pairing the experimental VSIE's for free M(III) ions [2] is a smooth function of the nuclear charge z and therefore of the number of d electrons n. Hence the VSIE can be expressed in terms of a reference value. ie:

$$VSIE_m^q = VSIE_{ref}^q\ (1 + \gamma n) \tag{5.27}$$

where γ is a constant (0.08 for first row transition metals) . Therefore equation 5.27 can be written

$$\mathrm{VSIE}_m^q = (\alpha_{ref} + \mathrm{k}\beta_{ref}\mathrm{q})\ (1 + \gamma \mathrm{n}) \tag{5.28}$$

From first order perturbation theory [127]

$$\Delta_\pi : \frac{1}{\Delta\varepsilon_{ML}} \tag{5.29}$$

$$\Delta\varepsilon_{ML} = \varepsilon_M - \varepsilon_L = \text{-}\mathrm{VSIE}_m^q - \varepsilon_L \tag{5.30}$$

where ε_L is the ligand orbital energy. Then

$$\frac{d\Delta_\pi}{d\mathrm{VSIE}_m^q} = \frac{d\Delta_\pi}{d\varepsilon_L} = \frac{\Delta_\pi}{\Delta\varepsilon_{ML}} \tag{5.31}$$

hence from 5.25

$$\frac{-d\varepsilon\ (\mathrm{t}_{2g})}{d\mathrm{VSIE}_m^q} = 1 - \frac{\Delta_\pi}{\Delta\varepsilon_{ML}} = A \tag{5.32}$$

5.11 Hexahalometallate electrode potentials and ε(redox)

The differences and sequential trends between the electrode potentials of the hexahalometallates are divisible into four main categories :

5.11.1

The difference between the electrode potentials of isovalent hexahalometallate neighbours within the same period which can be written as

$$E[MX_6]^z - E[M'X_6]^z \equiv \Delta(M,M') \tag{5.33}$$

$\Delta(M,M')$ defines the slope of $-\mathcal{E}(t_{2g})$ and is therefore the rate of change of $-\mathcal{E}(t_{2g})$ with increasing d-t_{2g} electron population, n. Neglecting any effects of n on k and q

$$\Delta(M,M') \equiv \frac{-d\mathcal{E}(t_{2g})}{dn} \simeq A\gamma(\alpha_{ref} + k\beta_{ref}q) - \frac{d\Delta_\pi}{dn}$$

$$\simeq \gamma(\alpha_{ref} + k\beta_{ref}q)\left(1 - 2\frac{\Delta_\pi}{\Delta\mathcal{E}_{ML}}\right) \tag{5.34}$$

$$\left(\frac{d\Delta_\pi}{dn} = \frac{d\Delta_\pi}{dVSIE_m^q}.\frac{dVSIE_m^q}{dn} = \frac{\Delta_\pi}{\Delta\mathcal{E}_{ML}}.\gamma(\alpha_{ref} + k\beta_{ref}q)\right) \tag{5.35}$$

In chapter one the properties of the metal-halogen bonds were discussed in terms of the differing electronegativities of the halide ligands which led to increasing σ-donation from the ligand to the metal in the order

$$[MF_6]^z < [MCl_6]^z < [MBr_6]^z \tag{5.36}$$

The gradient $\Delta(M,M')$ is influenced by the values of k, q and $\Delta_\pi/\Delta\mathcal{E}_{ML}$. k is a number between 0 and 1.0 which reflects the covalency of the M-L bonds and is approximately equal to 1.0 for a purely ionic bond. Similarly the effective nuclear charge q decreases with increasing electron donation of the ligand to the metal. Therefore,for hexahalometallates the decrease in both k and q will reflect the order 5.37.

$\Delta\mathcal{E}_{ML}$ can be approximated by the energy of the first charge transfer band of the hexahalometallate complex in the visible/ultra-violet region (section 1.9). Equation 1.7 indicates that when considering hexafluoro-, hexachloro- and hexabromometallates, $\Delta\mathcal{E}_{ML}$ will be greatest for hexafluorometallates and smallest for hexabromometallates. Δ_π is positive for halide ligands and increases in the order $F^- < Cl^- < Br^-$ and so the contribution of $-2\Delta_\pi/\Delta\mathcal{E}_{ML}$ to $\Delta(M,M')$ increases in the order 5.36.

Therefore the predicted gradients, $-d\mathcal{E}\ (t_{2g})/dn$ for the redox couples of isovalent hexahalometallate series should follow the order

$$[MF_6]^{z/z-1} > [MCl_6]^{z/z-1} > [MBr_6]^{z/z-1} \tag{5.37}$$

This trend was observed in this thesis. Provision for the difference in slope between the $d^{0/1}$,$d^{1/2}$,$d^{2/3}$ and $d^{3/4}$,$d^{4/5}$,$d^{5/6}$ couples can be made as in section 5.10.1 by introducing a new term into the spin pairing energy of the complexes with a greater than half filled d-t_{2g} manifold.

5.11.2

The difference between the electrode potentials of two consecutive electron transfer steps of the same hexahalometallate complex, often referred to as the redox stability of $[MX_6]^z$, can be written :

$$E[MX_6]^{z+1/z} - E[MX_6]^{z/z-1} \equiv \Delta(ox,red) \tag{5.38}$$

Δ(ox,red) is then a measure of the change in the energy $-\mathcal{E}(t_{2g})$ of a hexahalometallate complex with respect to the overall charge on the ion z. Neglecting any effects of z on A and k as relatively minor

$$\Delta(ox,red) \equiv \frac{-d\mathcal{E}\ (t_{2g})}{dz} \simeq Ak\beta_m \frac{dq}{dz} - \frac{d\Delta_\pi}{dz} \tag{5.39}$$

Equation 5.39 is difficult to assess in relation to the effect of varying the ligand of hexahalometallate complexes. However, one can interpret dq/dz as the extent of metal character of the redox orbital, which is expected to be greatest for the hexafluorometallates because the M-F bond is more ionic in nature. If the Δ_π contribution of F^-, Cl^- and Br^- is assumed to decrease by approximately the same amount with increase in z ($d\Delta_\pi/dz$ is probably smallest for F^- in fact) then the redox stability of isoelectronic $[MX_6]^z$ complexes should decrease in the order

$$\Delta(\text{ox,red}) : [MF_6]^z > [MCl_6]^z > [MBr_6]^z \quad (5.40)$$

In this thesis it was only possible to calculate the redox stabilities of $[MCl_6]^{2-}$ and $[MBr_6]^{2-}$ complexes. The results are listed in table 5.11. Clearly the redox stabilities listed in table 5.11 agree with the prediction of equation 5.40. Table 5.11 along with figures 5.2 - 5.6 also clearly illustrates the enhanced redox stability of d^3 hexahalometallates compared with other members of the same isovalent series.

Table 5.11: Redox stabilities (volts) of the second and third row $[MCl_6]^{2-}$ and $[MBr_6]^{2-}$ complexes.

M	X = Cl	X = Br
Nb	1.40	1.19
Mo	1.33	1.09
Tc	2.80*	2.40*
Ru	1.66	1.39
Rh	1.71	1.15*
Ta	1.50	1.19
W	1.55	1.34
Re	2.45	2.20
Os	1.92	1.79
Ir	1.76	1.48

* estimated value

5.11.3

The discontinuity in the progression of isovalent hexahalometallate redox couples has been discussed in section 5.10.

5.11.4

Equation 5.25 indicates that the higher electrode potentials of the second row $[MX_6]^z$ complexes compared with third row $[MX_6]^z$ complexes is governed by a larger $VSIE_m^q$ of second row metals compared with the analogous third row metals. This conclusion contradicts the available ionization data but adds support to the relativistic description of the orbital energies (section 5.9b). A series of theoretical calculations might be helpful to elucidate this problem.

5.12 The effect of the solvent (S) on the enthalpy term

In section 5.6 it was assumed that the solvent contribution to the enthalpy change of an $[MBr_6]^{2-/3-}$ couple could be approximated by :-

$$\sum H_{solv}[MBr_6]^{3-} - \sum H_{solv}[MBr_6]^{2-} \tag{5.41}$$

And in section 5.7.1 the ion-solvent interaction was interpreted by using the Born equation which led to equation 5.16 describing the contribution of the solvent to the enthalpy change during a typical one electron electrochemical reduction :-

$$(\Delta H)_{Born} = \frac{-\,Le_o^2}{8\pi\epsilon_o}\left(1 - \frac{1}{D} - \frac{T}{D^2}\frac{\partial D}{\partial T}\right)\left(\frac{z_{red}^2}{r_{red}} - \frac{z_{ox}^2}{r_{ox}}\right) \tag{5.42}$$

It would be unwise to relate solvation enthalpies calculated from the Born equation to the overall enthalpy change of reduction since a largely empirical approach has been adopted so far. But, it is useful to compare the effects of different solvents on the same system.

Table 5.12 summarises the calculated solvent contribution to the free energy, enthalpy and entropy of reaction for an $[MBr_6]^{2-/3-}$ couple in the three solvents H_2O, SO_2 and CH_2Cl_2 . For the three different solvents, one can say on purely electrostatic considerations that the solvent enthalpy contribution is relatively constant for solvents

of widely varying dielectric properties and is therefore probably only of importance when a specific chemical interaction occurs.

Table 5.12: Born solvation energies for an $[MBr_6]^{2-/3-}$ redox couple in different solvents.

	H_2O D^{293}=80.36	SO_2 D^{293}=14	CH_2Cl_2 D^{293}=9.09
ΔG ($KJmol^{-1}$)	-762	-716	-687
ΔH ($KJmol^{-1}$)	-776	-805	-793
ΔS ($Jmol^{-1}$)	-48	-304	-362

A feature of table 5.12 worth noting is that although it is small in comparison with the solvation enthalpy, the entropy contribution from the ordering of solvent molecules around ions is substantially smaller for solvents with large dielectric constants. The main reason for this may be that in solvents with a high dielectric constant the order of the system is already high and is therefore little affected by any small local increase in order around ions which gain a charge.

5.13 Summary of the energy contributions to the redox potentials of second and third row hexahalometallates

- The electrode potential of a reversible $[MX_6]^{z/z-1}$ redox couple is proportional to the free energy change during the redox reaction.
- The entropy contribution to the free energy change is assumed to only involve a rearrangement of the solvation sphere around the hexahalometallate complex. The Born equation predicts that the entropy contribution to the free energy change is likely to be small compared with the enthalpy contribution.
- The enthalpy contribution to the free energy change is responsible for the systematic trends observed within the hexahalometallate redox potentials. The principal contributions to the enthalpy arise from:-

1. The character of the metal which can be related to the VSIE of the metal with effective nuclear charge q.
2. The number of d electrons. The interelectronic repulsion energies can be combined into an interelectronic correlation scheme which can predict the relative slopes and discontinuities of a series of isovalent $[MX_6]^{z/z-1}$ couples.
3. The nature of the halogen ligands which influence the redox potentials by their nephelauxetic properties.
4. The nature of the solvent which affects the redox enthalpy by the formation of a secondary coordination sphere of solvent molecules.

5.14 The determination of unknown redox couples

A valuable outcome of the systematic pattern of hexahalometallate electrode potentials is that if some potentials are already known then the potential of an unknown redox couple can be predicted. This is accomplished by extrapolating the trend of known redox couples (figs. 5.2-5.6) to incorporate an unknown electrode potential. Where two unknown isovalent redox couples are side by side (eg. $[RhBr_6]^{1-/2-}$ and $[PdBr_6]^{1-/2-}$) then an informed guess of the gradient between the two electrode potentials can be interpolated and then the electrode potentials read off.

This procedure also proved to be of semi-diagnostic value as further verification of the successful synthesis of $[Bu_4N]_2[MoBr_6]$ (sections 3.4 and 6.9).

5.14.1 The determination of unknown $[MF_6]^{z/z-1}$ redox couples in acetonitrile

a) Hexahalotechnetates were not synthesized in this thesis because of the potentially dangerous radioactivity of technetium. However, extrapolating the $[NbF_6]^{1-/2-}$ and $[MoF_6]^{1-/2-}$ redox potentials gives an estimate of the $[TcF_6]^{1-/2-}$ redox potential:

$[TcF_6]^{1-/2-}$ at $E_{1/2} = +1.2$V (vs.S.C.E.) in CH_3CN.

The potential of the redox couple $[TcF_6]^{2-/3-}$ is more difficult to predict because the $[RhF_6]^{2-/3-}$ redox couple has not been determined. However, R appears to increase between $[MX_6]^{1-/2-}$ and $[MX_6]^{2-/3-}$ for second row hexahalometallates hence a value for the redox couple can be estimated:

$[TcF_6]^{2-/3-}$ at $E_{1/2} \simeq$ -1.8V (vs.S.C.E.) in CH_3CN.

b) Extrapolating the $[TcF_6]^{2-/3-}$ and $[RuF_6]^{2-/3-}$ redox potentials gives an estimate of the $[RhF_6]^{2-/3-}$ redox potential:

$[RhF_6]^{2-/3-}$ at $E_{1/2} \simeq$ 0.0V (vs.S.C.E.) in CH_3CN.

Both complexes, $[RhF_6]^{2-}$ and $[RhF_6]^{3-}$, have been prepared as alkali metal and alkaline earth salts [128,129] and are susceptible to hydrolysis. The anions should be suitable for electrochemical study in a dry organic solvent and since $[RhF_6]^{1-}$ salts have also been prepared [130] the $[RhF_6]^{1-/2-}$ redox potential should also be observable in dry CH_3CN at approximately +2.0V (vs.S.C.E.). Although RhF_6 is known [131], the $[RhF_6]^{0/1-}$ redox potential is predicted to lie well above the solvent range.

c) Extrapolating the $[OsF_6]^{1-/2-}$ and $[IrF_6]^{1-/2-}$ redox potentials gives an estimate of the $[PtF_6]^{1-/2-}$ redox potential:

$[PtF_6]^{1-/2-}$ at $E_{1/2} = +1.8$V (vs.S.C.E.) in CH_3CN.

5.14.2 The determination of unknown $[MCl_6]^{z/z-1}$ redox couples in methylene chloride

a) Extrapolating the $[MCl_6]^{1-/2-}$ redox potentials of Nb and Mo and the $[MCl_6]^{2-/3-}$ redox potentials of Ru and Rh gives an estimate of the $[TcCl_6]^{z/z-1}$ redox potentials:

$[TcCl_6]^{1-/2-}$ at $E_{1/2} = +2.0$V (vs.S.C.E.) in CH_2Cl_2
$[TcCl_6]^{2-/3-}$ at $E_{1/2} =$ -0.8V (vs.S.C.E.) in CH_2Cl_2

The electrochemistry of $[Bu_4N]_2[TcCl_6]$ was investigated in CH_3CN by previous workers [60]. At a rotating platinum electrode two irreversible processes at $E_{1/2}$= +1.88V and +2.30V (vs.S.C.E.) were observed and at a dropping mercury electrode (D.M.E.) four irreversible processes were observed at $E_{1/2}$= -0.34V, -0.68V, -1.11V and -1.83V (vs.S.C.E.). The predicted electrochemical behaviour in CH_2Cl_2 suggests that CH_3CN and Hg are not passive participants in the redox processes of $[TcCl_6]^z$.

(N.B. Moock [197] has determined the redox potentials of $[Ph_4P]_2[TcCl_6]$ in CH_2Cl_2. The complex exhibited one reversible oxidation $[TcCl_6]^{1-/2-}$ at $E_{1/2}$ = +1.98V (vs.S.C.E.) and a reversible reduction $[TcCl_6]^{2-/3-}$ at $E_{1/2}$ = -0.85V (vs.S.C.E.) in excellent agreement with the predicted values.)

b) Extrapolating the $[WCl_6]^{2-/3-}$ and $[TaCl_6]^{2-/3-}$ redox potentials gives an estimate of the $[HfCl_6]^{2-/3-}$ redox potential:

$[HfCl_6]^{2-/3-}$ at $E_{1/2}$ = -3.1V (vs.S.C.E.) in CH_2Cl_2.

5.14.3 The determination of unknown $[MBr_6]^{z/z-1}$ redox couples in methylene chloride

a) Extrapolating the $[NbBr_6]^{1-/2-}$ and $[MoBr_6]^{1-/2-}$ redox potentials gives an estimate of the $[TcBr_6]^{1-/2-}$ redox potential:

$[TcBr_6]^{1-/2-}$ at $E_{1/2}$ = +2.0V (vs.S.C.E.) in CH_2Cl_2

The $[TcBr_6]^{2-/3-}$ redox potential can be predicted in the same way as 5.14.1:

$[TcBr_6]^{2-/3-}$ at $E_{1/2} \simeq$ -0.4V (vs.S.C.E.) in CH_2Cl_2

The electrochemistry of $[Bu_4N]_2[TcBr_6]$ was previously investigated in CH_3CN [60]. Two irreversible processes at $E_{1/2}$ = +1.70V and +2.32V (vs.S.C.E.) were observed using a rotating platinum electrode and irreversible processes at -0.34V, -0.68V, -1.11V and -1.83V (vs.S.C.E.) were observed with a D.M.E. By analogy with the $[TcCl_6]^{z/z-1}$ complexes (5.14.2), the $[TcBr_6]^{z/z-1}$ complexes would presumably be more stable in dry CH_2Cl_2 than dry CH_3CN or dry CH_3CN/Hg.

b) By assuming the repulsion energy K is approximately the same for the second row transition metal series $[MBr_6]^{1-/2-}$ and $[MBr_6]^{2-/3-}$ then the predicted value for the hypothetical redox couple $[RhBr_6]^{1-/2-}$ is :-

$[RhBr_6]^{1-/2-}$ at $E_{1/2} \simeq +1.8V$ (vs.S.C.E.) in CH_2Cl_2.

Extrapolating to the $[PdBr_6]^{1-/2-}$ redox potential gives:

$[PdBr_6]^{1-/2-}$ at $E_{1/2} \simeq +2.1V$ (vs.S.C.E.) in CH_2Cl_2.

c) Extrapolating the $[TcBr_6]^{2-/3-}$ and $[RuBr_6]^{2-/3-}$ redox potentials gives an estimate of the $[RhBr_6]^{2-/3-}$ redox potential:

$[RhBr_6]^{2-/3-}$ at $E_{1/2} \simeq +0.65V$ (vs.S.C.E.) in CH_2Cl_2.

d) Extrapolating the $[WBr_6]^{2-/3-}$ and $[TaBr_6]^{2-/3-}$ redox potentials gives an estimate of the $[HfBr_6]^{2-/3-}$ redox potential:

$[HfBr_6]^{2-/3-}$ at $E_{1/2} = +2.2V$ (vs.S.C.E.) in CH_2Cl_2.

The latter section, 5.14.3, exemplifies the value of the concept since, even though the hexabromometallate salts of Pd and Rh could not be prepared in a form which was soluble in methylene chloride, their relative redox properties are predictable.

5.15 Applications of hexahalometallate redox potentials

Redox potentials are useful for numerous applications where thermodynamic information is required. Primarily, redox potentials can be used to predict whether species A can oxidize/reduce species B in order to determine whether the synthesis of a compound is thermodynamically feasible. In this section some useful applications of redox potentials are discussed by resorting to specific examples.

N.B. Reactions are divided into two half-cell reactions with the oxidation half-cell on the left hand side and the reduction half-cell on the right hand side. E_{cell} is then given by :-

$$E_{cell} = E_{RHS} - E_{LHS} \tag{5.43}$$

5.15.1

Hexachlorotungstates(V) are normally prepared by the reaction of tungsten hexachloride with either quaternary ammonium chlorides in thionyl chloride solution [132] or alkali-metal iodide in a sealed tube [133]. However, Dickinson *et al* [133] also discovered that tungsten hexachloride reacts with potassium hexachlorotungstate(IV) when they are ground together at room temperature to form the hexachlorotungstate(V) salt.

$$WCl_6 + [WCl_6]^{2-} \longrightarrow 2[WCl_6]^{1-} \tag{5.44}$$

This reaction was described as remarkable [13] but with $[WCl_6]^{0/1-}$ $E_{1/2} = +1.59$V and $[WCl_6]^{1-/2-}$ $E_{1/2} = +0.40$V then E_{cell}= +1.19V and the solution reaction 5.44 is evidently thermodynamically feasible.

Thus because hexahalometallate redox potentials increase as the charge on the metal increases, for a given metal, then reaction 5.44 should be thermodynamically feasible for the general preparation of other hexahalometallate(V) complexes.

The converse reaction, the disproportionation of $[WCl_6]^{1-}$ is thermodynamically unfavourable and is reflected by an absence of hexahalometallate complexes which disproportionate in organic solvents.

5.15.2

Tungsten hexachloride and tungsten hexabromide can be reduced to the hexahalotungstate(IV) by tetra-n-butylammmoniumiodide in CH_2Cl_2 (chapter 6). But the attempted reduction of hexabromotantalate(V) by iodide in CH_2Cl_2 was unsuccessful (chapter 6):

I_2/I^- $E_{1/2}$ = +0.80V (vs.S.C.E.) in CH_2Cl_2
$[TaBr_6]^{1-/2-}$ $E_{1/2}$ = -0.16V (vs.S.C.E.) in CH_2Cl_2

hence E_{cell}= -0.96V in CH_2Cl_2 and ΔG is unfavourable for the reduction of hexabromotantalate(V) by iodide.

5.15.3

$MoCl_6$ was reported [134] to be the product of prolonged refluxing of molydenum trioxide with thionyl chloride but could not be confirmed [13]. The $[MoCl_6]^{0/1-}$ redox potential at $E_{1/2}$ = +2.20V (vs.S.C.E.) suggests $MoCl_6$ should be accessible by chemical means.

5.15.4

$[NO]^{1+}$ can oxidize $[WF_6]^{1-}$ to WF_6 in CH_3CN but does not react with $[MoF_6]^{1-}$. The redox potentials in CH_3CN (vs. Ag/Ag^+) are :-

$[NO]^{1+}/NO$ $E_{1/2}$ = +0.87V
$WF_6/[WF_6]^{1-}$ $E_{1/2}$ = +0.51V
$MoF_6/[MoF_6]^{1-}$ $E_{1/2}$ = +1.60V
$UF_6/[UF_6]^{1-}$ $E_{1/2}$ = +2.31V
Cu(II)/Cu(I) $E_{1/2}$ = +0.71V [196]

hence the order of oxidizing ability [40] in CH_3CN is

$UF_6 > MoF_6 > [NO]^{1+}$(solvated) $> Cu^{2+}$ (solvated) $\geq WF_6$

5.16 Future work

The hexahalotechnetates (except $[TcCl_6]^{2-}$) and several hexafluoro- and hexabromometallate complexes have not been investigated experimentally. While the complexes $[ZrF_6]^z$, $[HfF_6]^z$, $[RhF_6]^z$ and $[PdF_6]^z$ have not yet been attempted they should

be synthesisable by standard methods [128,130,135,136,137]. The difficulties encountered with organic-soluble hexabromometallates have been outlined in chapters 3 and 6.

An obvious extension of this thesis would be a study of the redox potentials of second and third row transition metal hexaiodometallates. The preparative methods for hexaiodometallates, whether by chance or by design, appear to be restricted to those complexes which can be formed by the action of hydroiodic acid on a hexabromometallate,hexachlorometallate or an oxometallate (eg. ReO_4^-). The known hexaiodometallates are restricted to those elements to the right of the Periodic Table [13], which would hopefully exhibit redox activity which is congruent with the theories discussed in chapter 5. The preparation of hexaiodometallates of elements to the left of the Periodic Table would provide an interesting challenge to the synthetic chemist. Reaction in anhydrous organic solvents analogous to the preparation of $[ZrBr_6]^{2-}$ (chapter 6) would provide a possible route, (ZrI_4, HfI_4, TaI_4 and NbI_4 are all known), although it can be anticipated that the large steric requirement of six iodide ligands may inhibit complex formation particularly in the case of second row metals and large cations.

The redox properties of the first row transition metal hexahalometallates might also provide a fruitful topic of research although the hexahalometallates are only known comprehensively towards the left hand side of the first row elements.

Finally, it would be of further interest in this area of work to determine the first charge-transfer energies of as many hexahalometallate complexes as possible (chapter 1). It should then be possible to identify a relationship between the charge transfer energy and the redox potential, since both properties are primarily influenced by changes in the metal t_{2g} orbital energy.

Chapter 6

Experimental procedure

6.1 General information

All moisture sensitive hexahalometallate complexes were prepared on a Pyrex vacuum line fitted with a mercury diffusion pump and an Edwards high vacuum rotary oil pump. The vacuum manifold was fitted with Rotaflo Teflon stopcocks and reaction vessels were fitted with either Rotaflo or Youngs Teflon stopcocks. The status of the vacuum was measured with a mercury filled vacuostat and Apiezon-N or Kel-F greases were used throughout. Rotaflo reaction vessels were flamed out prior to use to remove surface moisture and solid compounds were handled under a dry-nitrogen atmosphere in a Lintott glove box. Those compounds which were not prepared under vacuum were rigorously dried on the vacuum line before use. Unless stated, dried solvents (section 6.23) were used throughout.

Infra-red spectra in the range 4000 to 180cm^{-1} were obtained on Perkin-Elmer 983 and 580 infra-red spectrophotometers. Samples were examined as solid mulls between silicon or caesium iodide plates with sodium dried Nujol as the mulling agent. Raman spectra were obtained with a Spex Ramanlog spectrometer from crystalline samples vacuum sealed into thin Pyrex glass capillaries. The laser lines used were 476.5nm, 488.0nm, 515.4nm, 568.2nm and 647.1nm. In this chapter vibrational data are listed with the preparation of each compound where appropriate, and in table 1.6.

Visible/ultra-violet absorption spectra were obtained using a Rotaflo vessel fitted with a 1mm path-length quartz glass optical cell attached to a side arm. The apparatus was designed to fit into the sample compartment of a Perkin-Elmer Lambda-9 or Beckman UV 5270 spectrophotometer. Dry compounds were weighed into the rotaflow compartment in the glove box, then dry solvent was distilled into the vessel on the vacuum line. Solution concentrations were approximately $5x10^{-3}$M (weight of solid ca. 0.02-0.03g in ca. 5ml of solvent). Extinction coefficients were not calculated because the concentration could not be measured accurately enough. The solution absorption data are listed with the preparation of each compound where appropriate.

C, H, N and Br microanalyses were determined by the University of Glasgow microanalysis department. The department could only analyse those compounds which could be handled in the open air. The author attempted to determine the bromine content of WBr_5 and WBr_6 by the Volhard method but found the analysis results were widely scattered and unreliable.

Electrochemical experiments were performed with the cell apparatus described in section 6.2. In total, three different sets of electrochemical apparatus were used: a PAR model 170 potentiostat and programmer, a Hi-Tek potentiostat type DT 2101 in conjunction with a Hi-Tek waveform generator type PPR1 and Hewlett-Packard X-Y recorder, and an EG&G PARC model 175 universal programmer with EG&G PAR model 173 potentiostat and EG&G PAR X-Y recorder. Sweep rates $\geq$ 1V sec^{-1} were monitored with a Telequipment model D66A oscilloscope.

6.2 The electrochemical cell

The requirement of strictly anhydrous conditions for the present work precluded the use of a conventional glass 'pot' as a useful electrochemical cell. To exclude moisture, the greatest efficiency is obtained by use of a vacuum tight electrochemical cell. Several workers have already tackled the problem of design previously. An example is the 'Anderson' cell [37,38] which employed a D.M.E. with a mercury pool counter electrode and a silver/silver perchlorate reference electrode. The reference, electrolyte

and sample solutions were made up individually in a glove box before the whole apparatus, (in effect two cells–a reference cell connected to the electrode cell *via.* a Luggin capillary), was joined together. The main drawback of this cell arrangement was the tedious handling procedures and the limited range of the mercury electrode.

The cell designed to study the redox potentials and reactions of transition metal hexafluorometallates [39,40] in acetonitrile proved to be much more versatile than the 'Anderson' cell and cleverly incorporated a silver/silver nitrate reference electrode built along the same lines as standard reference electrodes. Unfortunately this commendable feature made the cell very complex to manipulate. Consequently, the cell design chosen for the work in this thesis was that invented by Klaus Moock [31,41], a diagram of which is shown in figure 6.1. A major advantage of this design over the others was the incorporation of a cooling finger projecting into the electrolyte solution which permitted low temperature electrochemistry under vacuum conditions.

6.2.1 Cell construction and experimental procedure

The whole cell apparatus was made from Pyrex glass and the three electrodes from platinum wire. The auxiliary and quasi-reference electrodes were made from platinum wire (diameter 0.5mm) spot-welded to tungsten rod and encased in glass so that approximately 5mm of platinum wire protruded into the solution. The platinum micro-electrode was described in section 2.13. After the completion of experiments, the three electrodes were immersed in concentrated nitric acid to remove any inorganic and organic material adsorbed onto the electrodes.

In order to perform an experiment, the two side arms containing the supporting electrolyte and the compound were first loaded in a glove box and then evacuated on a vacuum line overnight. These were sealed and then glass-blown onto the main apparatus. Then, along with the reference compound and a small Teflon stirring bar the whole apparatus was flamed out and evacuated overnight. (The reference compound (here ferrocene) was initially weighed and introduced into a thin glass capillary which was evacuated and sealed such that the reference compound was sealed in a section of the capillary approximately 6cm long. This section of the

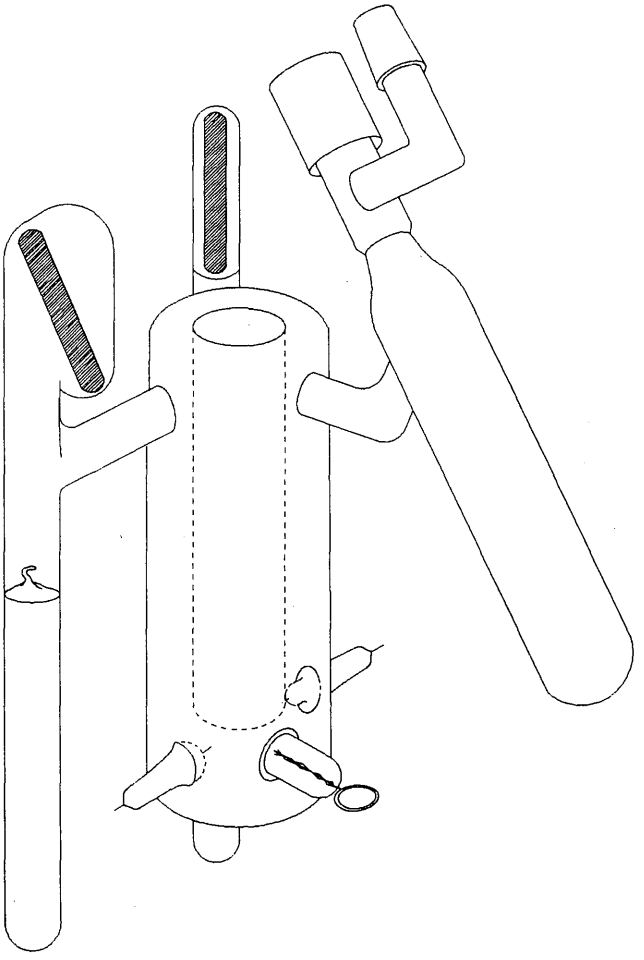

Figure 6.1: The electrochemical cell.

glass capillary had previously been deeply scored by a glass knife approximately 2cm from one end in order to facilitate the rupture of the ampoule by shaking.) The solvent was then vacuum distilled into the Rotaflo compartment and the breakseal of the electrolyte compartment broken. Once the electrolyte had dissolved, after careful manoeuvering of the cell, the working potential range of the solvent-electrolyte system was determined. Then the breakseal of the compound compartment was broken, the compound dissolved and its redox activity determined. The reference compound contained in the evacuated, frangible ampoule in the rotaflow compartment was dissolved in the solution at the end of the experiment by shaking the apparatus in order to break the ampoule. If cooling was required, a suitable slush mixture of solvent and dry-ice was made up in the cooling finger. Temperatures inside the cell were estimated by comparison with a conventional cell equipped with a thermocouple and by attaching a thermocouple to the underside of the cell used in this work, which indicated that temperatures around -40^oC were obtainable.

6.3 The preparation of metal bromides from the metal or metal oxide

6.3.1 General procedure

Transition metal halides are classically prepared by heating the reduced metal or a metal oxide/charcoal mixture in a stream of nitrogen and halogen [138]. The apparatus normally includes a horizontal glass reaction vessel which can be heated, and through which the nitrogen/halogen stream flows over the heated metal. The metal halide vapour formed is carried by the nitrogen stream along the reaction vessel until it condenses on a cooler surface. Once reaction is complete the desired product is then separated by sealing the appropriate section of glass apparatus under nitrogen.

Wilkinson and Lincoln [139] proposed the simple and effective modification whereby the horizontal reaction tube was replaced by a vertical system. The metal powder is supported on a glass wool plug (supported by indentations in the tube) and topped by a second plug. In this manner, the heavy metal halide vapour is removed from the

reaction zone in part by gravity. This method was successfully used in this thesis to synthesize tungsten pentabromide and zirconium tetrabromide from tungsten powder and a zirconium oxide/charcoal mixture respectively.

Because of the high temperatures required, the reactions were performed in a silica glass reaction tube which was connected to a Pyrex collection vessel by a silica-Pyrex graded seal. Bromine vapour was supplied by bubbling the nitrogen flow stream through a vessel containing bromine liquid. Interconnections other than glass between the various sections of apparatus were made of p.v.c. tubing which was renewed for each experiment. The apparatus was thoroughly flushed with nitrogen before each experiment to diminish the extent of moisture contamination from the p.v.c. tubing.

6.3.2 Tungsten pentabromide

(see Lincoln and Wilkinson [139])

Tungsten powder (1g, 5.4mmol) supported between two silica-wool plugs was pre-reduced by hydrogen gas at 250-300°C for approximately 30 minutes to remove any surface oxide. Then the hydrogen gas was replaced with nitrogen-gas and the collection apparatus was flamed-out with a gas torch to remove any condensed water. The furnace temperature was raised to 700°C and then bromine vapour admitted to the nitrogen stream at the rate of approximately one bubble per second. The initial light-brown product, which was flamed away, was followed by a black vapour/solid which descended into the collection vessel. When reaction had ceased the flow stream was reverted to nitrogen only and the system allowed to cool. The collection vessel containing approximately 2.7g of WBr_5 was sealed under nitrogen. Wt/mol = 583.3g, yield approx. 85%.

Infra-red: 330(s), 240(s)cm^{-1}

(cf. 260(sh), 230(sh), 205(vs)cm^{-1} [ref. 159], 280, 245cm^{-1} [ref. 183])

6.3.3 Zirconium tetrabromide

(see Young and Fletcher [140])

Zirconium dioxide (0.75g, 6.1mmol) and finely powdered sugar charcoal (1:4) were intimately mixed and placed between the two silica-wool plugs in the vertical bromination apparatus. With the nitrogen stream regulated to approximately one bubble every four seconds, the temperature was gradually raised to $700°C$ and bromine vapour was introduced to the nitrogen flow stream. Bromination occurred very slowly at approximately $750°C$ producing a white product after the initial yellowish-white product had been flamed away. The large volume of reaction mixture effectively blocked the reaction tube and a slow flow rate of nitrogen/bromine vapour was necessary to prevent any pressure build up. Reaction was stopped after five hours when approximately 1.3g of white $ZrBr_4$ had been collected and sealed under nitrogen. Wt/mol = 410.8g, yield approx. 40%.

6.3.4 Hafnium tetrabromide

A 4:1 mixture of powdered sugar charcoal and hafnium dioxide (1g, 4.7mmol) was brominated by the same method as 6.3.3 except the silica reaction tube was modified to include a right angle bend. The HfO_2/C mixture was spread horizontally between two silica-wool plugs approximately 10cm apart such that the reaction zone was approximately half filled. By this means, an adequate flow rate could be maintained without any pressure build up. The reaction mixture was placed as near to the right angle bend as possible to facilitate the removal of hafnium tetrabromide from the horizontal reaction zone by gravity. The reaction was maintained at $830°C$ for 3 hours during which time approximately 1.5g of cream coloured $HfBr_4$ was collected. Wt/mol = 498g, yield approx. 60%.

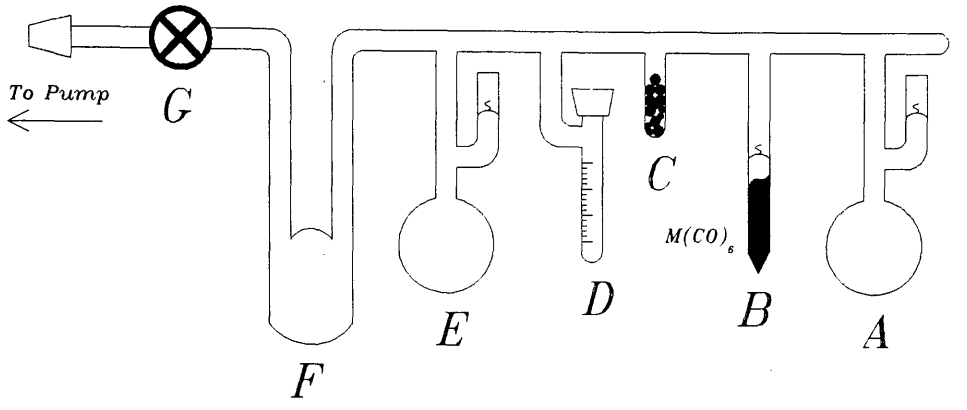

Figure 6.2: Apparatus design used to prepare metal bromides from the metal carbonyl.

6.4 The preparation of metal bromides from the metal carbonyl

Molybdenum hexacarbonyl and tungsten hexacarbonyl react with liquid bromine at room temperature to form molybdenum tetrabromide and tungsten hexabromide respectively. Both products are highly moisture sensitive hence the reactions were conducted in a vacuum system (figure 6.2).

6.4.1 General procedure

The metal carbonyl was weighed and evacuated under a dynamic vacuum for two to three days until dry, then sealed under vacuum into a glass vessel with a break-seal (B). Bromine was degassed over P_2O_5 by freeze-thaw, then distilled onto fresh P_2O_5 in a graduated rotaflow vessel (D). The glassware apparatus 6.2 was then constructed, checked for leaks, flamed out and evacuated overnight.

Using a magnet, the breakseal of vessel B was broken with the metal ball bearings which were then removed along with vessel C by a gas torch. Tap G was closed so that

the whole apparatus could be tipped to manipulate the metal carbonyl into vessel A, after which vessel B was removed by gas torch. With tap G closed and vessel A cooled with liquid nitrogen, excess bromine was distilled onto the metal carbonyl in vessel A. After vessel D had been removed the reaction mixture was allowed to warm to $0°C$. Reaction was allowed to proceed at $0°C$ for 30 minutes with tap G opened briefly every few minutes to allow the escape of carbon monoxide gas through trap F, which was cooled with liquid nitrogen. Reaction vessel A was then allowed to warm to room temperature and left to react for one hour after which the volatile materials were distilled into vessel E. Vessel E was removed with the gas torch, vessel F cooled with liquid nitrogen and then tap G opened and the residue in vessel A pumped under vacuum for 24 hours to remove any remaining traces of bromine. Vessel A containing the metal bromide was then sealed under vacuum with a gas torch.

6.4.2 Molybdenum tetrabromide

(see von Hieber and Romberg [141])

Following procedure 6.4.1, dried $Mo(CO)_6$ (0.7g, 2.6mmol) reacted quantitatively with excess bromine under vacuum to produce a dull black powder, $MoBr_4$. The powder exhibited a broad, medium-strong absorption at $290cm^{-1}$ in the infra-red region. Two other possible absorptions between $220cm^{-1}$ and $190cm^{-1}$ were unresolvable. No evidence for molybdenum-oxygen or carbonyl stretching modes could be detected. Infra-red data for $MoBr_4$ has not been previously published. The compound was not sublimed as $MoBr_4$ is thermally unstable [142] and was used without further purification. Wt/mol = 415.5g, yield quantitative.

6.4.3 Tungsten hexabromide

(see Shchukarev and Kokovin [143])

Following procedure 6.4.1, dried $W(CO)_6$ (5g, 14mmol) reacted quantitatively with excess bromine under vacuum to produce a grey-green powder, WBr_6. The powder exhibited a very strong, broad absorption in the infra-red region at $220cm^{-1}$ assigned

to the ν_3 stretching vibration of WBr_6 (cf. 217cm^{-1} [ref.159], 305cm^{-1} [ref.183]). No evidence for tungsten-oxygen or carbonyl stretching modes could be detected in the infra-red region. Raman signals observed at 209cm^{-1} and (possibly) 190cm^{-1} were tentatively assigned to the ν_1 and ν_2 vibrations of WBr_6 respectively by comparison with other hexabromometallates (table 1.6). There are no previous reports of Raman vibrational frequencies for WBr_6 in the literature. The compound was insoluble in CH_2Cl_2 even after shaking for several days. The visible/ultra-violet solution spectrum of the compound in CH_3CN changed over 25 hours until the spectrum resembled that of $WBr_4.2CH_3CN$ (section 3.5). The compound was used without further purification. Wt/mol = 663.25g, yield quantitative.

6.5 The preparation of bis tetra-n-butylammonium hexabromozirconate(IV)

Freshly sublimed $ZrBr_4$ (0.7g, 1.7mmol) and $[Bu_4N]Br$ (1.1g, 3.4mmol) were placed in one limb of a two-limbed glass Rotaflow vessel and CH_2Cl_2 (10ml) was distilled onto the mixture. The $ZrBr_4$ solid did not dissolve so the mixture was stirred under vacuum with a magnetic stirring bar for 5 days after which some of the $ZrBr_4$ was still unreacted. The solid was allowed to settle then the clear solution phase was decanted into the second limb and the solvent evacuated to leave a white solid product. Since the reaction had not proceeded quantitatively, the product was contaminated with $[Bu_4N]Br$ which is very soluble in CH_2Cl_2. The two-limbed vessel was evacuated overnight to remove any traces of solvent and then the two limbs were separated under vacuum. The mildly hygroscopic white product exhibited infra-red and visible/ultra-violet absorption spectra consistent with the formation of $[Bu_4N]_2[ZrBr_6]$. Wt/mol = 1054.6g.

Observed

$[Bu_4N]_2[ZrBr_6]$	
infra-red	ν_3 219cm^{-1}
Raman	sample burned in laser
vis/uv (CH_2Cl_2)	36.1, 39.9kK

Literature

$[Et_4N]_2[ZrBr_6]$		ref.
infra-red	ν_3 223cm^{-1}	144
vis/uv (CH_3CN)	34.5(sh), 38.9, 40.0(sh), 44.4kK	145

6.6 The preparation of bis tetra-n-butylammonium hexabromohafnate(IV)

Freshly sublimed $HfBr_4$ (0.75g, 1.5mmol) and $[Bu_4N]Br$ (0.97g, 3mmol) were placed in one limb of a two-limbed glass Rotaflow vessel and CH_2Cl_2 (10ml) was distilled onto the mixture. The $HfBr_4$ solid did not dissolve so the mixture was stirred under vacuum with a magnetic stirring bar for 3 days after which some of the $HfBr_4$ was still unreacted. The solid was allowed to settle then the clear solution phase was decanted into the second limb and the solvent evacuated to leave a white solid product. Since the reaction had not proceeded quantitatively, the product was contaminated with $[Bu_4N]Br$ which is very soluble in CH_2Cl_2. The two-limbed vessel was evacuated overnight to remove any traces of solvent and then the two limbs were separated under vacuum. The hygroscopic white product exhibited infra-red, Raman and visible/ultra-violet spectra consistent with the formation of $[Bu_4N]_2[HfBr_6]$. Wt/mol = 1141.9g.

Observed

$[Bu_4N]_2[HfBr_6]$	
infra-red	ν_3 189cm^{-1}
Raman	ν_1 200cm^{-1}
vis/uv (CH_2Cl_2)	39.1kK

Literature

$[Et_4N]_2[HfBr_6]$		ref.
infra-red	ν_3 189cm^{-1}	144
Raman	ν_1 197cm^{-1}	144
vis/uv (CH_3CN)	37.6(sh), 38.9, 42.9kK	146

6.7 The preparation of tetra-n-butylammonium hexabromoniobate(V)

Following the method of Dehnicke *et al* [105], freshly sublimed $NbBr_5$ (0.76g, 1.55mmol) and $[Bu_4N]Br$ (0.5g, 1.55mmol) were placed in one limb of a two-limbed glass Rotaflow vessel and CH_2Cl_2 (10ml) was distilled onto the mixture. The red $NbBr_5$ solid did not dissolve so the solution was stirred under vacuum with a magnetic stirring bar while the limbs of the Rotaflow vessel were suspended in an oil bath maintained at $40°C$. After 3 days stirring some of the $NbBr_5$ was still unreacted. The solid was allowed to settle then the red solution phase was decanted into the second limb and the solvent evacuated to leave a red/brown solid. Since the reaction had not proceeded quantitatively, the product was contaminated with $[Bu_4N]Br$ which is very soluble in CH_2Cl_2. The two-limbed vessel was evacuated overnight to remove any traces of solvent then the two limbs were separated under vacuum. The moderately hygroscopic reddish-brown product exhibited infra-red and visible/ultra-violet spectra consistent with the formation of $[Bu_4N][NbBr_6]$. A weak absorption in the infra-red spectrum of the compound at $963cm^{-1}$ indicated the product was contaminated with an oxyhalide compound, most probably $[Bu_4N]_2[NbOBr_5]$ or $[Bu_4N][NbOBr_4]$.

Observed

	$[Bu_4N][NbBr_6]$
infra-red	ν_3 $237cm^{-1}$/ (Nb-O str. $963cm^{-1}$)
vis/uv(CH_2Cl_2)	20.8(sh), 22.7, 26.8, 34.9,46.4kK

Literature

	$[Et_4N][NbBr_6]$ (reference [146])	$Cs_2[NbOBr_5]$ (reference[107])
infra-red	ν_3 $239cm^{-1}$	Nb-O str. $977cm^{-1}$
vis/uv	(CH_3CN/Br^-): ~ 210(sh),22.6, 26.9, 35.3, 43.7kK	(solid): 21.7(sh), 25.3, 28.0, 33.9kK

6.8 The preparation of tetra-n-butylammonium hexabromotantalate(V)

Following the method of Dehnicke *et al* [105], freshly sublimed $TaBr_5$ (2.2g, 3.7mmol) and $[Bu_4N]Br$ (1.2g, 3.7mmol) were placed in one limb of a two-limbed glass Rotaflow vessel and CH_2Cl_2 (15ml) was distilled onto the mixture. The yellow $TaBr_5$ solid did not dissolve so the mixture was stirred under vacuum with a magnetic stirring bar for 2 days after which time some of the $TaBr_5$ was still unreacted. The solid was allowed to settle then the yellow solution phase was decanted into the second limb and the solvent evacuated to leave a yellow solid product. Since the reaction had not proceeded quantitatively, the product was contaminated with $[Bu_4N]Br$ which is very soluble in CH_2Cl_2. (Repetition of the experiment with the reaction solution gently refluxed at $70°C$ did not increase the reaction yield by an appreciable amount.) The two-limbed vessel was evacuated overnight to remove any traces of solvent and then the two limbs were separated under vacuum. The moderately hygroscopic yellow product exhibited infra-red and visible/ultra-violet spectra consistent with the formation of $[Bu_4N][TaBr_6]$.

Observed

	$[Bu_4N][TaBr_6]$
infra-red	ν_3 211cm^{-1}
vis/uv(CH_2Cl_2)	22.0(sh), 26.0, 32.0, 33.3, 41.5kK

Literature

	$[Et_4N][TaBr_6]$	ref.
infra-red	ν_3 213cm^{-1}	147
vis/uv (CH_3CN/Br^-)	22.2, 26.1, 29.8(sh), 31.9, 33.6, 36.9kK	146

6.9 The preparation of bis tetra-n-butylammonium hexabromomolybdate

(see Dehnicke *et al* [58])

$MoBr_4$ (0.5g, 1.2mmol) and $[Bu_4N]Br$ (0.77g, 2.4mmol) were placed in one limb of a two-limbed glass Rotaflow vessel and CH_2Cl_2 (10ml) was distilled onto the mixture. The black $MoBr_4$ solid did not dissolve so the mixture was stirred under vacuum with a magnetic stirring bar for 3 days after which some of the $MoBr_4$ was still unreacted. The solid was allowed to settle then the black solution phase was decanted into the second limb and the solvent evacuated to leave a purple-black solid product. Since the reaction had not proceeded quantitatively, the product was contaminated with $[Bu_4N]Br$ which is very soluble in CH_2Cl_2. (The reaction was repeated with the reaction mixture gently refluxed at 70^oC without any appreciable increase in the reaction yield.) The two-limbed vessel was evacuated overnight to remove any traces of solvent then the two limbs were separated under vacuum. The very hygroscopic purple-black solid product exhibited an infra-red spectrum consistent with the formation of $[Bu_4N]_2[MoBr_6]$. The cyclic voltammetric study of the product (section 3.4) revealed the compound was contaminated with $[Bu_4N][MoOBr_4]$.

Observed

	$[Bu_4N]_2[MoBr_6]$
infra-red	ν_3 227cm^{-1}
vis/uv (CH_2Cl_2)	17.6, 21.3, 26.2, 28.2, 29.8, 36.4(sh)kK

The infra-red and visible/ultra-violet absorption spectra of the sample of $[Bu_4N]_2[MoBr_6]$ did not reveal any absorptions characteristic of $[Bu_4N][MoOBr_4]$.

Literature

infra-red	$[PPh_3Me]_2[MoBr_6].2CH_2Br_2$	ν_3 230cm^{-1}	[ref.58]
vis/uv (solid)	Cs_2MoBr_6	16.1, 19.6, 24.1, 28.0, 41.7kK	[ref.148]

6.10 The preparation of tetra-n-butylammonium oxytetrabromomolybdate(V)

$[Bu_4N][MoBr_4]$ was prepared by a variation of the method described by Allen and Neumann [149]. $[Bu_4N]Br$ (4.47g, 13.8mmol) dissolved in conc. HBr acid was added dropwise to a hot solution of MoO_3 (1g, 6.9mmol) in conc. HBr (40ml). The resulting solution was evaporated slowly on a hotplate until a yellow precipitate had formed. The cooled solution was suction filtered and a yellow powder with brown speckles recovered. The compound exhibited visible/ultra-violet absorption spectra in conc. HBr and CH_2Cl_2 solutions consistent with the formation of $[Bu_4N]_2[MoOBr_5]$ and $[Bu_4N][MoOBr_4]$ respectively. The compound was taken up in hot conc. HBr, hot filtered and recrystallised from conc. HBr under nitrogen. Ochre platelets of $[Bu_4N][MoOBr_4]$ which were moderately stable in air were obtained in approximately 50% yield.

Observed

	$[Bu_4N][MoOBr_4]$
infra-red	1002(s), 978(s), 288(s), 251(vs)cm^{-1}
vis/uv (CH_2Cl_2)	20.4, 23.7, 26.1kK

Literature

infra-red	unreported		
vis/uv (CH_3NO_2)	$[Ph_4As][MoOBr_4]$	13.8, 20.6, 23.8, 25.6kK	ref.[63]

Analysis

	$[Bu_4N][MoOBr_4]$
found	C(28.31), N(1.96), H(5.50), Br(47.45)
calculated	C(28.31), N(2.01), H(5.35), Br(47.45)

6.11 The preparation of tetra-n-butylammonium hexabromotungstate(V)

$[Bu_4N][WBr_6]$ was prepared by a modification of the method described by Walton and Brisdon [150]. WBr_5 (0.7g, 1.2mmol) and $[Bu_4N]Br$ (0.39, 1.2mmol) were placed in one limb of a two-limbed glass Rotaflow vessel and CH_2Cl_2 (10ml) was distilled onto the mixture. The WBr_5 solid did not dissolve completely so the mixture was stirred under vacuum with a magnetic stirring bar for 24 hours after which some of the WBr_5 was still unreacted. The solid was allowed to settle then the red solution phase was decanted into the second limb and the solvent evacuated to leave a red-brown solid product. Since the reaction had not proceeded quantitatively, the product was contaminated with $[Bu_4N]Br$ which is very soluble in CH_2Cl_2. The two-limbed vessel was evacuated overnight to remove any traces of solvent then the two limbs were separated under vacuum. The hygroscopic red-brown product exhibited infra-red and visible/ultra-violet absorption spectra consistent with the formation of $[Bu_4N][WBr_6]$.

Observed/ infra-red: $[Bu_4N][WBr_6]$ ν_3 212cm^{-1}

Literature/infra-red: $[PPh_4][WBr_6]$ ν_3 210cm^{-1} [ref.159]

The visible/ultra-violet absorption spectra are listed in table 3.5.1.

6.12 The preparation of bis tetra-n-butylammonium hexabromotungstate(IV)

Two methods of preparation were attempted:-

6.12.1 The attempted metathesis of Cs_2WBr_6 and $[Bu_4N]Br$

Cs_2WBr_6 was prepared by the method described by Peacock *et al* [157]. WBr_6 (0.5g, 0.75mmol) and CsI (0.39g, 1.5mmol) were intimately mixed and heated under vacuum in a sealed Carius tube for 4 days at $130°C$. The iodine which formed during the reaction was removed by slowly raising the temperature to $290°C$ whilst evacuating the solid under a dynamic vacuum. The green product was identified by infra-red spectroscopy as Cs_2WBr_6.

Observed/ infra-red: $Cs_2[WBr_6]$ ν_3 210cm^{-1}

Literature/infra-red: $Cs_2[WBr_6]$ ν_3 214cm^{-1} [ref.157]

$Cs_2[WBr_6]$ (0.25g, 0.27mmol) and $[Bu_4N]Br$ (0.17g, 0.54mmol) were placed in one limb of a two-limbed glass Rotaflow vessel and CH_2Cl_2 (10ml) was distilled onto the mixture. The mixture was stirred under vacuum with a magnetic stirring bar for 3 days but the $Cs_2[WBr_6]$ did not dissolve into solution and there was no reaction. CH_3CN (10ml) was substituted for CH_2Cl_2 because of the stronger solvating ability of CH_3CN but no reaction occurred.

6.12.2 Reduction of WBr_6 with $[Bu_4N]I$ in CH_2Cl_2

WBr_6 (0.46g, 0.7mmol) and $[Bu_4N]I$ (0.52g, 1.4mmol) were placed in one limb of a two-limbed glass Rotaflow vessel and CH_2Cl_2 (10ml) was distilled onto the mixture. The solution was shaken under vacuum for 4 days, the red solution phase decanted

into the second limb and the solvent evacuated to leave a red-brown solid. The visible/ultra-violet absorption spectrum taken in CH_2Cl_2 was dominated by the spectrum of $[Bu_4N]I$ + trace I_2 which is characterized by very intense, narrow absorptions at 27.4 and 34.0kK and which masked any other absorptions which were present. ($[Bu_4N]I$ alone does not exhibit any absorptions in CH_2Cl_2 down to a cut-off at 240nm while I_2 alone in CH_2Cl_2 exhibits broad, weak absorptions at 20.0, 27.0 and 35.5kK).

To remove the iodine, the solid was transferred to a clean Rotaflow vessel, CH_2Cl_2 (5ml) was distilled onto the solid, the solution shaken, then the solvent evacuated. The washing procedure was repeated eight times. Finally the solid was heated at $60°C$ for 24 hours under a dynamic vacuum to remove the last traces of I_2. The moderately hygroscopic reddish-brown product exhibited infra-red and visible/ultra-violet spectra consistent with the formation of $[Bu_4N]_2[WBr_6]$ which was obtained in almost quantitative yield.

Observed/ infra-red: $[Bu_4N]_2[WBr_6]$ $\nu_3 \simeq 200cm^{-1}$

Literature/infra-red: $Cs_2[WBr_6]$ ν_3 $214cm^{-1}$ [ref.157]

The visible/ultra-violet absorption spectra are listed in table 3.5.1.

6.13 The preparation of bis tetra-n-butylammonium hexabromorhenate(IV)

$[Bu_4N]_2[ReBr_6]$ was prepared from $K_2[ReBr_6]$. Potassium perrhenate ($KReO_4$) was prepared by titrating a solution of Re_2O_7 in distilled water with 3M KOH solution until the solution registered pH8. The white precipitate of $KReO_4$ was filtered and washed with a small volume of cold water.

6.13.1 The preparation of K_2ReBr_6

Following the method of Watt and Thompson [59], a 250ml beaker was charged with $KReO_4$ (1.82g, 6.3mmol), KBr (0.75g, 6.3mmol), conc.(48%) HBr (120ml) and 50% hypophosphorus acid (2ml). The solution was heated at $110 \pm 5°C$ until the solution volume had been reduced to approximately 5ml. The mixture was chilled with ice then suction filtered to collect the dark-red crystals. The compound was recrystallized from 4M HBr and identified as K_2ReBr_6 by infra-red spectroscopy and microanalysis.

Observed/ infra-red: K_2ReBr_6 ν_3 224cm^{-1}

Literature/infra-red: K_2ReBr_6 ν_3 217cm^{-1} [ref.153]

Analysis/ found: Br(64.28) calculated: Br(64.45)

6.13.2 The preparation of $[Bu_4N]_2[ReBr_6]$

K_2ReBr_6 (0.51g, 0.68mmol) dissolved in the minimum volume of 2M HBr solution was stirred in a beaker with acidified Dowex 50 W-X8 cation exchange resin (ca.3g) then rapidly filtered. $[Bu_4N]Br$ (0.44g, 1.3mmol) dissolved in the minimum volume of 1M HBr solution was added to the filtrate and a yellow compound precipitated. The

precipitate was suction filtered and washed with small volumes of ice cold water and diethyl ether. The air-stable yellow compound, $[Bu_4N]_2[ReBr_6]$, was obtained in a 55% yield (based on K_2ReBr_6).

Observed

$[Bu_4N]_2[ReBr_6]$	
infra-red	ν_3 209cm^{-1}
vis/uv (CH_2Cl_2)	13.2, 13.3, 15.0, 15.2kK

Literature

infra-red	$[(C_7H_{15})_4N]_2[ReBr_6]$ ν_3 208cm^{-1}	[ref.155]
vis/uv (24% HBr)	K_2ReBr_6 13.2, 13.3, 14.9, 15.2, 16.7kK	[ref.165]

Analysis

$[Bu_4N]_2[ReBr_6]$	
found	C(33.48), H(6.01), N(2.34), Br(41.75)
calculated	C(33.40), H(6.26), N(2.43), Br(41.70)

6.14 The preparation of bis tetra-n-butylammonium hexabromoruthenate(IV)

$[Bu_4N]_2[RuBr_6]$ was prepared from K_2RuBr_6.

6.14.1 The preparation of K_2RuBr_6

Following the method of Fergusson and Greenaway [163], bromine vapour was bubbled through a solution of K_3RuCl_6 (0.5g, 1.16mmol) dissolved in the minimum volume of conc. HBr acid (48%). A black precipitate was filtered and washed with small volumes of cold water and cold diethyl ether. Infra-red analysis indicated the compound was a mixture of chloro- and bromoruthenates. The black precipitate was then dissolved in 48% conc. HBr (50ml) and the solution slowly evaporated to a volume of 15ml. The cooled solution was filtered and bromine vapour bubbled through the filtrate precipitating small black crystals of K_2RuBr_6. Although the bromide microanalytical result indicated some HBr or possibly KBr had co-precipitated the compound was used without further purification.

Observed/ infra-red: K_2RuBr_6 ν_3 250cm^{-1}

Literature/infra-red: K_2RuBr_6 ν_3 263cm^{-1} [ref.158]

Analysis

K_2RuBr_6.HBr	
found: Br(76.98)	calculated: Br(75.63)

6.14.2 The preparation of $[Bu_4N]_2[RuBr_6]$

K_2RuBr_6 (0.58g, 0.88mmol) dissolved in the minimum volume of 2M HBr solution was stirred in a beaker along with acidified Dowex 50 W-X8 cation exchange resin (ca.3g)

then rapidly filtered. $[Bu_4N]Br$ (0.57g, 1.76m) dissolved in the minimum volume of 2M HBr solution was added to the filtrate and a blue compound precipitated. The precipitate was suction filtered and washed with small volumes of ice-cold water and diethyl ether. The air-stable blue product, $[Bu_4N]_2[RuBr_6]$, was obtained in a 55% yield (based on $K_2RuBr_6.HBr$).

Observed

	$[Bu_4N]_2[RuBr_6]$
infra-red	ν_3 235cm^{-1}
vis/uv (CH_2Cl_2)	13.4(sh), 14.1(sh), 14.7, 16.2, 18.1, 19.0, 19.8, 23.4(sh)kK

Literature

infra-red	Cs_2RuBr_6	ν_3 240cm^{-1}	[ref.163]
vis/uv	unreported		

Analysis

	$[Bu_4N]_2[RuBr_6]$
found	C(36.16), H(6.86), N(2.56), Br(46.86)
calculated	C(36.07), H(6.76), N(2.63), Br(45.04)

6.15 The preparation of bis tetra-n-butylammonium hexabromoosmate(IV)

$[Bu_4N]_2[OsBr_6]$ was prepared from K_2OsBr_6 by a modification of the method of Gutbier [95].

6.15.1 The preparation of K_2OsBr_6

A solution of K_2OsCl_6 (0.7g, 1.45mmol) in 48% HBr solution (50ml) was slowly reduced to a small volume on a hotplate. After cooling, the solution was filtered to collect a black crystalline precipitate which was washed with ice-cold absolute ethanol (5ml) and suction dried. Although the bromide microanalysis indicated some HBr or possibly KBr had co-precipitated the compound was used without further purification.

Observed/ infra-red: K_2OsBr_6 ν_3 226cm^{-1}

Literature/infra-red: K_2OsBr_6 ν_3 224cm^{-1} [ref.164]

Analysis

K_2OsBr_6	
found: Br(69.04)	calculated: Br(64.11)

6.15.2 The preparation of $[Bu_4N]_2[OsBr_6]$

K_2OsBr_6 (0.55g, 0.73mmol) dissolved in the minimum volume of 2M HBr solution was stirred in a beaker along with acidified Dowex 50 W-X8 cation exchange resin (ca. 3g) and the mixture filtered rapidly. $[Bu_4N]Br$ (0.48g, 1.5mmol) dissolved in the minimum volume of 2M HBr solution was added and a brown compound precipitated. The brown precipitate was filtered and washed with 5ml portions of ice-cold water and diethyl ether. Brown $[Bu_4N]_2[OsBr_6]$ was obtained in ca. 80% yield (based on K_2OsCl_6).

Observed

$[Bu_4N]_2[OsBr_6]$	
infra-red	ν_3 214cm^{-1}
vis/uv(CH_2Cl_2)	19.0(sh), 19.7(sh), 20.02, 22.1, 23.9, 24.7(sh)kK

Literature

infra-red	$[(C_7H_{16})_4N]_2[OsBr_6]$ ν_3 211cm^{-1} [ref.155]
vis/uv	$[Bu_4N]_2[OsBr_6]$ 18.9(sh), 19.5(sh),
$ClCH_2CH_2Cl$	20.1, 22.0, 23.6, 24.5(sh) [ref.166]

Analysis

$[Bu_4N]_2[OsBr_6]$	
found	C(33.17), H(5.99), N(2.23), Br(42.34)
calculated	C(33.28), H(6.24), N(2.43), Br(41.56)

6.16 The preparation of bis tetra-n-butylammonium hexabromoiridate(IV)

$[Bu_4N]_2[IrBr_6]$ was prepared from K_2IrBr_6 by a modification of the method of Fergusson and Rankin [91].

6.16.1 The preparation of K_2IrBr_6

A solution of K_2IrCl_6 (0.39g, 0.8mmol) in 48% HBr (60ml) was evaporated nearly to dryness. The procedure was repeated and then on a third evaporation the volume was only reduced to approximately 10ml. The solution was cooled by an ice-bath and bromine vapour poured over the solution. The black-blue precipitate which immediately formed was suction filtered and washed with ice-cold ethanol (5ml). Although a bromide microanalysis indicated that excess bromide in the form of HBr or possibly KBr had co-precipitated, the product K_2IrBr_6 was used without further purification.

Observed/infra-red: K_2IrBr_6 ν_3 231cm^{-1}

Literature/infra-red: K_2IrBr_6 ν_3 235cm^{-1} [ref.152]

Analysis

K_2IrBr_6	
found: Br(68.50)	calculated: Br(63.94)

6.16.2 The preparation of $[Bu_4N]_2[IrBr_6]$

K_2IrBr_6 (0.38g,0.5mmol) dissolved in the minimum volume of distilled water was stirred in a beaker along with acidified Dowex 50 W-X8 cation exchange resin (ca. 3g) and the mixture filtered rapidly. $[Bu_4N]Br$ (0.33g, 1mmol) dissolved in the minimum volume of distilled water was added and a blue compound precipitated. The precipitate was washed with 5ml portions of ice-cold water and diethyl ether. Blue $[Bu_4N]_2[IrBr_6]$ was obtained in approximately 50% yield (based on K_2IrCl_6).

Observed

$[Bu_4N]_2[IrBr_6]$	
infra-red	ν_3 221cm^{-1}
vis/uv (CH_2Cl_2)	13.3, 13.8, 14.4, 16.7, 18.1, 18.7kK

Literature

$[Bu_4N]_2[IrBr_6]$		ref.
infra-red	ν_3 221cm^{-1}	90,162
vis/uv (CH_3NO_2)	13.3, 14.0, 14.6, 16.7, 18.1, 18.8kK	166

Analysis

$[Bu_4N]_2[IrBr_6]$	
found	C(33.06), H(6.21), N(2.21), Br(41.32)
calculated	C(33.23), H(6.23), N(2.42), Br(41.48)

6.17 The preparation of bis tetra-n-butylammonium hexabromoplatinate(IV)

$[Bu_4N]_2[PtBr_6]$ (see ref.92) was prepared from K_2PtBr_6.

6.17.1 The preparation of K_2PtBr_6

Following the method of Gutbier and Bauriedel [167], a solution of K_2PtCl_6 (0.5g, 1mmol) dissolved in 48% HBr (50ml) was slowly evaporated to a small volume on a hotplate. The procedure was repeated and then on a third evaporation the volume was reduced to approximately 10ml. The solution was cooled by an ice-bath and bromine vapour poured over the solution. Red-black crystals of K_2PtBr_6 precipitated immediately and were suction-filtered and washed with 5ml portions of ice-cold ethanol and diethyl ether. (yield 85%).

Observed

K_2PtBr_6	
infra-red	ν_3 243cm^{-1}
Raman	ν_1 217cm^{-1}, ν_2 194cm^{-1}

Literature

K_2PtBr_6		ref.
infra-red	ν_3 243cm^{-1}	151
Raman	ν_1 217cm^{-1}, ν_2 195cm^{-1}	151

Analysis

K_2PtBr_6	
found: Br(63.80)	calculated: Br(63.66)

6.17.2 The preparation of $[Bu_4N]_2[PtBr_6]$

A solution of $[Bu_4N]Br$ (0.43g, 1.3mmol) dissolved in the minimum volume of 48% HBr was added to a saturated solution of K_2PtBr_6 (0.5g, 0.7mmol) in 48% HBr. A yellow

solid precipitated and was suction filtered and washed with 5ml portions of ice-cold water and diethyl ether. When the yellow precipitate was dried on the vacuum line, the compound changed from a yellow powder to a sticky brown solid. Therefore the compound was re-dissolved in excess 48% HBr solution and slowly evaporated to a small volume. When the solution cooled, dark red crystals of $[Bu_4N]_2[PtBr_6]$ formed. The crystals were suction filtered and washed with ice-cold ether. (Yield ca.40% based on K_2PtCl_6).

Observed

	$[Bu_4N]_2[PtBr_6]$
infra-red	ν_3 230cm^{-1}
vis/uv(CH_2Cl_2)	18.0(sh), 26.3, 31.0, 32.0(sh)kK

Literature

infra-red	$[(C_7H_{16})_4N]_2[PtBr]$	ν_3 230cm^{-1}	[ref.155]
vis/uv (CH_2Cl_2)	$[Bu_4N]_2[PtBr_6]$	18.9(sh), 22.6(sh), 26.3, 30.8, 32.2kK	[ref.92]

Analysis

	$[Bu_4N]_2[PtBr_6]$
found	C(32.23), H(6.38), N(2.11), Br(40.60)
calculated	C(33.15), H(6.22), N(2.41), Br(41.38)

6.18 The attempted preparation of tris tetra-n-butylammonium hexabromorhodate(III) - unintentional preparation of tris tetra-n-butylammonium nonabromodirhodate(III)

Following the method of Robb and Bekker [102], the precursor K_3RhBr_6 was prepared from $RhCl_3$ as follows:-

$RhCl_3.3H_2O$ (1g, 3.8mmol) was dissolved in distilled water and the pH altered to pH9 by addition of 1M KOH solution which resulted in a white precipitate. The solution and white precipitate were heated at ca. $80°C$ for 90 minutes to digest the solid then filtered (Whatman No.1 filter paper). The precipitate of $Rh(OH)_3.3H_2O$ was washed copiously with distilled water.

A solution of $Rh(OH)_3.3H_2O$ (0.8g, 3.8mmol) and KBr (1.24g, 11.5mmol) in 48% HBr (15ml) was heated at $50°C$ for 10 minutes. After cooling, a small amount of black precipitate was filtered off then absolute ethanol (1L) added to the solution. The solution wa left overnight during which time a fine light brown solid precipitated. The solid was filtered (Whatman No.1), dried in an oven then recrystallized from 4M HBr by addition of ethanol. The reddish-brown compound K_3RhBr_6 was obtained in 25% yield (based on $RhCl_3.3H_2O$).

K_3RhBr_6 (0.45g, 0.64mmol) dissolved in the minimum volume of 2M HBr was stirred in a beaker along with acidified Dowex 50 W-X8 cation exchange resin (ca. 3g) and the mixture filtered rapidly. When $[Bu_4N]Br$ (0.62g, 1.93mmol) dissolved in the minimum volume of 2M HBr was added to the solution, the expected product $[Bu_4N]_3[RhBr_6]$ did not precipitate. The mixture was gently evaporated to a small volume on a hot plate and a black solid obtained by filtering. The solid was washed with ice-cold ether (10ml) and suction dried to obtain a green powder which analysed as $[Bu_4N]_3[Rh_2Br_9]$. The experiment was repeated several times and on those occasions precipitates did form in the first instance when $[Bu_4N]Br$ was added to the solution of '$[H_3O]_3[RhBr_6]$'. However, the solids which were isolated were either green $[Bu_4N]_3[Rh_2Br_9]$ or a sticky black solid, identity unknown.

Observed

K_3RhBr_6	
infra-red	ν_3 249cm^{-1}
vis/uv(4M HBr)	18.0, 22.5kK

Literature

infra-red	Cs_3RhBr_6	ν_3 253cm^{-1}	[ref.96]
vis/uv(4M HBr)	K_3RhBr_6	18.1, 22.2kK	[ref.168]

Analysis

K_3RhBr_6	
found: Br(67.99)	calculated: Br(68.52)

Observed

$[Bu_4N]_3[Rh_2Br_9]$	
infra-red	ν 255, 250(sh)cm^{-1}
vis/uv(CH_2Cl_2)	17.4, 21.4(sh)kK

Literature

infra-red	$[Bu_4N]_2[H_3O][Rh_2Br_9]$	ν 250, 245cm^{-1}	[ref.103]
vis/uv(4M HBr)	$K_3Rh_2Br_9$	17.8kK	[ref.102]

Analysis

$[Bu_4N]_3[Rh_2Br_9]$	
found	C(34.21), H(6.90), N(2.68), Br(43.42)
calculated	C(34.89), H(6.54), N(2.54), Br(43.56)

6.19 The attempted preparation of tris tetra-n-butylammonium hexabromomolybdate(III) -unintentional preparation of tris tetra-n-butylammonium nonabromodimolybdate(III)

A solution of tervalent molybdenum in 48% HBr solution was prepared by the methods of Wardlaw [56] and Lohmann [169]. This required the steady electrolytic reduction of a solution of MoO_3 (3.5g, 24mmol) in 48% HBr (50ml) for ca. 3 hours under a stream of nitrogen gas. To 5ml of the reduced solution was added $[Bu_4N]Br$ (2.32g, 7.2mmol) dissolved in the minimum volume of 48% HBr. When the volume of solution was reduced by 75% a red-brown solid precipitated which was slightly moisture sensitive and analysed as $[Bu_4N]_3[Mo_2Br_9]$. In order to suppress dimerisation, the experiment was repeated with a three-fold excess of $[Bu_4N]Br$. Instead of reducing the solution volume to precipitate the complex the solution was extracted with deoxygenated CH_2Cl_2 and dark red crystals precipitated by addition of deoxygenated diethyl ether to the organic phase. The infra-red spectrum of the crystals was identical to that of the dimolybdenum complex obtained previously.

Observed

$[Bu_4N]_3[Mo_2Br_9]$	
infra-red	ν 249(vs), 219(s)cm^{-1}
vis/uv(48% HBr)	17.9, 19.6(sh), 22.2(sh), 23.8kK

Literature

$[Et_4N]_3[Mo_2Br_9]$		ref.
infra-red	ν 247(vs), 227(s)cm^{-1}	170
vis/uv(powder reflectance)	18.2, 20.0(sh), 22.5(sh), 23.5kK	171

Analysis

$[Bu_4N]_3[Mo_2Br_9]$	
found	C(34.17), H(6.45), N(2.53), Br(44.12)
calculated	C(35.19), H(6.60), N(2.57), Br(43.93)

6.20 The attempted preparation of bis tetra-n-butylammonium hexabromopalladate(IV) - unintentional preparation of bis tetra-n-butylammonium hexabromodipalladate(II)

K_2PdBr_6 was prepared by the method of Gutbier and Krell [101]:-

$PdCl_2$ (0.7g, 4mmol) was added to 48% HBr (50ml) in a 100ml beaker and the mixture heated to encourage bromination of the palladium. A saturated aqueous solution of KBr (1.0g, 8.4mmol) was added and the solution cooled in an ice-bath. When bromine vapour was poured over the solution, black crystals of K_2PdBr_6 precipitated from the solution.

Observed/infra-red: K_2PdBr_6 ν_3 266cm^{-1}

Literature/infra-red: K_2PdBr_6 ν_3 253cm^{-1} [ref.154]

The same method was unsuccessful when repeated with $[Bu_4N]Br$ substituted in place of KBr because $[Bu_4N]Br$ was found to precipitate from HBr (probably) as polybromides in the presence of bromine vapour.

K_2PdBr_6 (0.66g, 1mmol) dissolved in the minimum volume of 2M HBr was stirred in a beaker along with Dowex 50 W-X8 cation exchange resin (ca. 3g) and rapidly filtered. A saturated solution of $[Bu_4N]Br$ (0.64g, 2mmol) in 2M HBr solution was added to the filtrate and a sticky brown solid precipitated. The brown solid was washed with 5ml portions of ice-cold ethanol and diethyl ether. The brown product analysed as $[Bu_4N]_2[Pd_2Br_6]$.

If K_2PdBr_6 and $[Bu_4N]Br$ are stirred together in CH_2Cl_2 then $[Bu_4N]_2[Pd_2Br_6]$ is obtained in low yield. Similarly, $[Bu_4N]_2[Pd_2Br_6]$ is the only product from the metathesis of K_2PdBr_6 and $[Bu_4N]Br$ in CH_3CN. But, the metathesis of K_2PdBr_6 with $[Et_4N]Br$ in CH_3CN produced a red-brown compound which exhibited an infra-red

spectrum consistent with the formation of a mixture of $[Et_4N]_2[PdBr_4]$ (ν 255cm^{-1}) and $[Et_4N]_2[PdBr_6]$ (ν 227cm^{-1}).

Observed/infra-red: $[Bu_4N]_2[Pd_2Br_6]$ ν 256(s), 191(s)cm^{-1}

Literature/infra-red: $[Et_4N]_2[Pd_2Br_6]$ ν 266(vs), 262(vs), 192(m)cm^{-1} [ref.173]

Analysis

$[Bu_4N]_2[Pd_2Br_6]$	
found	C(32.52), H(2.06), N(6.25), Br(42.94)
calculated	C(32.65), H(2.38), N(6.12), Br(40.76)

6.21 The attempted preparation of bis(tetra-n-butylammonium)hexabromotantalate(IV)

The synthesis of this compound was desired as part of an investigation into the correlation between charge transfer energies and $E_{1/2}$ values, as well as offering a useful cross-reference for the $[TaBr_6]^{z/z-1}$ redox couples already determined. Two methods of preparation were attempted:

6.21.1

$[Bu_4N][TaBr_6]$ and $[Bu_4N]I$ in the mole ratio 1:1 were gently refluxed in CH_2Cl_2 under vacuum for 3 days. When the solvent was evacuated, the unreacted starting materials were recovered.

6.21.2

$TaBr_4$ was prepared by reduction of $TaBr_5$ with aluminium powder in a Carius tube at $250°C$ for 3 days according to the method of McCarley and Boatman [97]. When $TaBr_4$ and $[Bu_4N]Br$ (mole ratio 1:2) were gently refluxed in CH_2Cl_2 under vacuum for 3 days no reaction occurred. NB: Reaction 6.21.2 could have been attempted in CH_3CN solution as the reaction is known to proceed when $NbBr_4.2CH_3CN$ and $[Et_4N]Br$ are used (Walton *et al* [108]). However, Walton *et al* found the reaction of $TaBr_4$ with CH_3CN formed an unidentifiable product.

6.22 The preparation of supporting electrolytes

The necessary requirements of a supporting electrolyte were considered in chapter 2.

Two similar supporting electrolytes were used in this thesis, tetra-n-butylammoniumhexafluorophosphate ($[Bu_4N]PF_6$) and tetra-n-butylammoniumtetrafluoroborate ($[Bu_4N]BF_4$). Both compounds were prepared and purified in the same manner, therefore the preparation of $[Bu_4N]PF_6$ will only be discussed (in the case of $[Bu_4N]BF_4$ substitute $H[BF_4]$ for KPF_6):

KPF_6 (15g, 0.081mol) was dissolved in excess distilled water and the solution filtered (Whatman No.1 filter paper). A slight excess of $[Bu_4N]OH$ was added slowly to the filtrate while stirring the solution with a glass rod until precipitation of white $[Bu_4N]PF_6$ was complete. The white compound was filtered with a sintered glass funnel and washed with lukewarm (ca. $40°C$) distilled water. The solid was transferred to a 500ml beaker, thoroughly stirred with luke warm distilled water (ca. 250ml) then filtered with a sintered glass funnel. The washing procedure was repeated until the washings registered pH7 (approximately 6 times). After washing, the compound was transferred to a 250ml round bottomed flask and evacuated under a dynamic vacuum for 2-3 hours. After drying, the solid was dissolved in CH_2Cl_2 and filtered (Whatman No.1) then the solvent evacuated by a dynamic vacuum. This process was repeated until the filtered solvent was crystal clear (approximately 4 times). Finally, the white powder of $[Bu_4N]PF_6$ was transferred to a large Rotaflow vessel and dried on the vacuum line for several days with occasional shaking before transferral to the glove box for storage.

6.23 Purification of solvents

6.23.1 Methylene chloride

Analar CH_2Cl_2 (200ml) was refluxed over P_2O_5 (5g) for 15 minutes then rapidly distilled directly into a Quickfit flask to minimise contact with the open air, topping

and tailing' by 20% (discarding the first and last 20% of distillate). The distillation was repeated with the distillate collected directly into a large Rotaflow vessel. The Rotaflow vessel was transferred to the vacuum line and the solvent degassed three times by the freeze-thaw method: (This requires the solvent to be frozen very slowly starting from the bottom of the vessel and gradually moving to the top. As gas bubbles effervesce, the stopcock is opened briefly to allow the escape of the gas. The slowly rising solidified solvent effectually 'pushes' the dissolved gas out of solution.) When the solvent was thoroughly degassed, the solvent was distilled over into a 100ml graduated Rotaflow vessel (on the vacuum line) containing 4Åmolecular sieves. (The molecular sieves were previously dried by heating at $180^{o}C$ overnight while evacuating on the vacuum line.) The dried and degassed solvent was protected from light by surrounding the Rotaflow vessel with aluminium foil.

6.23.2 Acetonitrile

CH_3CN was purified by the method of J.M. Winfield [172] which required several stepwise distillations performed in a Pyrex still equipped with a 0.75m vacuum jacket separating column and protected from moisture.

1. HPLC grade acetonitrile (350ml) was refluxed over anhydrous $AlCl_3$ (ca. 6g) for 1 hour then rapidly distilled, 'topping and tailing' the solvent by 3%.

2. $KMnO_4$ (2g) and Li_2CO_3 (2g) were refluxed with the solvent for ca. 15 minutes then the solvent rapidly distilled, 'topping and tailing' the solvent by 3%.

3. The solvent was refluxed over $KHSO_4$ (5g) for ca. 1 hour then rapidly distilled, 'topping and tailing' the solvent by 3%.

4. The solvent was refluxed over CaH_2 (6g) for ca. 1 hour then rapidly distilled, 'topping and tailing' the solvent by 3%.

5. The solvent was refluxed over P_2O_5 (4g) for 30 minutes then rapidly distilled, 'topping and tailing' the solvent by 3%.

6. Step 5) was repeated then the solvent transferred to a large Rotaflow vessel in a dry box and degassed and distilled onto activated molecular sieves as for CH_2Cl_2.

Appendix A

Calculation of the interelectronic correlation terms (k+r), K and R.

All the values were calculated from the data in tables 5.2, 5.3 and 5.4 and wherever possible gradients were calculated by a least-squares best fitting line analysis.

A.1 Second row $[MF_6]^{1-/2-}$; M = Nb, Mo, Tc*, Ru

x = k + r = +1.21
z = 3R - 2(k + r) = -0.02
R = [-0.02 + 2(+1.21)]/3 = +0.80
K unobtainable

A.2 Third row $[MF_6]^{1-/2-}$; M = Ta, W, Re, Os, Ir

x = k + r = +1.18
y = k + K + r = +0.60 therefore K = -0.58
z = 3R - 2(k + r) = +0.45
R = [+0.45 + 2(+1.18)]/3 = +0.93

A.3 Second row $[MCl_6]^{1-/2-}$; M = Nb, Mo, Tc*, Ru, Rh, Pd

x = k + r = +0.96
y = k + K + r = +0.65 therefore K = -0.31
z = 3R - 2(k + r) = -0.39
R = [-0.39 + 2(+0.96)]/3 = +0.51

A.4 Third row $[MCl_6]^{1-/2-}$; M = Ta, W, Re, Os, Ir, Pt

x = k + r = +0.94
y = k + K + r = +0.51 therefore K = -0.43
z = 3R - 2(k + r) = -0.05
R = [-0.05 + 2(+0.94)]/3 = +0.61

A.5 Second row $[MBr_6]^{1-/2-}$; M = Nb, Mo, Tc*, Ru

x = k + r = +0.85
z = 3R -2(k + r) = -0.48
R = [-0.48 + 2(+0.85)]/3 = +0.41
K unobtainable

A.6 Third row $[MBr_6]^{1-/2-}$; M = Ta, W, Re, Os, Ir, Pt

x = k + r = +0.74
y = k + K + r = +0.63 therefore K = -0.11

$z = 3R - 2(k + r) = -0.07$
$R = [-0.07 + 2(+0.74)]/3 = +0.47$

A.7 Second row $[MCl_6]^{2-/3-}$; M = Zr, Nb, Mo, Tc*, Ru, Rh

$x = k + r = +1.12$
$y = k + K + r = +0.76$ therefore $K = -0.36$
$z = 3R - 2(k + r) = -0.52$
$R = [-0.52 + 2(+1.12)]/3 = +0.57$

A.8 Third row $[MCl_6]^{2-/3-}$; M = Hf*, Ta, W, Re, Os, Ir

$x = k + r = +0.98$
$y = k + K + r = +0.55$ therefore $K = -0.43$
$z = 3R - 2(k + r) = +0.03$
$R = [+0.03 + 2(+0.98)]/3 = +0.66$

A.9 Second row $[MBr_6]^{2-/3-}$; M = Nb, Mo, Tc*, Ru

$x = k + r = +0.95$
$y = k + K + r = +0.53$ therefore $K = -0.42$
$z = 3R - 2(k + r) = -0.46$
$R = [-0.46 + 2(+0.95)]/3 = +0.48$

A.10 Third row $[MBr_6]^{2-/3-}$; M = Ta, W, Re, Os, Ir

x = k + r = +0.60

y = k + K + r = -0.52 therefore K = -0.08

z = 3R - 2(k + r) = -0.14

R [-0.14 + 2(+0.60)]/3 = +0.35 (* estimated value)

Appendix B

Chemicals

Chemical	Supplier
diethylether	May and Baker Ltd.
acetonitrile	Rathburn Chemicals Ltd.
dichloromethane (Pron.AR)	May and Baker Ltd.
abs. ethanol	James Burrough PLC.
hydrobromic acid (48%)	BDH chemicals Ltd.
fluoroboric acid	Aldrich Chemical Company Ltd.
phosphorus pentoxide	Koch-light laboratories Ltd.
Dowex 50 W-X8 cation exchange resin	BDH chemicals Ltd.
tungsten wire	Jenkins
platinum wire	Johnson Matthey Metals Ltd.
tungsten powder	Ventron Alpha products
bromine	May and Baker Ltd.
tetra-n-butylammoniumhydroxide	Aldrich Chemical Company Ltd.
tungsten hexacarbonyl	Fluka AG

cont.

Chemical	Supplier
potassiumhexafluorophosphate	Aldrich Chemical Company Ltd.
molybdenum trioxide	Hopkins and Williams Ltd.
rhenium oxide	Ventron G.m.B.H. Karslruhe,WG
zirconium(IV) oxide	Aldrich Chemical Company Ltd.
Hafnium(IV) oxide	Aldrich Chemical Company Ltd.
tetra-n-butylammoniumbromide (HPLC. grade)	Fisons PLC.
tetra-n-butylammoniumiodide (HPLC. grade)	Fisons PLC.
tetraethylammoniumbromide	Koch-light laboratories Ltd.
molybdenum hexacarbonyl	BDH chemicals Ltd.
niobium pentabromide	Ventron Alpha products
tantalum pentabromide	Ventron Alpha products
palladium(II) chloride	Johnson Matthey chemicals Ltd.
trispotassiumhexachloro-ruthenate(III)	Johnson Matthey chemicals Ltd.
bispotassiumhexachloro-osmate(IV)	Johnson Matthey chemicals Ltd.
bispotassiumhexachloro-iridate(IV)	Aldrich Chemical Company Ltd.
bispotassiumhexachloro-platinate(IV)	Johnson Matthey chemicals Ltd.
rhodiumtrichloride	Johnson Matthey chemicals Ltd.

Appendix C

References

[1] J.P.Fackler Jnr., "Symmetry in Chemical Theory", Benchmark papers in inorganic chemistry, Vol.4, 1973.

[2] J.S.Griffith, "The Theory of Transition Metal Ions", Cambridge University Press, 1964.

[3] H.L.Schlaffer and G.Gliemann, "Ligand Field theory", Wiley-Interscience, 1969.

[4] A.Liberles, "Introduction to Molecular Orbital Theory", Holt, Rinehart and Winston, 1966.

[5] M.Orchin and H.H.Jaffe,"Symmetry, Orbitals and Spectra", Wiley-Interscience, 1971.

[6] H.von Bethe, **Ann.Phys**, (1929),**5**, 133.

[7] B.N.Figgis, "Ligand Field Theory", Comprehensive Coordination Chemistry Vol.1, Pergamon Press, 1987.

[8] C.K.Jorgensen,"Absorption Spectra and Chemical Bonding", Pergamon Press, 1962.

[9] J.Sadlej, "Semi-Empirical Methods in Quantum Chemistry", Ellis Horwood Ltd., 1985.

[10] C.J.Ballhausen and H.B.Gray, "Electronic Structure of Metal Complexes", Coordination Chemistry Vol.1, ACS monograph, Van Nostrand Reinhold, 1971.

[11] See reference [5].

[12] R.B.Heslop and K.Jones, "Inorganic Chemistry", Elsevier Scientific Publishing Co., 1976.

[13] J.H.Canterford and R.Colton, "Halides of the Second and Third Row Transition Metals", Wiley-Interscience, 1968.

[14] L.Pauling, "The Nature of the Chemical Bond", Cornell University Press, 1945.

[15] A.N.Pandey, D.K.Sharma, U.F.Verma,**Acta.Phys.Polon. A**, (1977),**A51**, 475.

[16] C.K.Jorgensen, "Essay's in Coordination Chemistry", Birkhauser Verlag, 1964.

[17] N.Bartlett,**Angew.Chem.Int.Ed.**, (1968),**7**, 433.

[18] D.S.Dyer and R.O.Ragsdale,**JCS Chem.Comm.**, (1966), 601.

[19] M.Kubo and D.Nakamura,**Adv.Inorg.Chem.Radiochem.**, (1966),**8**, 257.

[20] L.A.Woodward and M.J.Ware,**Spectrochim.Acta A**, (1963), **A19**, 775.

[21] T.Hiraishi, I.Nakagawa, T.Shimanouchi, **Spectrochim.Acta A**, (1964),**A20**, 819.

[22] F.A.Cotton and C.B.Harris,**Inorg. Chem.**, (1967),**6**, 376.

[23] J.Owen and K.W.H.Stevens,**Nature London**, (1953),**171**, 836.

[24] J.H.E.Griffiths and J.Owen,**Proc.Roy.Soc.**,(1954),**A226**, 96.

[25] E.Deutsh, K.Libson, S.Jurisson, L.F.Lindsay, **Prog.Inorg.Chem.**, (1983),**30**, 75.

[26] D.R.Crow, "Principles and Applications of Electrochemistry", 2^{nd} Edn., Chapman and Hall, 1979.

[27] Southhampton electrochemistry group, "Instrumental methods in electrochemistry", J.Wiley and Sons, 1985.

[28] A.J.Bard and L.R.Faulkner, "Electrochemical Methods", J.Wiley and Sons, 1980.

[29] J.Heinze,**Angew.Chem.Int.Ed.**, (1984),**23**, 831.

[30] R.S.Nicholson and I.Shain,**Anal.Chem.**, (1964),**36**, 706.

[31] K.Moock, Ph.D. Thesis, University of Glasgow. 1985

[32] R.H.Wopscall and I.Shain,**Anal.Chem.**, (1967),**39**, 1514.

[33] D.Bauer and M.Breant,**Electroanalytical Chem.**,(1975),**8**,281.

[34] H.J.Emeleus and G.S.Rao,**J.Chem.Soc.**, (1958), 4245.

[35] E.A.Allen, B.J.Brisdon, G.W.A.Fowles,**J.Chem.Soc.**,(1964), 4531.

[36] C.K.Mann,**Electroanalytical Chem.**,**3**, 57.

[37] J.L.Mills, R.Nelson, S.G.Shore, L.B.Anderson, **Anal.Chem.**, (1971),**43**, 157.

[38] C.D.Schmulback and T.V.Oomen,**Anal.Chem.**, (1973),**45**, 820.

[39] G.A.Heath, G.T.Hefter, T.W.Boyle, C.D.Desjardins, D.W.A.Sharp,**J.Fluorine Chem.**, (1978),**11**, 399.

[40] G.M.Anderson, J.Iqbal, D.W.A.Sharp, J.M.Winfield, **J.Fluorine Chem.**, (1984),**24**, 303.

[41] G.A.Heath, K.A.Moock, D.W.A.Sharp, L.J.Yellowlees, **JCS Chem.Comm.**, (1985), 1503.

[42] B.H.Loo and Y.G.Lee,**Appl.Surf.Science**, (1984),**18**,345.

[43] I.Rubinstein,**J.Phys. Chem.**, (1981),**85**, 1899.

[44] M.Mastragostino and C.Gramellini,**Electrochim. Acta**, (1985),**30**, 373.

[45] P.K.Adanuvor, R.E.White, S.E.Lorimer, **J.Electrochem.Soc.**, (1987),**134**, 625.

[46] M.Mastragostino, S.Valcher, P.Lazzari,**J.Electroanal. Chem.Interfac.Electrochem.**, (1981),**126**, 189.

[47] M.W.Breitner,**Electrochim. Acta**, (1963),**8**, 925.

[48] D.K.Kyriacou, "Basics of Electroorganic Synthesis", Wiley-Interscience, 1981.

[49] I.V.Nelson and R.T.Iwamoto,**J.Electroanal.Chem. Interfac.Electrochem.**, (1964),**7**, 218.

[50] A.P.Tomilov,**Russ.Chem.Rev.**, (1962),**31**, 569.

[51] D.T.Sawyer and J.L.Roberts Jnr., "Experimental Electrochemistry for Chemists", Wiley-Interscience, (1974).

[52] A.A.Vlcek,**Prog.Inorg.Chem.**,**5**, 211.

[53] J.Koryta and J.Dvorak, "Principles of Electrochemistry" J.Wiley and Sons, 1987.

[54] E.R.Brown and R.F.Large "Physical Methods of Chemistry" Part IIA, Wiley-Interscience, 1971.

[55] S.Brownstein, G.A.Heath, A.Sengupta, D.W.A.Sharp, **JCS Chem.Comm.**, (1983), 669.

[56] W.Wardlaw and A.J.I.Harding,**J.Chem.Soc.**, (1926), 1592.

[57] A.Rosenheim and H.J.Braun,**Z.Anorg.Chem.**, (1905),**46**, 311.

[58] I.Schmidt, U.P.Siebel, U.Müller, K.Dehnicke, **Z.Anorg.Allgem.Chem.**, (1988),**556**, 57.

[59] G.W.Watt and R.J.Thompson,**Inorg. Synth.** ,**7**, 189.

[60] H.S.Trop, A.Davidson, G.H.Carey, B.V.de Pamphilis, A.G.Jones, M.A.Davis,**J.Inorg.Nucl.Chem.**, (1979),**41**, 271.

[61] G.Rouschias and G.Wilkinson,**J.Chem.Soc.A**, (1968), 489.

[62] F.A.Cotton, N.F.Curtis, B.F.G.Johnson, W.R.Robinson, **Inorg. Chem.**, (1965),**4**, 326.

[63] B.J.Brisdon, D.A.Edwards, D.J.Machin, K.S.Murray, R.A.Walton,**J.Chem.Soc.A**, (1967), 1825.

[64] R.A.Walton, P.C.Crouch, B.J.Brisdon,**Spectrochim.Acta A**, (1968),**24A**, 601.

[65] L.von Rudzik and W.Preetz,**Z.Anorg.Allg.Chem.**,(1978),**443**, 118.

[66] H.von Muller, P.Bekk, I.Hagenlocher, **Z.Anorg.Allg.Chem.**, (1983),**503**, 15.

[67] M.F.Ghorab Ph.D. Thesis, University of Glasgow, 1988

[68] R.K.Sharma and J.L.Fry,**J.Org. Chem.**, (1983),**48**, 2112.

[69] J.Emsley, O.P.A.Hoyle, R.E.Overill,**JCS Chem.Comm.**,(1977), 225.

[70] P.Reeb, Y.Mugnier, A.Dormond, E.Laviron, **J.Organomet.Chem.**, (1982),**239**, C1.

[71] N.V.Sidgwick, "The Organic Chemistry of Nitrogen", 3rd Edn., Clarendon Press, 1966.

[72] C.M.Langkammerer, E.L.Jenner, D.D.Coffman, B.W.Houk, **J.Amer.Chem.Soc.**, (1960),**82**, 1395.

[73] R.H.Magnusson,**Inorganic Chem.**, (1984),**23**, 387.
[74] I.M.Kolthoff and J.F.Coetzee,**J.Amer.Chem.Soc.**,(1957),**79**, 1852.
[75] A.I.Popov and D.H.Geske,**J.Amer.Chem.Soc.**, (1958),**80**, 1340.
[76] J.D.Voorhies and E.J.Schurdak,**Anal.Chem.**, (1962),**34**, 939.
[77] G.Dryhurst and P.J.Elving,**Anal.Chem.**, (1967),**39**, 606.
[78] see reference [42].
[79] A.S.Hinman, S.Pons, J.Cassidy,**Electrochim.Acta**,(1985),**30**, 95.
[80] K.J.Hanson and C.W.Tobias,**J.Electrochem.Soc.**,(1987),**134**, 2204.
[81] M.Biserni and M.Mastragostino,**Ann.Chimica.(Roma)**,(1985),**75**, 195.
[82] J.I.Song,*unpublished work.*
[83] A.T.Hubbard, R.A.Osteryoung, F.C.Anson,**Anal.Chem.**,(1966),**38**, 692.
[84] G.M.Anderson and J.M.Winfield,**JCS Dalton**, (1986), 337.
[85] A.I.Popov, "Halogen Chemistry", Vol.1, Academic Press, 1967.
[86] R.L.Benoit and C.louis,**Inorg.Nucl.Chem.Lett.**, (1970),**6**, 817.
[87] W.M.Latimer, "Oxidation Potentials", 2^{nd} Edn.,Prentice-Hall, 1952.
[88] F.P.Dwyer, H.A.McKenzie, R.S.Nyholm,
J.Proc.Roy.Soc.N.S.Wales, (1946),**80**, 183.
[89] F.P.Dwyer, H.A.McKenzie, R.S.Nyholm,
J.Proc.Roy.Soc.N.S.Wales, (1947),**81**, 216.
[90] W.Preetz and H.J.Steinebach,**Z.Naturforsch.B**, (1985),**40b**, 745.
[91] J.E.Fergusson and D.A.Rankin,**Aust.J.Chem.**, (1983),**36**, 863.
[92] D.L.Swihart and W.R.Mason,**Inorg. Chem.**, (1970),**9**, 1749.
[93] A.T.Hubbard and F.C.Anson,**Anal.Chem.**, (1966),**38**,1887.
[94] N.Bartlett, F.Einstein, D.F.Stewart, J.Trotter,
JCS Chem.Comm., (1966), 550.
[95] A.Gutbier,**Ber.**, (1913),**46**, 2098.
[96] T.S.Kuan,**Inorg. Chem.**, (1974),**13**, 1256.
[97] R.E.McCarley and J.C.Boatman,**Inorg. Chem.**, (1963),**2**, 547.
[98] R.W.Mertes, W.R.Crowell, R.K.Brinton,**J.Amer.Chem.Soc.**,
(1950),**72**, 4218.
[99] R.N.Goldberg and L.G.Hepler,**Chem.Rev.**,(1968),**68**, 229.
[100] D.L.Kepert, "The Early Transition Metals",Academic Press, 1972.

[101] A.Gutbier and A.Krell,**Ber.**, (1905),**38**, 2385.

[102] W.Robb and P.van Bekker,**Inorg.Chim.Acta**, (1973),**7**, 626.

[103] J.E.Fergusson and R.R.Sherlock,**Aus.J.Chem.**,(1977),**30**, 1445.

[104] F.A.Cotton and D.A.Ucko,**Inorg.Chim.Acta**, (1972),**6**, 161.

[105] U.von Muller, R.Dubgen, K.Dehnicke,
Z.Anorg.Allg.Chem., (1981),**473**, 115.

[106] A.Sabatini and I.Bertini,**Inorg. Chem.**, (1966),**5**, 204.

[107] S.M.Horner, R.J.H.Clark, B.Crociani, D.B.Copley, W.W.Horner,
F.N.Collier, S.Y.Tyree,**Inorg. Chem.**,(1968),**7**, 1859.

[108] G.W.A.Fowles, D.J.Tidmarsh, R.A.Walton,
Inorg. Chem., (1969),**8**, 631.

[109] V.T.Coombe, G.A.Heath, T.A.Stephenson, D.K.Vattis,
JCS Dalton, (1983), 2307.

[110] W.P.Griffith, "The Chemistry of the Rarer Platinum
Metals", Wiley-Interscience, 1967.

[111] C.K.Jorgensen,**Acta Chem.Scand.**, (1956),**10**, 518.

[112] J.Burgess, "Metal Ions in Solution", J.Wiley and Sons, 1978.

[113] P.George and D.S.McClure,**Prog. Inorg. Chem.**,
Vol.1, Wiley-Interscience, 1959.

[114] H.L.M.van Gaal and J.G.M.van der Linden,
Coord.Chem.Rev., (1982),**47**, 41.

[115] B.N.Figgis, "Introduction to Ligand Fields",
Wiley-Interscience, 1966.

[116] D.A.Johnson, "Some Thermodynamic Aspects of Inorganic
Chemistry", 2^{nd} Edn., Cambridge University Press,1982.

[117] A.K.Sengupta, D.W.A.Sharp, G.A.Heath, S.Brownstein,
J.Fluorine Chem., (1982),**21**, 38.

[118] J.R.W.Warn, "Concise Chemical Thermodynamics",
Van Nostran Reinhold, 1969.

[119] C.J.Pickett, Comprehensive Coordination Chemistry Vol.1, Pergamon Press, 1987.

[120] Y.Marcus, "Introduction to Liquid State Chemistry",
Wiley-Interscience, 1977.

[121] J.O'M.Bockris and A.K.N.Reddy,
"Modern Electrochemistry", Plenum Press, 1970.

[122] "Handbook of Chemistry and Physics", Vol.68,
C.R.C. Press, 1987.

[123] T.C.Waddington, "Non-aqueous Solvents", studies in
modern chemistry, Pitman Press, 1969.

[124] P.Pyykkö and J.-P.Desclaux,**Acc. Chem.Res.**, (1979),**12**, 276.

[125] E.U.Condon and H.Odabasi, "Atomic Structure",
Cambridge University Press, 1980.

[126] G.H.Aylward and T.J.V.Findlay, "S.I. Chemical Data",
2^{nd} Edn., J.Wiley and Sons, 1974.

[127] J.N.Murrell, S.F.A.Kettle, J.M.Tedder, "The Chemical
Bond", John Wiley and Sons, 1978.

[128] B.Cox, D.W.A.Sharp, A.G.Sharpe,**J.Chem.Soc.**,(1956),1242.

[129] R.D.Peacock,**J.Chem.Soc.**, (1955), 3291.

[130] J.H.Holloway, P.R.Rao, N.Bartlett,**JCS Chem.Comm.**,(1965), 306.

[131] C.L.Chernick, H.H.Claasen, B.Weinstock,
J.Amer.Chem.Soc., (1961),**83**, 3165.

[132] K.W.Bagnall, D.Brown, J.G.H.du Preetz,**J.Chem.Soc.**,(1964), 2603.

[133] R.N.Dickinson, S.E.Feil, F.N.Collier, W.R.Horner,
S.M.Horner, S.Y.Tyree,**Inorg. Chem.**, (1964),**3**,1600.

[134] M.Mercer,**JCS Chem.Comm.**, (1967), 119.

[135] H.Bode and G.Teufer,**Z.Anorg.Allg.Chem.**, (1956),**283**, 18.

[136] R.Hoppe and W.Klemm,**Z.Anorg.Allg.Chem.**, (1952),**268**, 364.

[137] A.G.Sharpe,**J.Chem.Soc.**, (1953), 197.

[138] G.Brauer, "Handbook of Preparative Inorganic
Chemistry", 2^{nd} Edn., Academic Press, 1965.

[139] R.Lincoln and G.Wilkinson,**Inorg Synth**.,
Vol.XX, Wiley-Interscience, 1980.

[140] R.C.Young and H.G.Fletcher,**Inorg. Synth**.,
Vol.I, McGraw-Hill, 1939.

[141] W.von Hieber and E.Romberg,**Z.Anorg.Allg.Chem.**,

(1935),**221**, 321.

[142] P.J.H.Carnell, R.E.McCarley, R.D.Hogue,
Inorg. Synth., Vol.X, McGraw-Hill, 1967.

[143] S.A.Shchukarev and G.A.Kokovin,**Russ.J.Inorg.Chem.**,
(1964),**9**, 715.

[144] W.van Bronswyk, R.J.H.Clark, L.Maresca,
Inorg. Chem., (1969),**8**, 1395.

[145] B.J.Brisdon, T.E.Lester, R.A.Walton,
Spectrochim.Acta A, (1967),**23A**, 1969.

[146] B.J.Brisdon, G.W.A.Fowles, D.J.Tidmarsh, R.A.Walton,
Spectrochim.Acta A, (1969),**25A**, 999.

[147] I.R.Beattie, T.R.Gilson, G.A.Ozin,**J.Chem.Soc.A**,(1968), 2765.

[148] A.J.Edwards, R.D.Peacock, A.Said,**J.Chem.Soc.**, (1962), 4643.

[149] J.F.Allen and H.M.Neumann,**Inorg. Chem.**, (1964),**3**, 1612.

[150] B.J.Brisdon and R.A.Walton,**J.Chem.Soc.**, (1965), 2274.

[151] D.M.Adams and D.M.Morris,**J.Chem.Soc.A**, (1967), 1666.

[152] M.Debeau,**Spectrochim.Acta A**, (1969),**25A**, 1311.

[153] L.A.Woodward and M.J.Ware,**Spectrochim.Acta A**, (1964),**20A**, 711.

[154] P.J.Hendra and P.J.D.Park,**Spectrochim.Acta A**, (1967),**23A**, 1635.

[155] D.A.Kelly and M.L.Good,**Spectrochim.Acta A**, (1972),**28A**, 1529.

[156] Y.M.Bosworth and R.J.H.Clark,**JCS Dalton**, (1974),1749.

[157] D.M.Adams, H.A.Gebbie, R.D.Peacock,**Nature London**,(1963),**199**, 278.

[158] J.E.Fergusson and P.V.Heveldt,**Aus.J.Chem.**, (1974),**27**, 661.

[159] P.Ruschke and K.Dehnicke,**Z.Naturforsch. B**, (1980),**35b**, 1589.

[160] R.J.H.Clark and T.J.Dines,**Mol.Phys.**, (1984),**52**, 859.

[161] J.P.Spoonhower,**J.Raman.Spec.**, (1981),**11**, 180.

[162] W.Preetz and H.J.Steinebach,**Z.Naturforsch. B**, (1985),**40b**, 745.

[163] J.E.Fergusson and A.M.Greenaway,**Aust.J.Chem.**, (1978),**31**, 497.

[164] D.H.Brown, K.R.Dixon, C.M.Livingston, R.H.Nuttall,
D.W.A.Sharp,**J.Chem.Soc.A**, (1967), 100.

[165] C.K.Jorgensen and K.Schwachau,**Z.Naturforsch. A**,(1965),**20a**, 65.

[166] C.K.Jorgensen,**J.Inorg.Nucl.Chem.**, (1962),**24**, 1587.

[167] A.Gutbier and F.bauriedel,**Ber.**, (1909),**42**, 4243.

[168] C.K.Jorgensen,**Acta Chem.Scand.**, (1956),**10**, 500.

[169] K.H.Lohmann and R.C.Young,**Inorg. Synth.** ,Vol.IV, 97.

[170] I.E.Grey and P.W.Smith,**Aus.J.Chem.**, (1968),**22**, 1627.

[171] P.W.Smith and A.G.Wedd,**J.Chem.Soc.A**, (1970), 2447.

[172] J.M.Winfield,**J.Fluorine Chem.**, (1984),**25**, 91.

[173] D.M.Adams, P.J.Chandler, R.G.Churchill,**J.Chem.Soc.A.**,(1967), 1272.

[174] J-C.Marchon and J.Badoz-Lambling,**Bull.Soc.Chim.**,(1967),**4**, 4660.

[175] G.Cauquis and D.Serve,**Bull.Soc.Chim.**, (1966),**1**, 302.

[176] M.Mastragostino, G.Casalbore, S.Valcher,
J.Electroanalytical Chem.Interfac.Electrochem.,
(1973),**48**, 419.

[177] L.Sereno, V.A.Macagno, M.C.Giordano,
Electrochim.Acta., (1972),**17**, 561.

[178] G.M.Anderson, unpublished work.

[179] J-C.Marchon,**C.R.Acad.Sci.Paris Ser.C.**, (1968),**267**,
1123. (**C.A.** 70, 33757a).

[180] M.Novak and Cs.Visy,**J.Electroanalytical Chem.**
Interfac. Electrochem., (1986),**210**, 251.

[181] B.Weinstock and G.L.Goodman,**Adv.Chem.Phys.**, (1965),**9**, 169.

[182] L.A.Woodward and J.A.Creighton,**Spectrochim.Acta**, (1961),**17**, 594.

[183] A.K.Brisdon, E.G.Hope, W.Levason, J.S.Ogden,
JCS Dalton, (1989),**2**, 313.

[184] R.J.P.Williams and J.D.Hale,**Structure and Bonding**,(1966),**1**, 249.

[185] K.Nakamoto, "Infra-red and Raman Spectra of Inorganic
and Coordination Compounds", Wiley-Interscience, 1986.

[186] R.J.H.Clark, "Halogen Chemistry", Vol.III,A¿¿cademic Press, 1967.

[187] D.E.Lightner Jnr., J.R.Kirk, V.Katovic,**J.Coord.Chem.**,
(1988),**19**, 223.

[188] R.R.Gagne, C.A.Koval, G.C.Lisenski,**Inorg. Chem.**,
(1980),**19**, 2854.

[189] A.Gutbier and C.Fellner,**Z.Anorg.Chem.**, (1916),**95**, 129.

[190] R.N.Goldberg and L.G.Hepler,**Chem.Rev.**, (1968),**68**, 229.

[191] J.A.Plambeck, "Electroanalytical Chemistry", Wiley-Intersciece, 1982.

[192] C.W.Davies, "Ion Association", Butterworths, 1962.

[193] L.McGhee,*personal communication.*

[194] T.A.O'Donnell,**Chem.Soc.Rev.**, (1987),**16**, 1.

[195] P.C.Couch, G.W.A.Fowles, R.A.Walton, **J.Inorg.Nucl.Chem.**, (1970),**32**, 329.

[196] G.M.Anderson, J.H.Cameron, A.G.Lappin, J.M.Winfield, **Polyhedron**,**1**, 467.

[197] K.Moock, *personal communication.*